PRELIMINARY EFFORTS TOWARDS ACHIEVING TRANSIENT DIRECTING GROUP CHEMISTRY ENABLED VIA A TANDEM AND COOPERATIVE CONCURRENT CHEMOENZYMATIC CASCADE

By

Ali Farzam

A thesis submitted to the University of Ottawa
in partial fulfillment of the requirements for the
Master of Science degree in Chemistry

Department of Chemistry and Biomolecular Sciences
Faculty of Science
University of Ottawa

Abstract.

Directing groups (DGs) are moieties installed onto organic molecules to confer regioselectivity in subsequent reactions. DGs have found utility in selective CH activations catalyzed by transition metal (TM) catalysis on starting materials with multiple CH bonds. Despite their utility, DGs are scarcely used in industrial applications due to the generally wasteful nature of conventional DG strategies and their associated increase in step-count. Transient directing groups (TDGs) have been developed to overcome these limitations, with additives reversibly forming adducts with compounds of interest prior to the DG-mediated CH activation, in one-pot processes. However, the use of TDGs still requires harsh conditions to achieve significant yields, hindering broad applications. Chemoenzymatic catalytic cascades have attracted attention due to the mild and environmentally friendly nature of biocatalysis, with the greatest challenge being compatibility issues between biocatalytic and traditional chemical transformations. Here we propose a concurrent chemoenzymatic catalytic cascade that would enable TM-catalyzed DG chemistry via flanking biocatalytic reductive amination to install, and oxidative deamination to remove, a TDG. Preliminary efforts have identified some incompatibilities arising from the biocatalytic portion of the cascade, namely substrate specificity and organic co-solvent tolerance, that need to be addressed to achieve the proposed chemoenzymatic cascade in a one-pot concurrent protocol.

Acknowledgements.

To my family:

"I sound my barbaric yawp over the roofs of the world."
- Walt Whitman

To my friends and colleagues:

"Gather ye rose-buds while ye may,
Old Time is still a-flying,
And this same flower that smiles today,
Tomorrow will be dying."
- Robert Herrick

To my supervisors and committee:

"... My name is Ozymandias, King of Kings;
Look on my works, ye Mighty, and despair! ..."
- Percy Bysshe Shelley

O captain, my captain:

"I went to the woods because I wanted to live deliberately,
I wanted to live deep and suck out all the marrow of life!
To put to rout all that was not life,
And not, when I had come to die, discover that I had not lived."
- Henry David Thoreau

Table of Contents.

List of Symbols, Abbreviations, and Nomenclature

% v/v	Percent volume by volume
% w/v	Percent weight by volume
ACN	Acetonitrile
ADH	Alcohol dehydrogenase
*Ad*RedAm	RedAm from *Ajellomyces dermatitidis*
*Asp*RedAm	RedAm from *Aspergillus oryzae*
ATHase	Artificial Transfer Hydrogenase
*At*RedAm	RedAm from *Aspergillus terreus*
B_2pin_2	Bis(pinacolato) diboron
BSA	Bovine serum albumin
CH	Carbon-hydrogen
CuAAC	Copper-catalyzed azide-alkyne cycloaddition
CV	Column volume
DAAO	D-amino acid oxidase
DG	Directing group
DKR	Dynamic kinetic resolution
DMSO	Dimethyl sulfoxide
DNA	Deoxyribose nucleic acid
dNTP	Deoxyribose nucleotide triphosphate
dsDNA	Double stranded DNA
EAS	Electrophilic aromatic substitution
EDG	Electron donating group
Equiv.	Equivalents
EWG	Electron withdrawing group
FG	Functional group
GC-FID	Gas chromatography – flame ionization detector
GC-MS	Gas chromatography – mass spectroscopy
GDH	Glucose dehydrogenase
HbpA	2-hydroxybiphenyl monooxygenase
HFIP	Hexaflouroisopropanol
HPLC	High performance liquid chromatography
IPTG	Isopropyl β-d-1-thiogalactopyranoside
IRED	Imine reductase
kDa	Kilodalton
LAAO	L-amino acid oxidase
LB	Lysogeny broth/ Luria-Bertani
MAO	Monoamine oxidase
min	minute(s)
M	moles per liter
mM	millimoles per liter
mol %	Percent mole by mole
NAD+	Oxidized nicotinamide adenine dinucleotide
NADH	Reduced nicotinamide adenine dinucleotide
NADP+	Oxidized nicotinamide adenine dinucleotide phosphate

NADPH	Reduced nicotinamide adenine dinucleotide phosphate
Ni-IMAC	Nickel immobilized-metal affinity chromatography
NMR	Nucleic magnetic resonance
NuH	Protonated nucleophile
PCR	Polymerase chain reaction
Pd-NP	Palladium nanoparticle
PVDF	Polyvinylidene fluoride
RAIR	*RecA* independent recombin
RCM	Ring closing metathesis
RedAm	Reductive aminase
rpm	Revolutions per minute
s	second(s)
SDS-PAGE	Sodium dodecyl sulfate – polyacrylamide gel electrophoresis
T4 PNK	T4 polynucleotide kinase
TDG	Transient directing group
TFE	Triflouroethanol
THF	Tetrahydrofuran
TM	Transition metal
Tris	Tris(hydroxymethyl)aminomethane
WT	Wild-type

List of Schemes.

List of Figures.

List of Tables.

1. Introduction

1.1. General Introduction

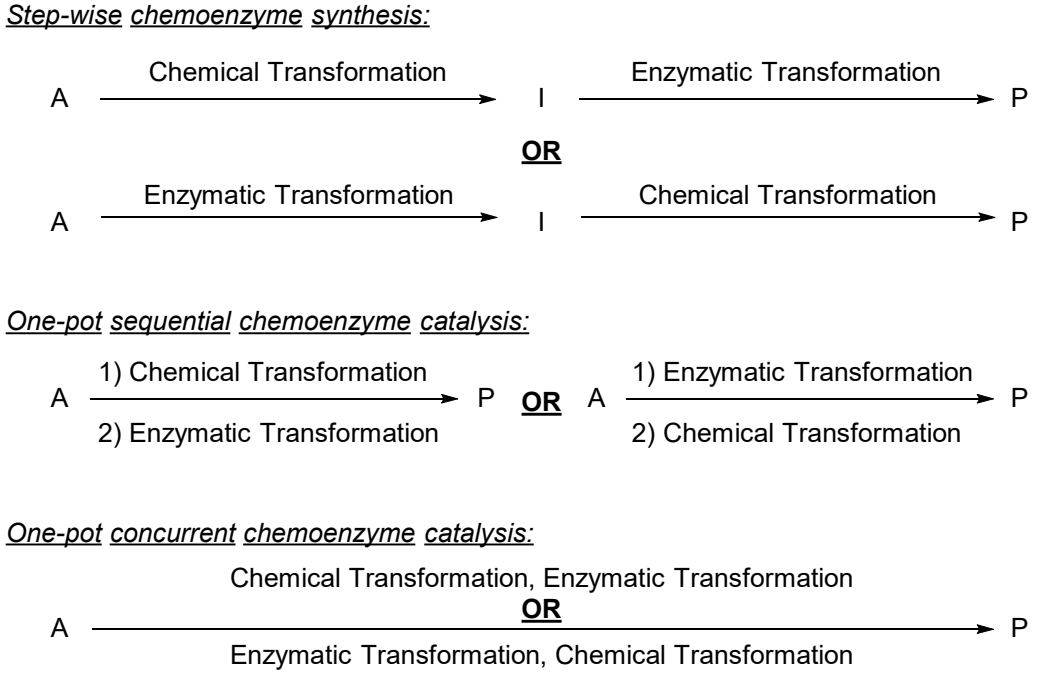

Figure 1. Different applications of chemoenzymatic chemistry.

Chemoenzymatic chemistry involves the integrated use of enzymatic and chemical transformations to produce small molecule compounds of interest (**Figure 1**). A rudimentary application of this concept is step-wise chemoenzymatic synthesis, which only differs from traditional chemical synthesis due to the use of a biocatalytic reaction in at least one synthetic step; while examples of this form of chemoenzymatic chemistry have been reported,[1] further discussion on chemoenzymatic synthesis has been omitted in favour of discussions on other applications of chemoenzymatic chemistry that are more appropriate for our scope, specifically, chemoenzymatic catalysis (see Section 1.3). Chemoenzymatic catalysis involves the integrated use of biocatalysts and chemo-catalysts to achieve multiple transformations in one-pot protocols. Chemoenzymatic catalysis in the form of one-pot sequential protocols involves the use of one mode of catalysis with subsequent alteration of the reaction conditions

to conduct the alternative mode of catalysis, without isolating the intermediate formed in between. Since the two catalytic cycles do not operate in concert, it is not necessary to optimize the reaction conditions to be mutually favourable for both catalytic cycles (for further discussion on sequential chemoenzymatic catalysis, see Section 1.3.1). In contrast, concurrent chemoenzymatic catalysis involves one-pot protocols wherein both bio- and chemo-catalysts are operating under the same reaction conditions. Since chemical transformations and enzymatic catalysis are often carried out under conflicting conditions, finding optimal conditions that are suitable for both types of catalysis is a challenge (for further discussion on concurrent chemoenzymatic catalysis, see section 1.3.2).

Here, our group is proposing a concurrent chemoenzymatic cascade with three catalytic cycles operating in tandem. Specifically, we aim to achieve a one-pot protocol wherein an intermediary organometallic catalytic cycle is flanked by a primary and a secondary biocatalytic cycle, ultimately achieving three transformations in a single reaction vessel (**Figure 2**). The chemical transformation we would like to achieve as a part of this cascade is a group-directed CH activation; a directing group moiety on the first intermediate (I^1) facilitates a regioselective CH activation by templating the organometallic catalyst (for further discussion on directing group chemistry, see sections 1.2–1.2.4). The purpose of the first and last biocatalytic cycles is to install the directing group on the starting material (A) and cleave it from the second intermediate (I^2), respectively; we propose to achieve this enzymatic loading and unloading through biocatalytic reductive amination and oxidative deamination, respectively (for further discussion on biocatalytic reductive aminations and the enzymes facilitating these transformations, see section 1.3.3-1.3.5).

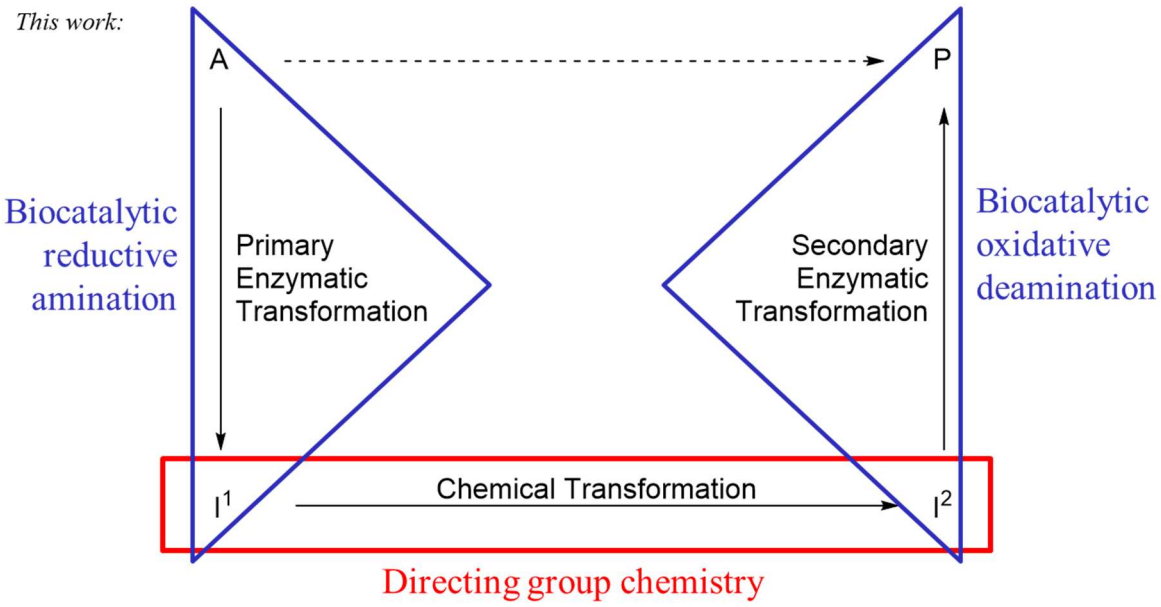

Figure 2. General scheme for our proposed tandem and cooperative concurrent chemoenzymatic cascade to enable transient directing group chemistry.

1.2. Directing Group Chemistry

The use of directing groups (DGs) on organic molecules is a classic strategy that can be employed in synthesis to selectively functionalize specific CH bonds, an otherwise difficult endeavour due to the pervasive presence and inert nature of CH bonds in organic molecules.[2] Very simply, DGs can be described as a moiety on a starting material that enables regioselectivity under reaction conditions that would otherwise yield different regioisomers. The concept of DGs was first described over a century ago with the substituent effects of mono-substituted arenes on the *ortho/meta/para* regioselectivity of electrophilic aromatic substitutions (EAS).[3] Since, the use of DGs to overcome the innate reactivity of arenes and heterocyclic aromatics has been extensively studied.[4–8] DGs have also been used to enable directed ortho metalations, a protocol complementary to metal halogen exchange.[9,10] In general, these DGs achieve regioselectivity through steric bulk, electronic effects, and templating/co-ordination of a reactive species to the desired CH bond (**Figure 3**).

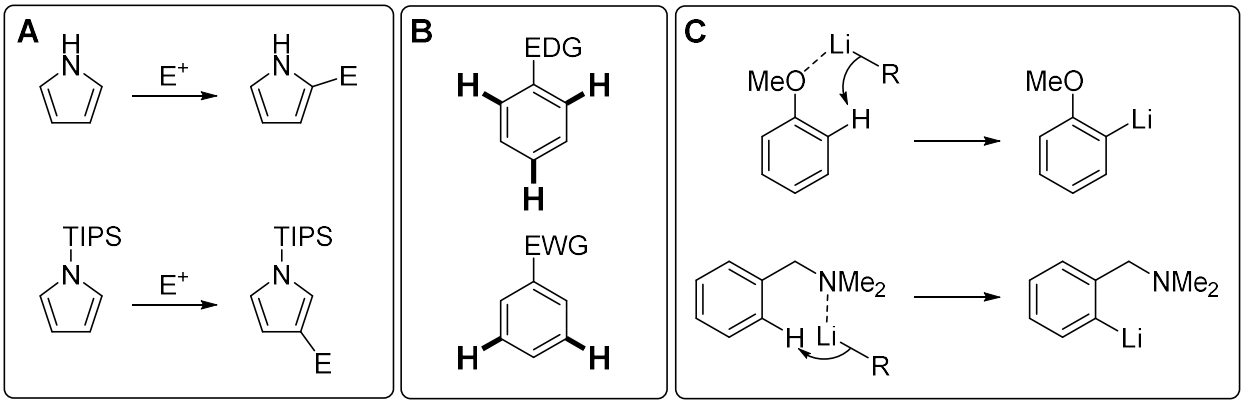

Figure 3. Simple examples of DGs in classic organic reactions. **(A)** Bulky alkyl-silyl substituent hinders the more reactive C2 position of pyrrole, conferring C3 regioselectivity in electrophilic aromatic substitutions (EAS). **(B)** The effect of electron donating groups (EDGs) and electron withdrawing groups (EWGs) on EAS. **(C)** Directed ortho lithiation of phenyl CH through templating of alkyllithium to the ortho C-H bond

Despite their long-standing history, DG chemistry garnered significant attention after a landmark paper describing the use of a DG in transition metal (TM)-catalyzed CH functionalization.[6,11] Specifically, this paper described the use of a ketone DG on (hetero)arenes for a regioselective *ortho* alkylation using olefins, which was later recognized as the Murai reaction. The selectivity was achieved through a metalacyclic intermediate formed through chelation of ruthenium with the ketone DG during the catalytic cycle (**Figure 4**). This contribution was the first example of efficient and selective CH bond cleavage and C-C bond formation mediated by TM catalysis, improving on the established protocols of CH bond cleavage with stoichiometric equivalents of metals.[6,12,13] Moreover, this development increased the attention received by DGs due to the increasing popularity of TM-catalyzed C-C couplings that coincided in the literature at the time.[14–16] Indeed, the use of DGs has evolved since the initial inception of the strategy in electrophilic aromatic substitutions; since the Murai reaction was published, advancements in DG-assisted TM-catalyzed CH activations have widened in scope, extending beyond alkylations and broadening the scope of functionalities that act as DGs.[17]

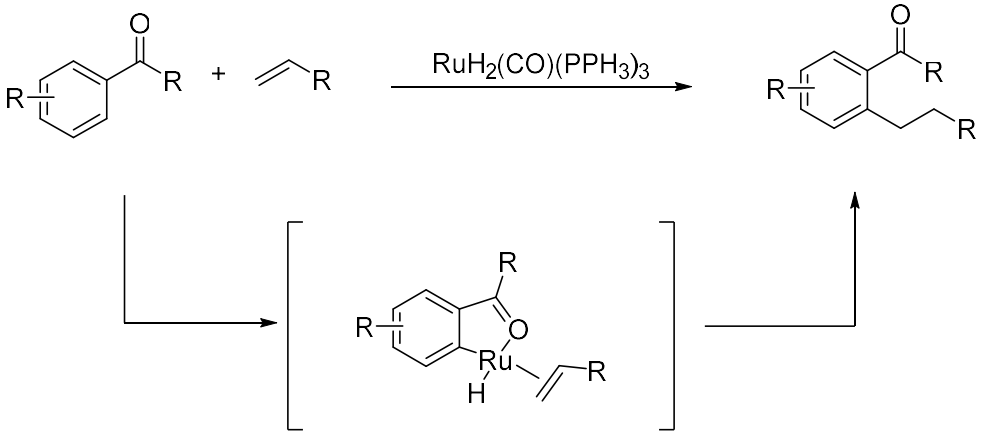

Figure 4. The Murai reaction: a ketone-directed *ortho* alkylation mediated via a ruthenacyclic intermediate formed in the catalytic cycle.

1.2.1. Modern DG-assisted C-H Activations.

Despite their ability to affect the yields of regioisomers through steric and electronic effects, the most popular DG strategy employed in modern CH activations is the use of σ-donor motifs to chelate reactive TM complexes and coordinate them to the desired CH bond.[6,17] Extending on the framework established by the Murai reaction, the protocol for ketone-directed alkylations has been diversified; it has been reported that the reactive ruthenium species can be generated in situ using inexpensive ruthenium trichloride.[18] Moreover, the Markovnikov-like selectivity of the alkylation with respect to the olefin has been shown to be tunable using an iridium based catalyst system; although, while the *ortho* regioselectivity can be attributed to DG chelation, the selectivity of branched and linear products was shown to be a consequence of the external ligands used.[19] The synthetic utility of the transformation has been further improved by the development of ketone-directed olefinations,[20–22] arylations,[23] alkynylations,[24] and acylations.[25]

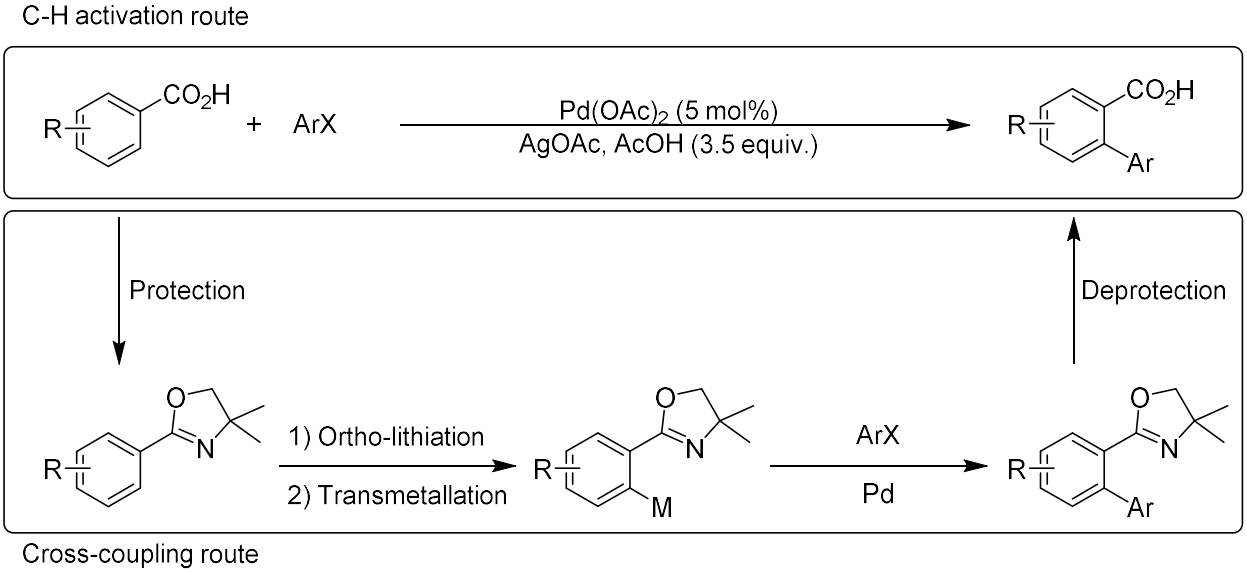

Scheme 1. Pd-catalyzed *ortho* directed arylation of benzoic acids enabling a quicker route to biaryl products compared to the Pd-catalyzed cross-coupling strategy required for the same starting materials.

Expanding on the use of ketones as DGs, carboxylic acids have found a place in the DG toolbox. The carboxylate moiety possesses a number of advantages when used as a DG, including its natural abundance, ease of installation, and the ready ability to be cleaved/modified by decarboxylation or further transformations.[6] The *ortho* arylation of benzoic acid derivatives is one of the most investigated CH activations mediated by carboxylate DGs; indeed, these CH activations have been reported using electrophilic and nucleophilic arylating reagents as well as cross-dehydrogenative coupling processes.[2] The palladium-catalyzed synthesis of biarylcarboxylates using benzoic acids and aryl halides is one of the first examples of such carboxylate-directed arylations.[26] This strategy enabled a more step-economical approach to the synthesis of 1,2-arylbenzoic acids in contrast to a traditional cross-coupling based synthesis using the same starting materials (**Scheme 1**).[27–29] Compared to ketones, a broader range of *ortho* directed CH activations have been reported using carboxylate DGs, including alkylations, olefinations, alkynylations, allylations, acylations, alkoxylations, aminations, and even halogenations.[2,6] More importantly, the use of carboxylate DGs is not limited to aromatic C(sp^2)-H activations. The rhenium(V) catalyzed β-allylation of acrylic acids using allylic alcohols is an example of carboxylate-directed vinyl CH activation (**Scheme 2**).[30] Furthermore, the palladium(II) catalyzed β-arylation of aliphatic acids using either phenylboronic esters (**Scheme 3A**) or aryl iodides are examples of carboxylate-directed C(sp^3)-H activations (**Scheme 3B**).[31]

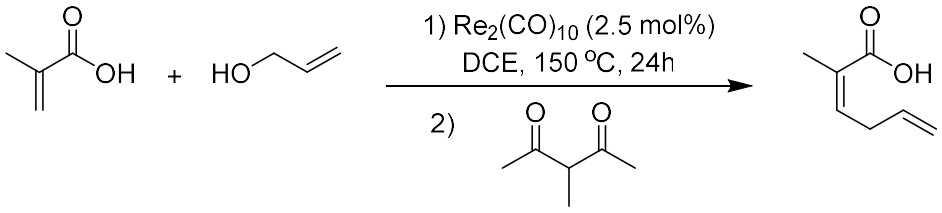

Scheme 2. Rhenium-catalyzed β-allylation of acrylic acids.

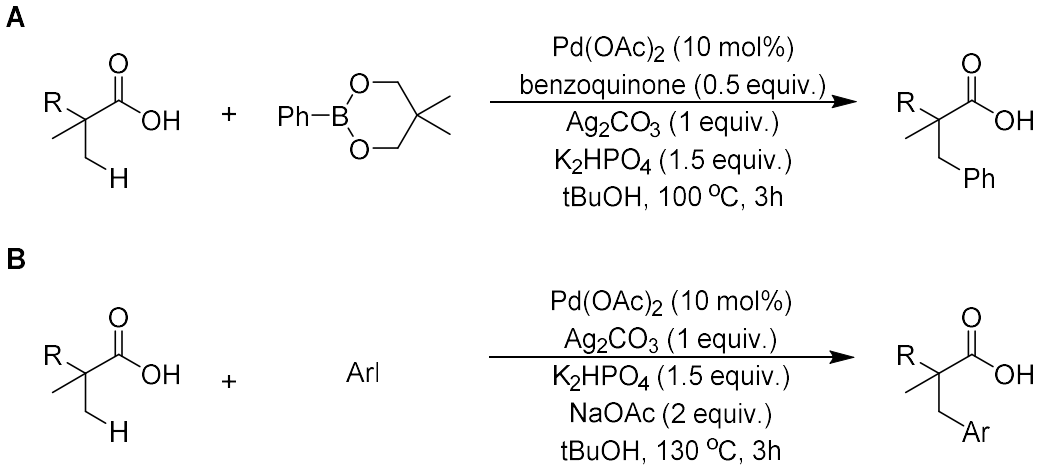

Scheme 3. Pd-catalyzed β-arylation of aliphatic acids using **(A)** phenylboronic esters and **(B)** aryl iodides.

A functional group related to the carboxylic acid is the ester moiety, which can be prepared from a free acid by Fischer-Speier esterification or a more contemporary protocol, like the Steglich esterification.[32,33] Both acids and esters coordinate weakly to metal catalysts, increasing the difficulty of developing successful protocols wherein they act as DGs. While this has not slowed the development of procedures employing carboxylate DGs, contributions to the field utilizing an ester DG have been limited. Nonetheless, ester DGs have found an interesting use in directed borylations to yield synthetically useful organoboron compounds. This direct synthetic route provides advantages over the previously reported indirect metalation/transmetalation sequence[34] in terms of functional group compatibility and more lenient reaction conditions (i.e. protic solvents, ambient temperatures, moisture sensitivity).[35] An iridium-catalyzed ester-directed *ortho* CH borylation of benzoates was reported using B_2pin_2 as the boron source (**Scheme 4A**).[36] This protocol was modified to achieve the borylation at the vinylic β-CH of α,β-unsaturated esters (**Scheme 4B**);[37] even when the ester substituent was a phenyl ring, the borylation occurred exclusively at the vinylic CH, illustrating the excellent selectivity of these conditions. DG-mediated borylations are also

possible at the *para* CH position of benzoates by utilizing a specific ligand-supported iridium based catalytic system.[38] Here the use of the ligand is crucial, as it is the non-covalent interaction between the ligand and the ester DG, and not the ester and TM, that is responsible for the *para* selectivity (**Scheme 5**).

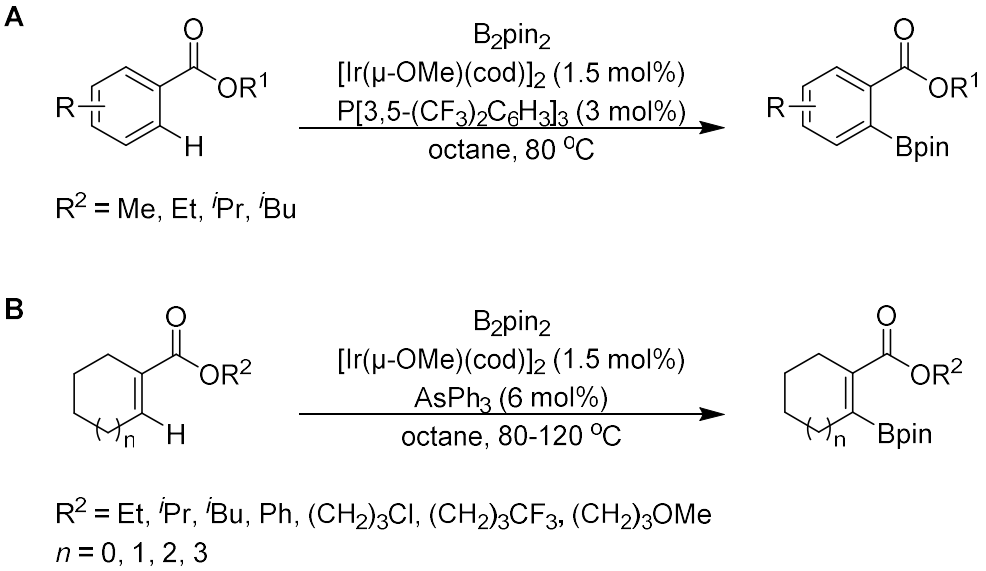

Scheme 4. Ir-catalyzed ester-directed borylations. **(A)** *Ortho* borylation of benzoates. **(B)** β-borylation of α,β-unsaturated esters.

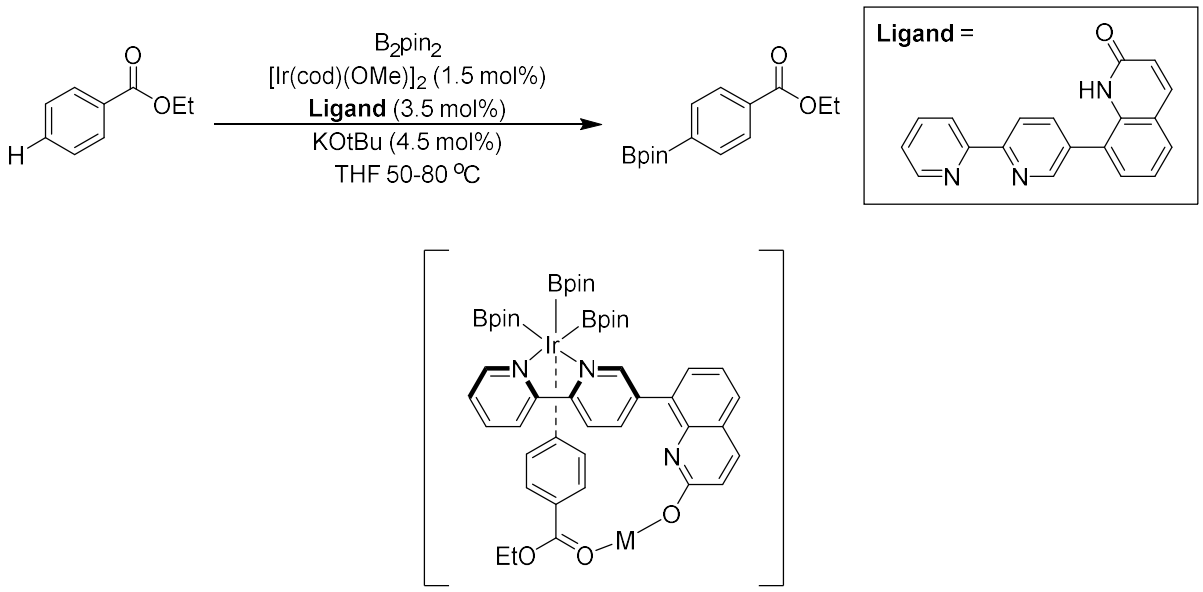

Scheme 5. *Para* selective borylations of (hetero)arenoates using a special iridium-ligand catalyst system. The selectivity is achieved via interactions between the ester substrate and ligand.

While pioneering work in the field of CH activations has been accomplished with oxygen-containing DGs, recent advancements have been dominated by nitrogen-based DGs. Isosteres of ester moieties and products of the coupling of carboxylic acids with amines, amides are an excellent example of DGs frequently used for the purposes of CH activations. A solitary amide has the capacity to act as a monodentate DG, and examples of both substituted and unsubstituted amides have been reported as DGs in CH activations. Like the previously described monodentate DG functionalities, amides have been used to direct numerous types of C-C bond forming C(sp^2)-H activations (i.e. arylations,[39] alkylations,[40] allylations,[41] alkenylations,[42] and acylations[43]). An interesting example is the amide-directed alkenylation of α,β-unsaturated amides with internal alkynes, at the olefinic β-C(sp^2)-H position, to yield dienamide products (**Scheme 6A**).[44] Another notable transformation is the DG-assisted alkylation (**Scheme 6B**) and alkenylation of formyl C(sp^2)-H bonds, using alkenes and alkynes respectively.[45] However, these formyl CH activations were not exclusive to amides as the transformations could be achieved with both esters and ketones, suggesting the importance of the carbonyl oxygen in directing these reactions.[6]

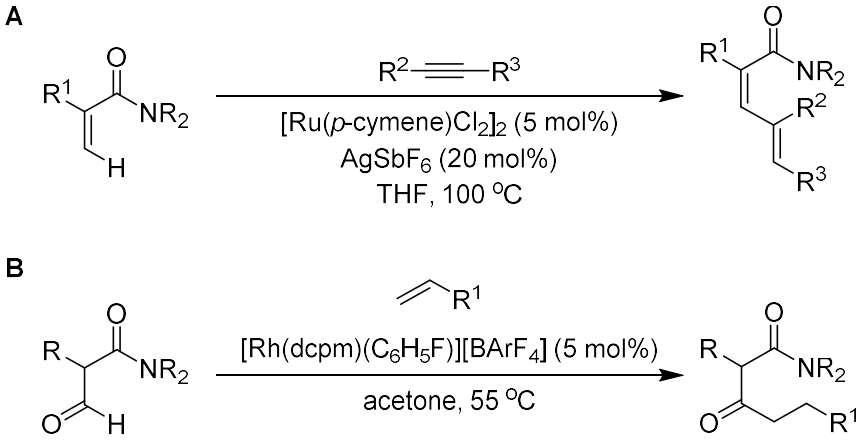

Scheme 6. Amide-directed C(sp^2)-H activations. **(A)** Alkenylation of α,β-unsaturated amides with internal alkynes. **(B)** Alkylation of formyl C(sp^2)-H using terminal olefins.

Although there are several examples of amide based DGs, the repertoire of transformations possible/available are not, for the most part, exclusive to the amide functionality. The *ortho* directed CH functionalization of (hetero)arenes is a good example to illustrate the state of the field in this regard. The application of nitriles as DGs has helped to diversify the toolbox by activating the more remote *meta* and *para* positions of (hetero)aromatic systems. While *para* selectivity has been achieved with ester DGs (**Scheme 5**), this required a special external ligand and was an example that was an exception to the norm. In contrast, examples of *ortho* directed functionalizations directed by nitriles are outnumbered by examples of *para* directed functionalizations, which are themselves outnumbered by examples of *meta* directed functionalizations.[6,17] Selectivity at the *para* and *meta* positions is typically achieved by placing the nitrile moiety at the end of a spacer, exploiting its linear geometry to activate the desired CH bond. For *meta* directed reactions, the nitrile is present as an *ortho* substituted benzonitrile separated from the target aromatic system by a 3-4 atom spacer (**Scheme 7**);[6,46] *para* substitutions are achieved using a biphenyl template and a silyl spacer (**Scheme 8**).[47] Despite the versatility displayed by nitriles as *meta/para* directors of aryl CH activations, reported transformations have mostly been limited to olefinations using electron deficient terminal olefins.[46–50]

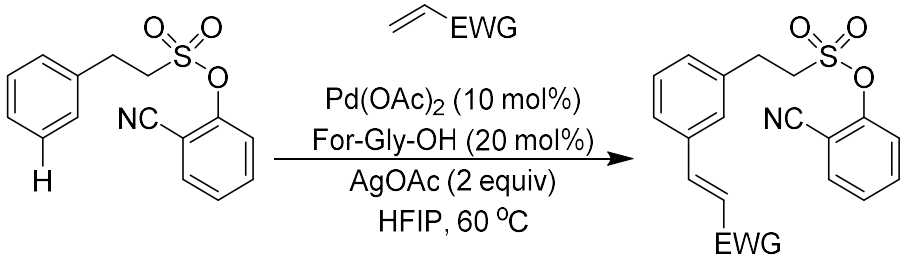

Scheme 7. Nitrile-directed *meta* CH olefination using electron deficient terminal olefins. The benzonitrile functionality is separated from the target arene by a 4-atom spacer.

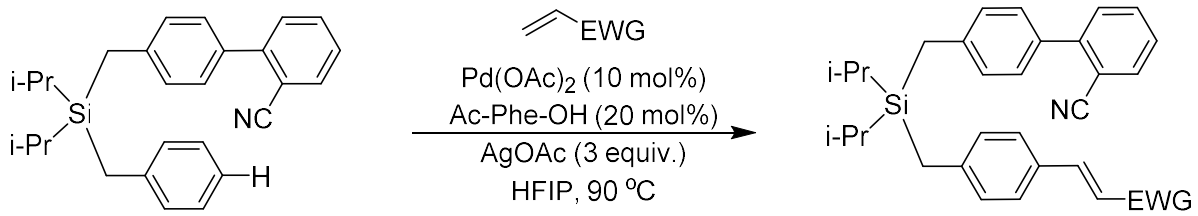

Scheme 8. Nitrile-directed *para* CH olefination using electron deficient terminal olefins. The nitrile functionality is separated from the target arene by a biphenyl template and silyl spacer.

While there are many examples of monodentate N-containing DGs, nitrogen is more frequently found in polydentate DGs wherein multiple N-atoms contribute to the DG's denticity. Recently published examples of polydentate N-containing DGs demonstrate their utility in modulating regioselectivity. Indeed, the palladium-catalyzed functionalization of unactivated olefins,[51–58] controlled using bidentate or tridentate DGs coordinating through N-atoms, demonstrates the versatility of nitrogen in DG chemistry. Here, the key to regioselectivity is the formation of a stable palladacyclic intermediate (**Scheme 9**) prior to proto-depalladation.[51,53] Chelation of the metal is often achieved with N-heteroarenes, particularly the aminoquinoline moiety.[6,59] These polydentate DGs have also been used to activate other C(sp^2)[60,61] and C(sp^3)[62–65] centers. Moreover, this strategy has been extended to nickel-catalyzed protocols,[66] including halogenations.[67]

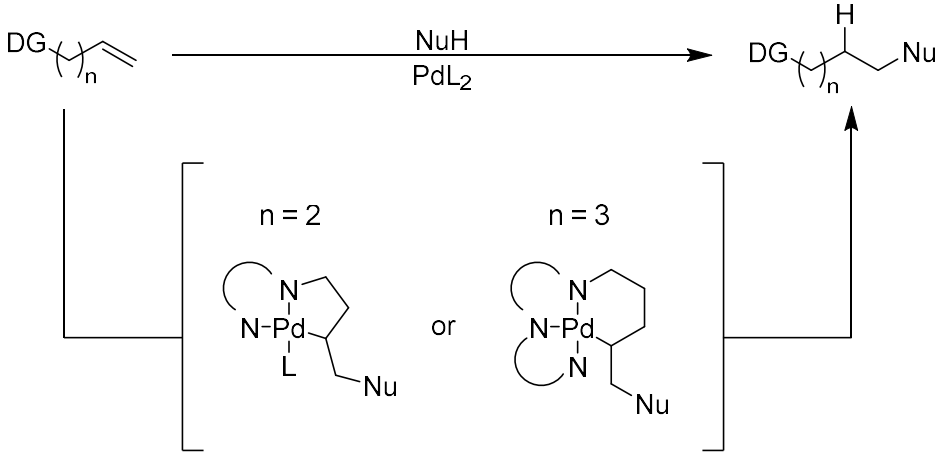

Scheme 9. Palladium-catalyzed functionalization of unactivated alkenes using polydentate directing groups chelating through nitrogen atoms.

1.2.2. Our Contributions to DG Chemistry

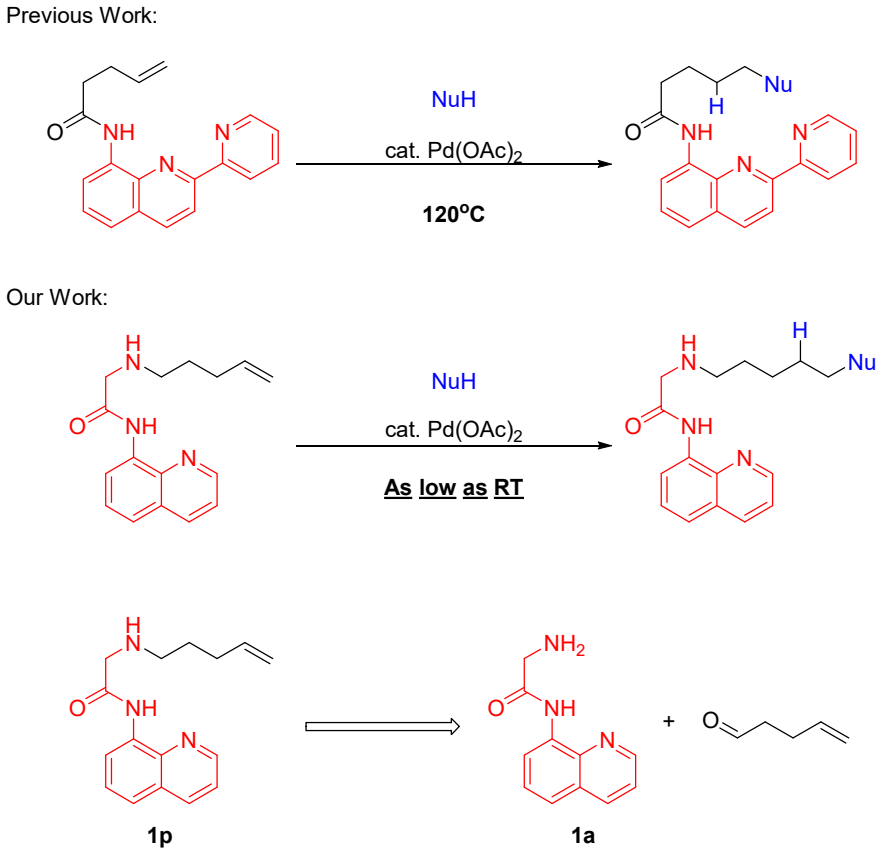

Scheme 10. Optimization of previously reported anti-Markovnikov alkene functionalizations to achieve CH activations at ambient temperatures. The design of a new tridentate DG (**1p**) reduces the heteroaromatic bulk present on previously reported DGs. A secondary amine sigma donor enables the preparation of **1p** from the primary amine **1a** via reductive amination.

Recently, efforts have been made by our group to extend on the conditions and moieties used for the previously reported anti-Markovnikov olefin functionalizations.[59] These efforts include successful transformations conducted under ambient temperatures, and a new aminoquinoline-based tridentate DG moiety with a secondary amine as a sigma donor (**Scheme 10**; **1p)**. The structure of the new tridentate DG moiety eliminates some of the heteroaromatic bulk on previously reported tridentate DGs by replacing the pyridyl ring and extending the aminoquinoline moiety with glycine. Moreover, utilizing the amine of glycine as a secondary amine sigma donor enables a straight-forward preparation of **1p** via the

reductive amination of 4-pentenal with the primary amine, **1a**. Interestingly, our results have shown that the optimal solvent for these vinylic CH activations are polyfluorinated alcohol solvents, particularly 2,2,2-triflouroethanol (TFE) and 1,1,1,3,3,3-hexaflouro-2-propanol (HFIP). Indeed, it has been previously suggested that the unique properties of these solvents, such as their acidity, high hydrogen bonding ability, and polarity, can help promote metal-mediated CH activations through a number of mechanisms like stabilizing cationic metallic species and facilitating proton transfer; however, these benefits have been proposed from empirical observation as the accurate roles of these solvents have not been studied in-depth.[68] Nevertheless, the ability to conduct these CH activations at room temperature is a promising property that could enable their congruence with biocatalytic transformations.

1.2.3. Drawbacks to DG Chemistry

Despite their potential to introduce versatility to synthetic strategies, reports of DG-mediated transformations in synthetic efforts are largely absent from the literature and industry applications.[69–72] This may be attributed to the limitations that are associated with the conventional use of DGs. Employing DGs creates an undesirable increase in step-count, as the DG-mediated transformation would often be accompanied by steps to install/remove the DG in a conventional synthesis. This multiple step requirement of applying a DG strategy in a total synthesis renders the approach a more complex implementation than simple one-step/one-pot transformations. As well, the increase in steps ultimately results in lower overall yields. Moreover, in the design of an appealing synthetic approach, DGs introduce unappealing atom economy: directly, through the moiety itself, and indirectly, through the reagents needed to install and remove it. The issue of atom economy is additionally compounded when the DG moiety itself and/or the reagents involved in its installation/removal are expensive. Another

concern arises from the need for harsh conditions to remove the DG, limiting the complexity of molecules that can be obtained when employing DG strategies.[73–75]

A simple example of conventional DG chemistry, a recently published protocol describing a DG-mediated transannular CH activation, is a recently published use of a DG that also demonstrates some of the previously mentioned limitations of DG chemistry (**Scheme 11**).[76] Here, the CH activation step is flanked by the steps required to install and remove the DG, reducing the yield of the final product to 52% over 4 steps. Moreover, the removal of the DG required supra-stoichiometric equivalents of samarium(II) iodide, increasing the cost of the synthesis. This, and the use of a fluorinated DG moiety, demonstrate the unappealing atom economy of a conventional DG strategy in synthesis. It is interesting to note the similarities between this synthetic scheme and the general scheme of the concurrent chemoenzymatic cascade that was proposed (**Figure 2**), as we propose to surpass these limitations via tandem chemoenzymatic transformations in one-pot.

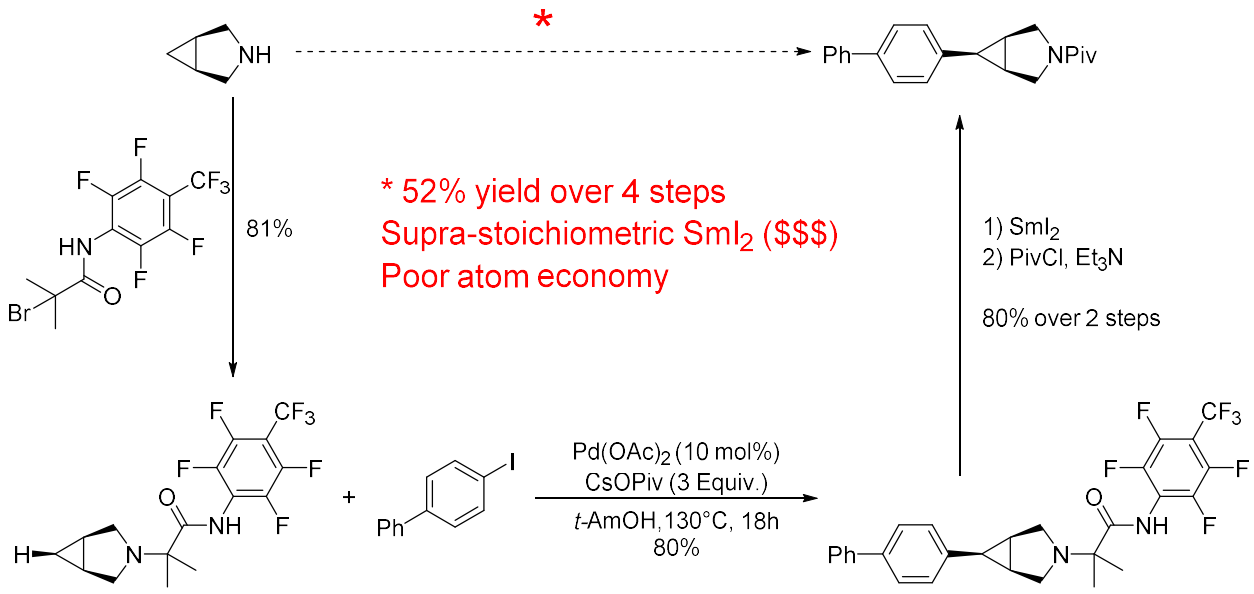

Scheme 11. Palladium-catalyzed DG-assisted transannular CH arylation of alicyclic amines demonstrating some of the drawbacks to a classically employed DG strategy.

1.2.4. Transient Directing Group Chemistry

While the traditional DG strategy suffers from limitations that have restricted its application, its potential in selectively activating otherwise inert CH bonds for efficient functionalization have not been ignored. Indeed, in the last two decades, significant efforts have been made to address some of the shortcomings of employing a conventional DG approach in a synthesis. Most notably, the emergence of transient directing groups (TDGs) has been an interesting strategy to overcome the poor atom and step economy associated with DG-mediated CH activations.[73–75] The TDG strategy involves the reversible installation and removal of the chelating σ-donor motif for a one-pot regioselective CH activation (**Figure 5**). The coordinating TDG is generated *in situ* from a reversible reaction between the starting material and a co-catalytic additive. The resulting Lewis basic intermediate chelates a reactive TM complex to confer regioselectivity in the subsequent CH activation, before the TDG is cleaved to yield the desired product and regenerate the co-catalytic additive, which is free to react again with the starting material.

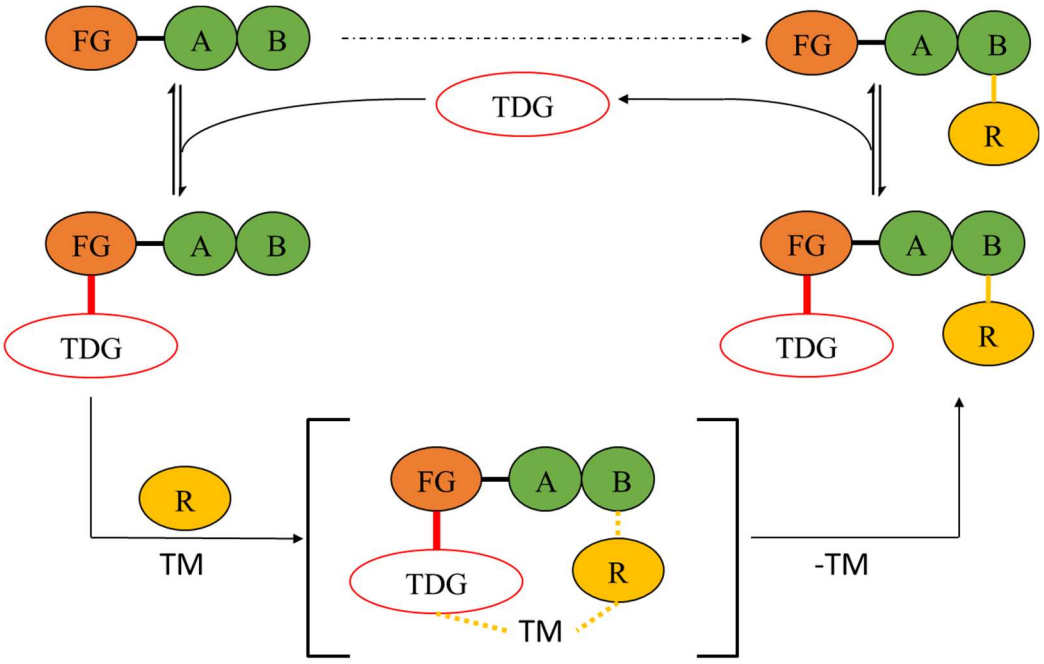

Figure 5. Overview of using a transient directing group (**TDG**) for regioselective transition metal (**TM**) catalyzed functionalization. The TDG is reversibly installed onto the starting material *in situ* through a reversible reaction with an appropriate functional group (**FG**). The coupling partner (**R**) is directed to reactive site B on the starting material through coordination with the TDG-TM complex. The TDG is cleaved to yield the final product.

Seminal work on TDGs was reported in 1996 with the hydroacylation of terminal olefins using Wilkinson's catalyst and 2-amino-3-picoline as a co-catalyst TDG (**Scheme 12A**);[77] however, the field did not attract significant attention until 2016,[74] following a report of amino acids used as TDG co-catalysts to direct palladium-catalyzed C(sp^3)-H activations (**Scheme 12B**).[78] Since, significant contributions have been made to advance the use of TDGs in CH activation chemistry with multiple reviews published to cover the subject in 2018 alone.[73–75] Interestingly, many examples utilize imine formation (a reversible condensation reaction between an amine and carbonyl) as a strategy to install and remove the TDG *in situ.* Consequently, an amine/carbonyl pair must be present on the starting material and TDG co-catalyst. Indeed, several imine-enabled TDG-mediated CH activations have been reported in response to the landmark paper in 2016, with examples of both aldehyde-based and amine-based TDG co-catalysts.

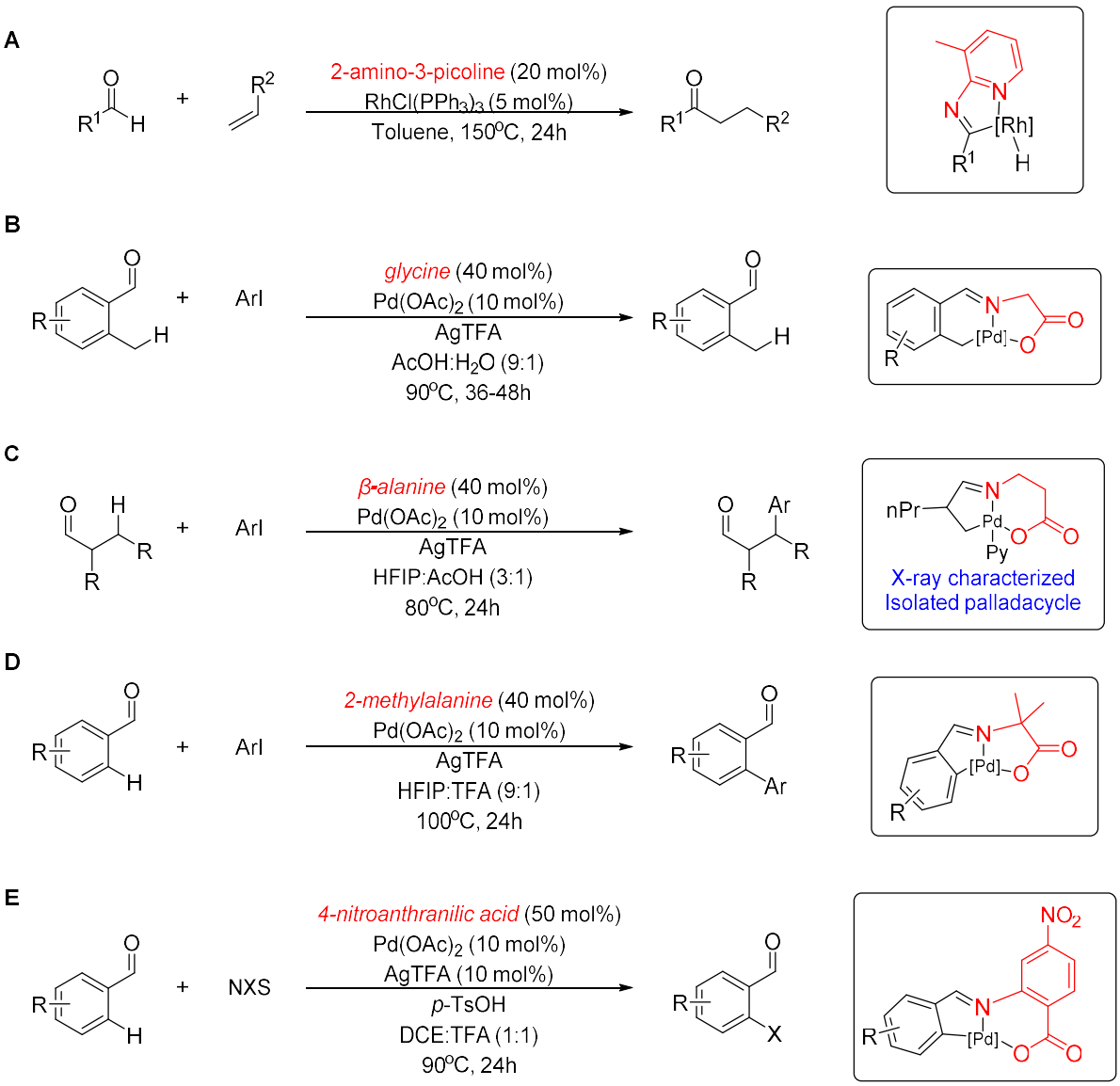

Scheme 12. Regioselective CH activations of aldehydes using amine-based TDGs with proposed or isolated palladacyclic intermediates. **(A)** Aldehydic CH alkylation using terminal olefins. **(B)** Benzylic CH arylation. **(C)** β-methylene CH arylation with isolated and characterized palladacycle. **(D)** Arylic *ortho* CH arylation. **(E)** Arylic *ortho* CH halogenation.

Considerable contributions have been made using amine-based TDGs for regioselective CH activations on aldehyde substrates, owing to the facile imine condensation/hydrolysis that occurs between amines and aldehydes.[74] Indeed, including the landmark reports mentioned previously, amine-based TDGs have been used in aldehydic (**Scheme 12A**), benzylic (**Scheme 12B**), β-methylene (**Scheme 12C**), and *ortho* arylic

(**Scheme 12D/E**) C($sp^{2/3}$)-H activations.[77–82] Ketones are more challenging substrates due to the slower rates of imine condensation/hydrolysis, and the possibility of forming imines with inactive geometries.[74] Nonetheless, protocols for CH activations of ketones enabled by amine-based TDGs have been reported.[78,79,83–86] The CH activation of amine substrates, accessed through aldehyde-based TDGs, are far less common and more challenging to achieve due to the high affinity of free amines for metal centers.[74] This is evident in the scarcity of reports that were able to achieve CH activation on amine substrates using the TDG approach; while it has been reported, most examples require additional workup steps or stoichiometric equivalents of the TDG (**Scheme 13**).[87–89]

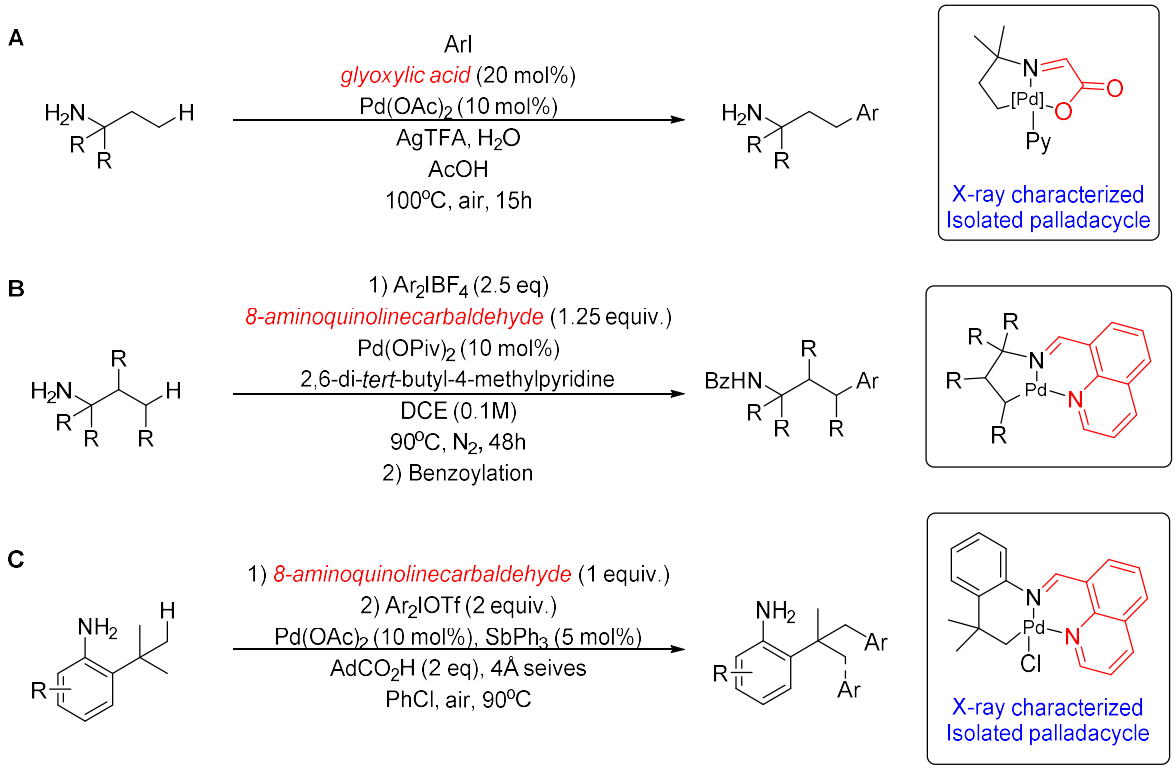

Scheme 13. Regioselective CH activations of amines using aldehyde-based TDGs with proposed or isolated palladacyclic intermediates. **(A/B)** C(sp^3)-H activation of aliphatic amine substrates. **(C)** C(sp^3)-H activation of aniline derivatives.

It's important to note that while the use of TDGs has been an expanding topic in response to the limitations of conventional DG-assisted CH activations, TDG-based protocols, particularly imine-forming TDGs, are not without their own drawbacks. The use of acidic conditions (**Scheme 12B-E**, **Scheme 13A/C**) and high temperatures (**Scheme 12A**) can limit the substrate scope of these protocols. Furthermore, the issues of high temperatures coupled with long reaction times reduce the economic viability of such strategies for large-scale industrial pursuits.

The use of multidisciplinary approaches to solve problems and overcome the limitations of traditional techniques has become very commonplace.[90,91] In particular, the combined use of enzymes and organic/organometallic catalysts has been a promising interdisciplinary field of study.[92–94] Therefore, utilizing a chemoenzymatic strategy to address the shortcomings of DG- and TDG-mediated transformations could serve to increase their incidence in the industrial setting.

1.3. Chemoenzymatic Catalysis

Chemoenzymatic catalysis is loosely defined as the integrated use of biocatalysts and chemical catalysts in one-pot protocols, attempting to improve on traditional strategies or overcome challenges when either mode of catalysis is utilized independently.[92–96] Despite the traditional separation of the two modes of catalysis, chemoenzymatic catalysis was an idea first proposed more than 40 years ago in 1980.[97] However, significant contribution to the field was not made until 1996, with two successive examples of chemoenzymatic dynamic kinetic resolutions (DKR) of secondary alcohols mediated by organometallic racemization and biocatalytic enantiomer enrichment.[98–100] While DKRs are also possible using a pure chemocatalytic approach,[101] a chemoenzymatic approach has the potential to yield improvements in selectivity and economic efficiency.[94] Indeed, the use of water as a solvent

is favourable due to its environmental friendliness, lack of toxicity, and low cost.[95] Moreover, reactions catalyzed by enzymes are very often carried out under mild conditions,[92] furthering efforts to achieve the industrial goals of economically and environmentally friendly transformations.[102] Thus, it is not surprising that the field of chemoenzymatic DKRs has flourished since the seminal reports in the 1990s.[102,103] Extending beyond DKRs, integrated chemoenzymatic approaches can allow several synthetic steps in one pot, which is favourable for process simplification, and more importantly, reducing the cost of product separation by decreasing the number of workups in a synthesis. With this potential, and advancements in modifying the activities and stability of enzymes,[104–106] a surge of efforts to innovate integrated chemoenzymatic catalysis have been published.[92,94]

The broad definition of chemoenzymatic catalysis can be attributed to the several strategies employed to achieve one-pot protocols of intrinsically incompatible catalyst systems.[92–95] The incompatibilities between the general operating conditions of enzymes and chemocatalysts can indeed be numerous. For example, most organometallic catalysts work efficiently at high temperatures and in organic solvents, while most biocatalysts' native activities were evolved in aqueous buffers and physiological temperatures. Only a minority of enzyme classes, such as lipases and serine proteases, are known to act in organic solvents,[95,96] and a limited number of thermozymes discovered in thermophiles and hyperthermophiles can operate at temperatures higher than 100°C (and only for a limited period of time).[107,108] Conversely, many chemical reactions and organometallic catalysts are very sensitive to (even traces of) water and/or air.[93] Moreover, biocatalyst inhibition by organic/organometallic compounds and chemocatalyst inactivation by biological buffers and compounds further complicate the issue of mutual incompatibility.[93,96]

One-pot integrated chemoenzymatic catalytic processes can be separated into two domains: i) one-pot sequential chemoenzymatic protocols and ii) one-pot concurrent chemoenzymatic catalysis.[92–96] One-pot sequential methodologies involve operating the first catalytic cycle to completion under one set of conditions, then modifying these conditions to be more conducive for the second catalytic cycle before the addition of the second catalyst. These processes can be initiated with either chemocatalysts or biocatalysts, though it is important to note that the change to the second set of conditions often inactivates the initial catalytic system. Thus, this approach can almost neglect the problem of mutual inactivation, and in fact embraces it; however, it is still important that the leftover components of the first catalytic system are not deleterious to the activity of the second. Consequently, it should not be surprising that the majority of examples of chemoenzymatic catalysis employ this approach to achieve operating methodologies.[94,95] Concurrent chemoenzymatic catalysis entails the simultaneous operation of both bio- and chemocatalyst in one-pot under the same conditions, necessitating careful consideration of the reaction conditions to ensure synergistic and orthogonal operation of the two different catalytic cycles. It is therefore not surprising that reports of concurrent chemoenzymatic processes are more infrequent than their sequential counterparts.[94] However, it is interesting to note that the first report of chemoenzymatic catalysis employed concurrent conditions, as did the seminal work on chemoenzymatic DKRs.[97–99]

1.3.1. One-Pot Sequential Chemoenzymatic Catalysis

Since achieving sequential chemoenzymatic protocols does not require reaction conditions that are simultaneously amenable to each catalyst used in the one-pot multi-step process, the majority of recent reports have been of sequential protocols.[94,95] Interesting examples include combining cross-couplings, metathesis, and click chemistry with biocatalysts to achieve chemoenzymatic synthesis.[109–111] Following the first report of an integrated chemoenzymatic synthesis of D-mannitol in 1980,[97] an enantioselective sequential chemoenzymatic synthesis of alanine was reported, 26 years later.[112] The chemoenzymatic catalytic sequence was achieved in water with an initial hydrogenation catalyzed by an immobilized rhodium complex, which was filtered off before the addition of an acylase and phosphate buffer **(Scheme 14A)**; it is worthwhile to note that this was also attempted as a concurrent process under modified conditions and with both catalysts immobilized, but with a significant decrease in conversion owing to intrinsic incompatibilities of the catalytic cycles. Following this development in the field, reports of integrated chemoenzymatic synthesis were made more frequently.[94] An interesting example of combining palladium-mediated cross-coupling with biocatalysts involved a sequential Suzuki-Miyaura reaction with an asymmetric ketone reduction mediated by an alcohol dehydrogenase (**Scheme 14B**).[109] The sequential protocol was necessary as the phenyl boronic acid inhibited the biocatalysis, requiring complete conversion from the cross-coupling before the addition of the alcohol dehydrogenase. Cleverly, the stoichiometric use of NADH was avoided by the oxidation of isopropanol by the same enzyme, allowing the co-factor to be recycled. Due to the bioorthogonal nature of copper-catalyzed cycloadditions, it is not surprising that they have found use in integrated chemoenzymatic catalytic cascades. Indeed, a copper-catalyzed azide-alkyne cycloaddition (CuAAC) reaction was used in sequential conjunction with a biocatalytic

ketone reduction mediated by bits of plant tissue from *Daucus carota*, also known as Queen Anne's lace **(Scheme 14C)**.[111] A distinct feature of this chemoenzymatic sequence is the initial use of enzyme catalysis followed by chemocatalysis. Interestingly, this chemoenzymatic cascade was also attempted in a concurrent protocol; however, the CuAAC reaction proceeded at a much faster rate than the biocatalysis, yielding a sterically hindered biphenyl product that was not tolerated by the *D. carota* enzyme(s).

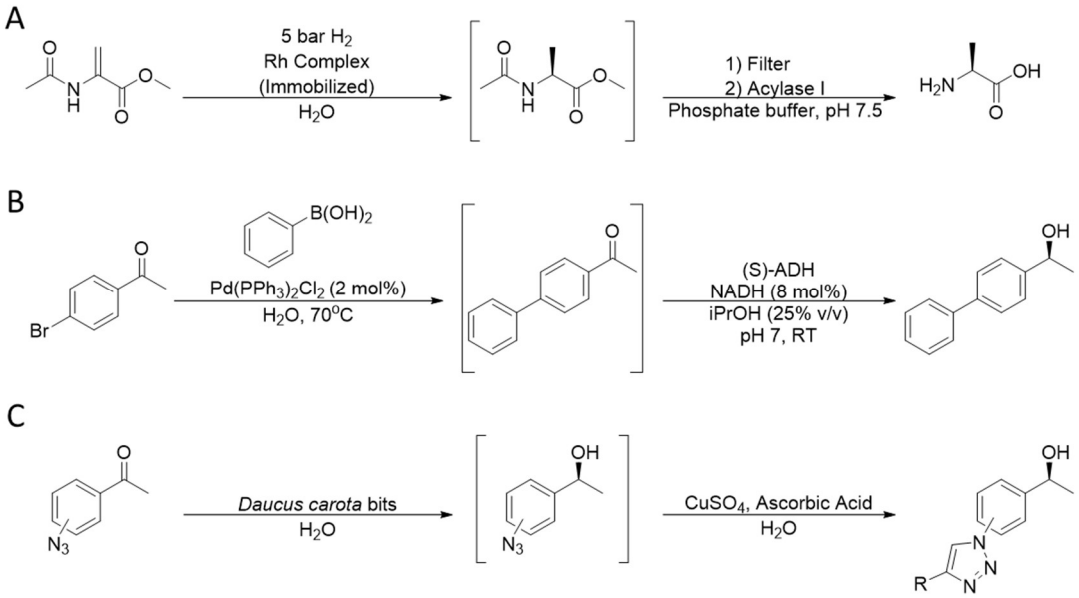

Scheme 14. One-pot sequential chemoenzymatic syntheses using organometallic catalysts and enzymes. **(A)** Enantioselective synthesis of alanine with rhodium-catalyzed hydrogenation and biocatalyzed hydrolysis. **(B)** Sequential Suzuki-Miyaura cross-coupling followed by alcohol dehydrogenase (ADH) catalyzed reduction. **(C)** Sequential biocatalyzed reduction using *D. carota* followed by copper catalyzed azide-alkyne cycloaddition (CuAAC).

While the sequential use of organometallic catalysts and biocatalysts in one pot is an achievement that demonstrates the merging of two traditionally independent forms of catalysis, the extent of integrating the chemo and biocatalysts is limited; only the costs of separation/isolation and, to an extent, intermediary steps are spared.[94] Sequential chemoenzymatic catalysis does not truly integrate two catalytic cycles in one step as adjustments to the reaction conditions must be made. Thus, concurrent chemoenzymatic protocols, though more sparse, are more innovative.[92,94]

1.3.2. One-Pot Concurrent Chemoenzymatic Catalysis

Achieving concurrent chemoenzymatic catalytic cascades are much more challenging endeavours due to innately incongruous catalytic cycles, which is, in part, an explanation for the scarcity of reports of such nature. Indeed, most concurrent chemoenzymatic processes described have been limited to DKRs, and deracemizations.[94] However, concurrent chemoenzymatic catalysis has been achieved by strategies that incorporate organometallic catalysts into supramolecular hosts and assemblies.[92–94,113–115] Interesting examples include the use of organometallic catalysts incorporated into protein scaffolds to make artificial metalloenzymes,[114] encapsulating organometallic catalysts into supramolecular gallium clusters,[113] the concentration of organometallic catalysts in micelles with surfactants,[115] and the use of two-phase solvent systems.[116] These strategies enable concurrent processes by increasing the effective solubility of the organometallic catalyst in aqueous buffers, preventing unwanted interaction between metals and the residues of enzymes, accelerating the rate of organometallic catalysis, and 'separating' the two catalytic cycles in one-pot. A unique strategy to achieve concurrent chemoenzymatic catalysis has been the use of the desired enzyme in whole cell systems; whole cell catalysis has been used with homogenous transition metal catalysis **(Scheme 15A)** and nanoparticles embedded on the cell membrane **(Scheme 15B)**.

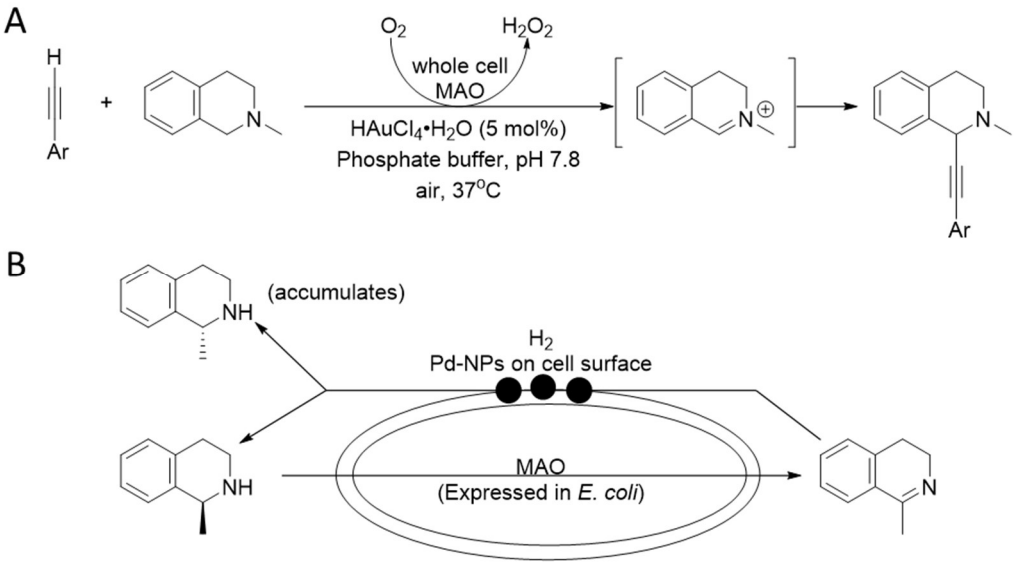

Scheme 15. Concurrent chemoenzymatic catalysis enabled with whole cell systems. **(A)** Concurrent biocatalytic oxidation by a monoamine oxidase (MAO) and gold catalyzed C-C coupling. **(B)** Deracemization enabled by a MAO expressed in *E. coli* coated with palladium nanoparticles (Pd-NPs).

Another promising use of whole cell systems in concurrent chemoenzymatic catalysis is their application in the valorization of bio-based feedstocks. A notable example involves the production of cycloalkenes from biologically relevant fatty acids and oils. Here, artificially engineered enzyme cascades, designed to produce long-chain dicarboxylic acids from fatty acids,[117] were coupled with the activity of a decarboxylase, to produce diolefins from the diacids, and a final ring closing metathesis (RCM) achieved with a Hoveyda-Grubbs catalyst, to yield the desired cycloalkenes. Engineering of the enzyme cascades enabled control over the different cycloalkene product that was obtained from the same fatty acid starting material. Interestingly, these transformations were performed both concurrently and sequentially with general success seen with both methodologies; in cases were the concurrent protocol achieved greater conversions, the authors suggested that the inferior performance of the sequential protocol was in large due to the decreased reaction time of the final organometallic catalyst. Moreover, the use of these chemoenzymatic cascades has been extended to produce these cycloalkenes from readily available olive oil (**Scheme 16**).[116]

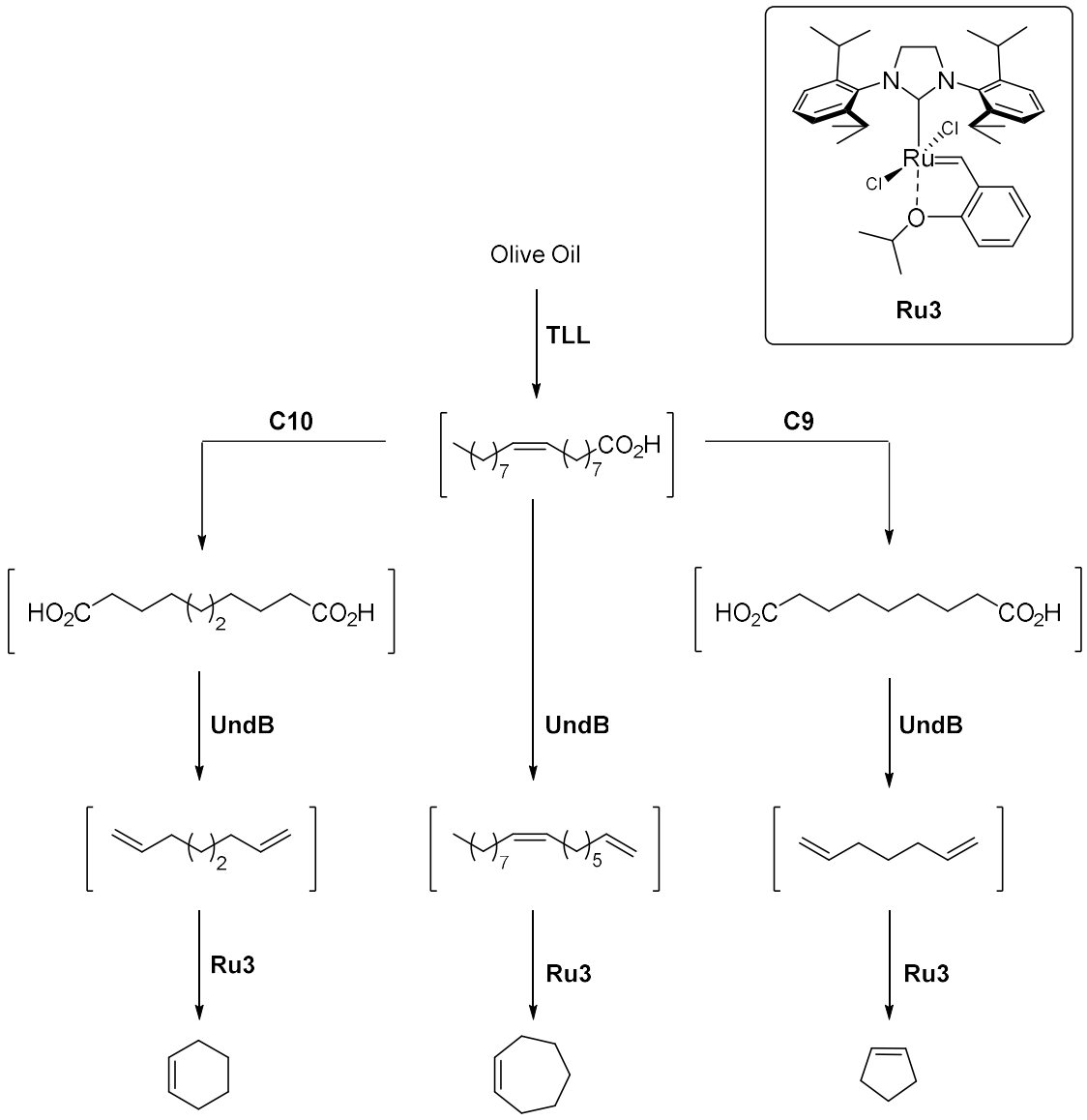

Scheme 16. Chemoenzymatic cascades for the valorization of biological feedstock to produce cycloalkenes. Oleic acid obtained from the hydrolysis of olive oil is converted to into diolefins via enzymatic cascades expressed in whole cell *E. coli* systems. Subsequent RCM of the diolefins yields the final cycloalkene. **TLL** – *Thermomyces lanuginosis* lipase. **C9** – engineered enzyme cascade with OhyA2 (oleate hydratase), MlADH (alcohol dehydrogenase), PpBVMO (Baeyer-Villiger monooxygenase), TLL, with ChnD and ChnE (dehydrogenases). **C10** – engineered enzyme cascade with OhyA2, MlADH, PfBVMO, and TLL. **UndB** – membrane bound decarboxylase. **Ru3** – Hoveyda-Grubbs catalyst.

Incorporating organometallic catalysts and enzymes to form enzyme-metal hybrid catalysts has been a well investigated topic. An interesting application of this technique has been the synthesis of an artificial transfer hydrogenase (ATHase) metalloenzyme by incorporating a biotinylated iridium complex into streptavidin (**Figure 6A**), essentially generating an organometallic catalyst with a protein ligand.[93] Several variants of this ATHase have been used in concurrent chemoenzymatic synthetic cascades, deracemizations of amines, and cofactor regeneration processes.[92,94] The enantioselective synthesis of L-pipecolic acid from L-lysine is a cleverly designed chemoenzymatic cascade that utilizes multiple converging catalytic cycles to generate and deracemize pipecolic acid using an L-amino acid oxidase (LAAO), D-amino acid oxidase (DAAO), and the ATHase metalloenzyme, with catalase employed to break down the hydrogen peroxide generated from the oxidations that would otherwise poison the other catalysts (**Figure 6B**).[95] Deracemizations and cofactor regeneration enabled by organometallic catalysts in concurrent chemoenzymatic cascades have been extensively studied,[94] and the use of organometallic catalysts in the form of artificial metalloenzymes has expanded these toolboxes.

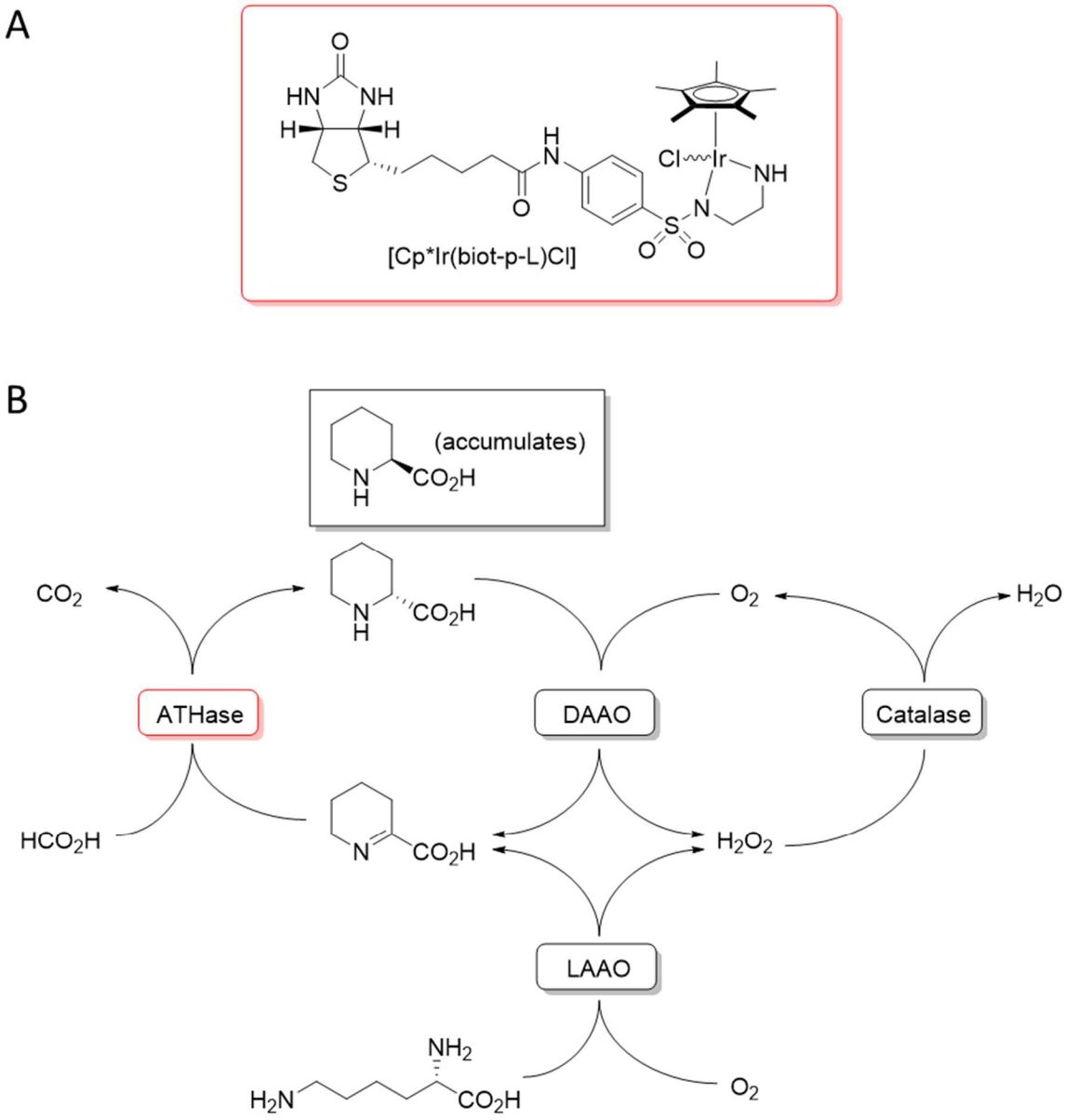

Figure 6. Concurrent chemoenzymatic catalysis enabled by an artificial metalloenzyme/organometallic catalyst with a protein ligand. **(A)** Biotinylated iridium complex that was incorporated into streptavidin to form an artificial transfer hydrogenase (ATHase). **(B)** Generating L-pipecolic acid from L-lysine using a concurrent chemoenzymatic cascade involving an ATHase metalloenzyme, L-amino acid oxidase (LAAO), D-amino acid oxidase (DAAO), and catalase.

1.3.3. Biocatalytic Reductive Aminations

Asymmetric reductive aminations are a powerful synthetic tool for the production of chiral amines, a functionality that maintains a significant presence in active pharmaceutical compounds.[118–120] TM catalysis has been employed to achieve asymmetric reductive aminations;[121–123] however, the challenges that still persist with these protocols have directed research efforts to achieving reductive aminations enzymatically.[120] The reduction of imine bonds has been described as a physiological reaction in biosynthetic pathways by NADPH-dependent imine reductases (IREDs), though the originally reported narrow substrate scope of these enzymes had limited their use in synthetic applications.[124] In 2010, two IREDs from *Streptomyces* were reported to catalyze the reduction of a synthetic heterocyclic imine,[125,126] which was followed by their use in the reduction of an expanded substrate scope and incorporation into biocatalytic cascades;[124] these studies prompted the discovery and characterization of several homologues of these IREDs that showed greater promise in synthetic applications.[127,128] While IREDs are known for their ability to reduce imines, their use in reductive aminations, by reducing imines formed *in situ* through the dehydration reaction between amines and carbonyls, has been of significant synthetic interest.[118,124,129] A recently developed high-throughput screen has been used to assay over 400 IRED orthologs against 50 amine and 50 carbonyl substrates.[130] Moreover, the tunability of IREDs has been demonstrated through successful attempts to engineer the substrate specificity of these enzymes.[105] Finally, IREDs have found use in a sequential chemoenzymatic cascade coupling the reduction of an imine with a Buchwald-Hartwig amination (**Scheme 17**).[115]

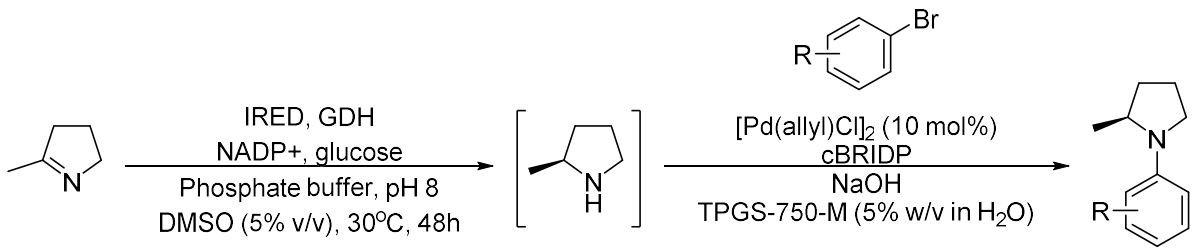

Scheme 17. Sequential chemoenzymatic cascade with an enantioselective IRED catalyzed imine reduction followed by a Buchwald-Hartwig amination achieved in micellar aqueous conditions.

While prokaryotic IREDs have attracted significant attention, the discovery of eukaryotic reductive aminases (RedAms), a subclass of IREDs, has been especially exciting for the synthetic application of biocatalytic reductive aminations.[119,120,129] Indeed, these RedAms have found use in artificial biocatalytic cascades,[131] and the deracemization of racemic amines,[132] though their use in concurrent chemoenzymatic cascades have not yet been reported. The first RedAm was reported and characterized in 2017, isolated from *Aspergillus oryzae* (*Asp*RedAm),[119] with a follow up study describing homologues from *A. terreus* (*At*RedAm) and *A. dermatitidis* (*Ad*RedAm).[120] A notable characteristic of these RedAms is their ability to catalyze both imine formation and reduction, which is made more intriguing by their wide substrate scope; imine reductase activity has also been described with heterocyclic imine starting materials. Importantly, these RedAms have shown potential for engineering with their enantioselectivity and substrate specificity modulated through site-directed mutagenesis.[119,120]

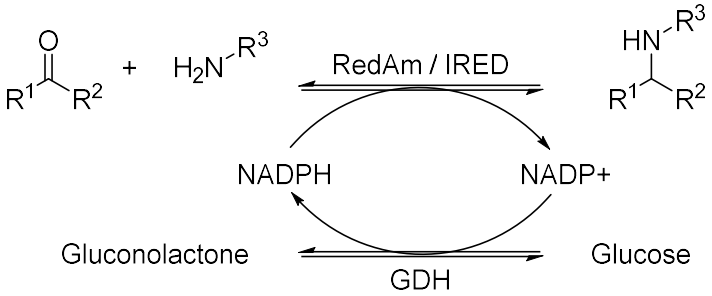

Scheme 18. RedAms/IREDs coupled with GDH in a cooperative coenzyme recycling process. The oxidation of glucose regenerates the NADPH needed for the reductive aminations.

Reductive aminations catalyzed by IREDs/RedAms operating in a single enzyme system would require stoichiometric amounts of NADPH, an expensive coenzyme. However, when they are cleverly coupled with a glucose dehydrogenase (GDH) in a cooperative coenzyme recycling process, the reductive aminations can be driven by the oxidation of excess glucose and sub-stoichiometric amounts of NADP+ (**Schemes 17** and **18**).[115,119] This is an alternative economical strategy that employs the use of cheaper coenzymes and reagents.

1.3.4. Engineering RedAms Through Rational Protein Design.

Rational protein design involves the efforts made to enhance existing activity, generate novel activity, or advance the basic understanding of protein function by making hypothesis-driven changes to the polypeptide sequence of a protein of interest. This approach to protein engineering is better facilitated when there is an advanced understanding of the protein of interest, such as the mechanism of catalysis and the catalytic triad, the key residues involved in substrate binding, and crystallographic information on the tertiary/quaternary structures. Indeed, the rigorous approach that was taken to characterize the recently discovered fungal RedAms has provided the opportunity for engineering via rational design.[119,120] In particular, site-directed mutagenesis guided by crystallographic imaging has enabled the preparation of mutant variants of these fungal RedAms with modulated stereoselectivities and substrate specificities. In the case of *Asp*RedAm, W210 and Q240 were identified as key target residues for modulating stereoselectivity, with the W210A and Q240A variants often favouring opposing enantiomers. More extensive crystallographic data was obtained in the study of *At*RedAm, which prompted the engineering of its substrate binding pockets. In these efforts, L96 and I123 were identified as critical residues that impose steric constraints in the amine binding pocket. Both L96A and I123A mutant variants and a L96A/I123A double mutant

variant were generated and shown to have substrate specificities that contrast with what is displayed by the wild-type enzyme. Specifically, higher specific activity was observed with larger amine substrates which was accompanied by lower specific activities observed with smaller amines. This change in substrate specificity strongly implicates the role of those residues in restricting the size of the amine binding pocket. Similar mutations have not yet been reported for *Asp*RedAm, despite the strong homology between these two enzymes.

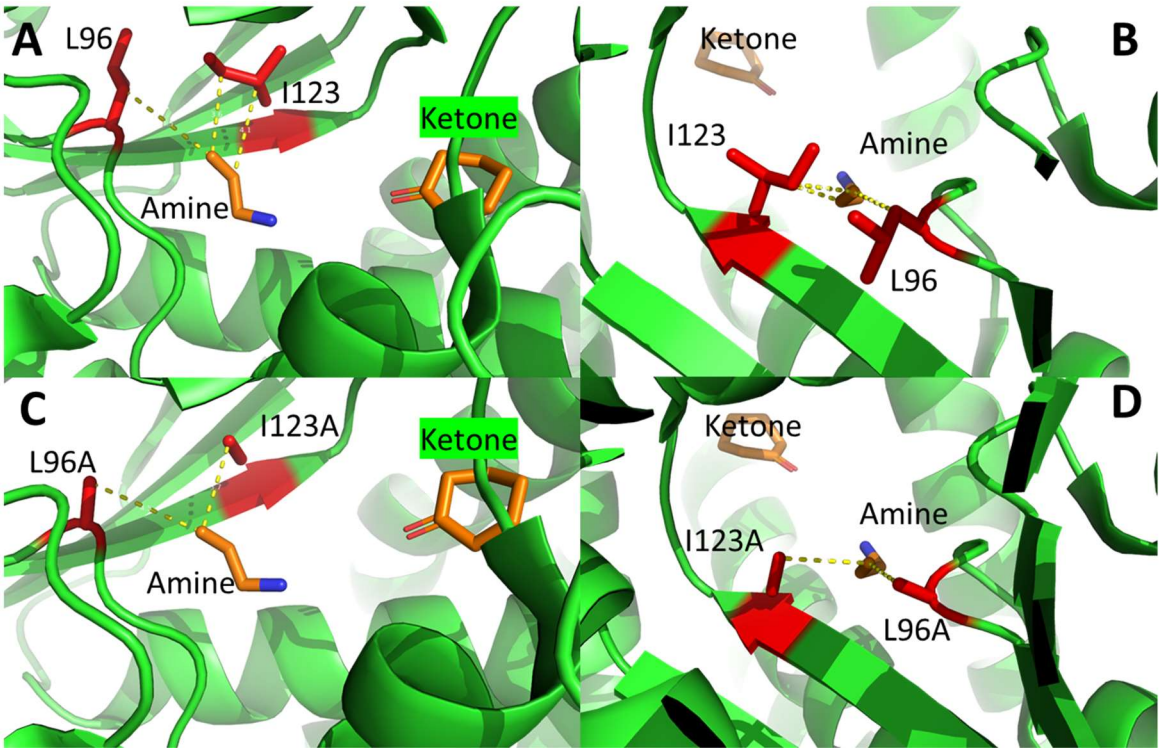

Figure 7. Crystal structure of *At*RedAm in complex with $NADPH_4$ (hidden), cyclohexanone, and allylamine with the L96 and I123 residues in the amine binding pocket highlighted in red (**A/B**).[120] The L96A/I123A double mutant of *At*RedAm in complex with $NADPH_4$ (hidden), cyclohexanone, and allylamine with the mutated residues highlighted in red (**C/D**).The structure of the mutant was modeled using PyMOL software.[133]

1.3.5. Our Contributions to RedAm Catalysis.

Previous efforts have been made by our group to study the substrate scope of *Asp*RedAm beyond what has been previously reported. These efforts have identified both a new carbonyl and a new amine substrate. The *Asp*RedAm-catalyzed reductive amination of cyclohexanone, a previously reported carbonyl substrate, with glycinamide, a novel amine substrate, was confirmed by qualitative GC-FID analysis. An attempt to further expand the amine substrate scope was made with the reductive amination of cyclohexanone with glycine *tert*-butyl ester, however, the product of this reductive amination was not observed. Using the newly identified glycinamide as an amine substrate, a reductive amination was successfully achieved with 4-pentenal, further expanding the carbonyl substrate scope of *Asp*RedAm. The ability of *Asp*RedAm to catalyze reductive aminations with glycinamide but not with glycine *tert*-butyl ester is suggestive of steric encumbrance in the amine binding pocket of the enzyme.

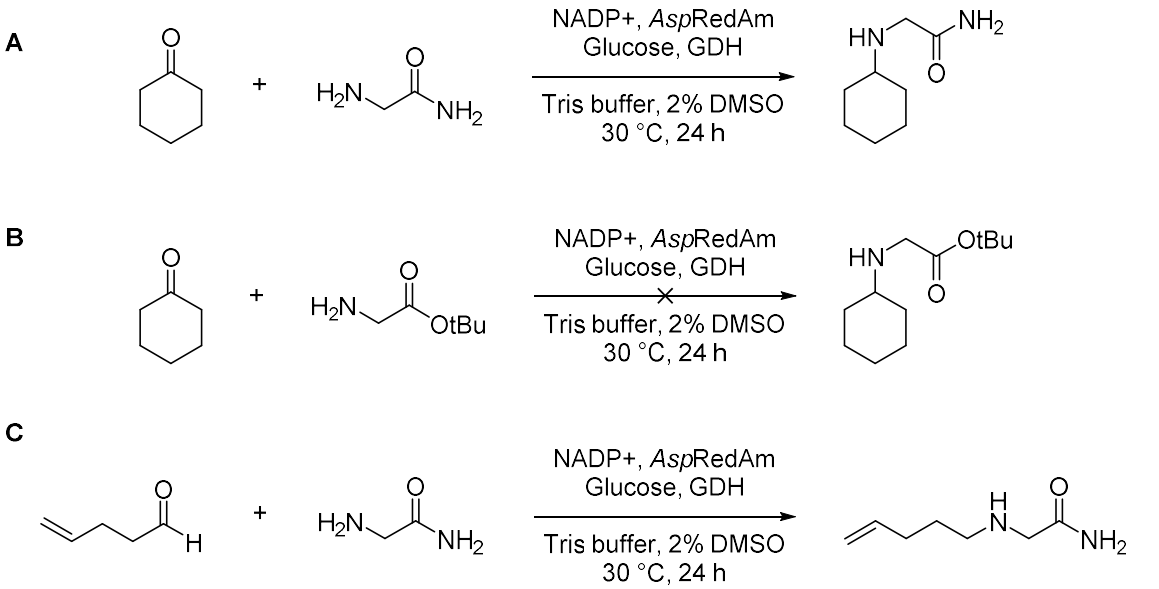

Figure 8. *Asp*RedAm catalyzed reductive aminations previously attempted by our group. (**A**) The reductive amination of cyclohexanone with glycinamide was successfully performed. (**B**) The reductive amination of cyclohexanone with glycine *tert*-butyl ester was not achieved. (**C**) The reductive amination of 4-pentenal with glycinamide was successful.

1.4. Proposed Concurrent Chemoenzymatic Cascade to Enable Transient Directing Groups

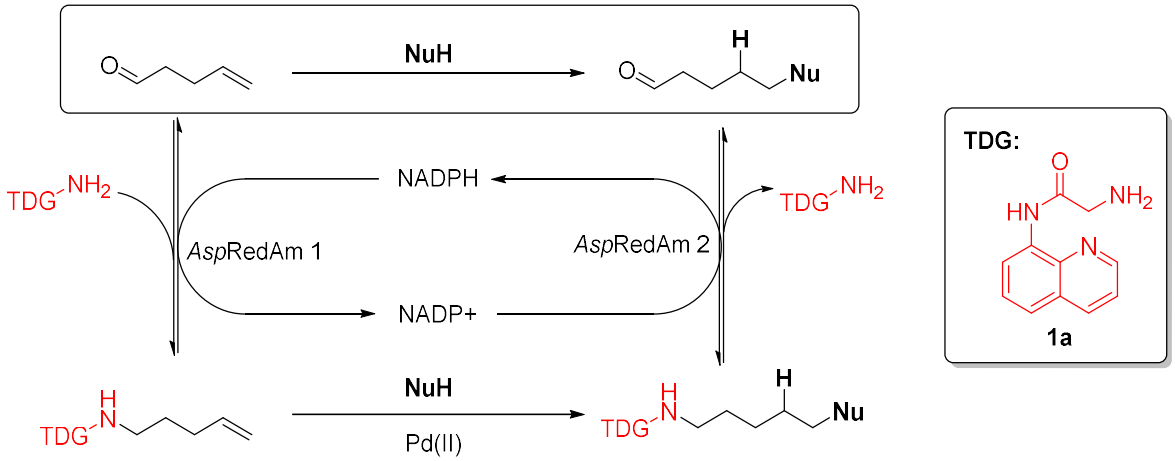

Figure 9. Hydrocarbofunctionalization of an alkenyl aldehyde substrate by concurrent chemoenzymatic reductive amination, hydrofunctionalization, and oxidative deamination**.** Akin to a metabolic pathway, the concurrent catalytic cycles would turnover synergistically, where the product generated from one catalytic transformation is used as a substrate for the subsequent reaction.

The use of DGs on organic molecules is a classic strategy to selectively functionalize specific CH bonds, which would otherwise be challenging due to the prevalence of CH bonds in organic molecules. Recently, advancements in TM catalyzed CH functionalization have fostered the discovery of a variety of DGs that are able to guide the chemistry towards otherwise unreactive CH bonds[76,134,135] or unsaturated moieties.[51,53,55,56] Unfortunately, the classical approach to DG chemistry has some inherent drawbacks that has limited its impact on the industrial setting; recent developments regarding DGs have been mostly neglected by the industry, largely due to an undesirable step-count, unappealing atom economy (both in regard to the directing group and the reagents needed to install and remove it), and complex considerations that render the strategy unapparent in a retrosynthetic analysis in comparison to simple oxidation/reduction, substitution, and C-C cross-coupling reactions.[6] Notable attempts to address these issues have involved the use of TDGs where (sub/super)stoichiometric additives transform a functional group on a reagent into a temporary

DG capable of imparting auxiliary effects on subsequent but concurrent TM-catalyzed CH functionalizations;[78,87] however these reactions often require harsh reaction conditions.

The strategy of employing selectivity in a transient manner is the principal function of enzymes and this native property can be exploited to install and remove a TDG under conditions that are orthogonal to TM-catalyzed chemistry. This tandem and concurrent chemoenzymatic catalysis approach addresses the shortcomings of TDGs that are achieved through strictly chemical methods by employing mild reaction conditions. The discovery of *Asp*RedAm, a NADPH-dependent reductive aminase capable of catalyzing the reductive amination of primary/secondary amines and ammonia with aldehydes/ketones,[119,120] has provided a means to achieve the primary and tertiary catalytic steps in the concurrent chemoenzymatic TDG cascade. The reversible nature of enzymatic reactions enables a cooperative process, allowing the recycling of coenzymes and substrates between the first and last catalytic cycles, facilitating the use of catalytic amounts of NADPH and TDGs. The biochemical transformations can be performed in conjunction with recently reported DG-mediated hydrofunctionalizations of olefins with tridentate DGs that coordinate to palladium through Lewis-basic nitrogen atoms.[53,55,56] Our group has developed a tridentate DG based on these previous reports to act as the TDG/substrate for the reductive amination (**Scheme 10;** compound **1a**).[59] The TDG (**1a**) is not a reported substrate for *Asp*RedAm, thus, engineering a mutant variant for the reductive amination of **1a** and a variant for the oxidative deamination of the functionalized product of the palladium chemistry will be necessary.

1.5. Plan of Study

As previously discussed, achieving concurrent chemoenzymatic cascades requires overcoming challenges associated with the general mutual incompatibility of conditions that are optimal for chemocatalysis versus those necessary for biocatalysis. In terms of conditions

for *Asp*RedAm catalyzed reductive aminations, a relatively broad pH range and multiple aqueous buffers have been established in the literature. However, performing these reactions in the presence of organic co-solvents has not been extensively studied, with DMSO at low concentrations (1-2% v/v) being the only reported co-solvent. Thus, the study of *Asp*RedAm catalyzed reductive aminations in the presence of other organic co-solvents is an essential step to understanding how this enzyme will perform in a concurrent chemoenzymatic cascade. The DG-mediated CH activations that we are pursuing have only been reported in halogenated organic solvents, particularly TFE and HFIP,[59] making these solvents a priority in these preliminary studies. For a more thorough analysis, a panel of polar protic and polar aprotic water-miscible co-solvents will be screened to understand the effects of organic co-solvents on the catalytic activity of the enzyme.

Previous efforts in our group have identified compound **1p** as a viable tridentate DG for the previously reported anti-Markovnikov olefin hydrofunctionalizations.[53,59] These efforts have resulted in CH activations achieved at ambient temperatures, a critical parameter that makes these transformations compatible with biocatalysis. Compound **1p** could be prepared by a RedAm with the primary amine **1a** and 4-pentenal used as substrates (**Figure 9**). Our group has been able to achieve reductive aminations with 4-pentenal using *Asp*RedAm, demonstrating that that carbonyl substrate scope of the enzyme is suitable for our proposed chemoenzymatic cascade. Compound **1a** has not been reported as a substrate for *Asp*RedAm, and the structure is much bulkier than the amine substrates that have previously been reported.[119] Modulating substrate specificity through site-directed mutagenesis has been reported for *At*RedAm,[120] an *Asp*RedAm homologue, allowing more efficient catalysis with larger amine substrates. With this precedent, the analogous residues in *Asp*RedAm have been chosen as targets for site-directed mutagenesis, invoking a rational protein design approach to

achieve biocatalytic reductive amination with our TDG (**1a**). Site-directed mutagenesis will be performed using mutagenic polymerase chain rection (PCR) protocols, and mutants will be tested with novel amine substrates to probe the effects of mutations in the amine binding site.

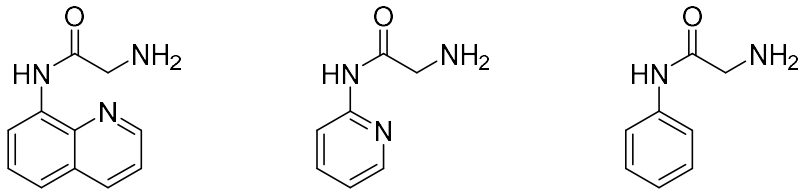

Figure 10. A panel of primary amines used to assess the substrate scope of WT and mutant *Asp*RedAm variants with novel amine substrates. Amine **1a** is the proposed TDG that we would like to load and unload using *Asp*RedAm. Amines **2a** and **3a** are novel amine substrates with less (hetero)aromatic bulk than **1a**.

The structure of **1a** consists of glycine extended by an aminoquinoline ring at the C-terminus through a peptide bond. Successful reductive aminations achieved with WT *Asp*RedAm using glycinamide as an amine substrate suggest that the glycine moiety of **1a** should have favourable interactions in the binding pocket of *Asp*RedAm; however, unsuccessful reductive aminations using glycine *tert*-butyl ester suggest that larger structures like the aminoquinoline ring of **1a** may produce unfavourable steric interactions. Due to the size and heteroaromatic structure of **1a**, amines **2a** and **3a** were chosen as alternative amine substrates to screen the mutants with. Both are smaller than **1a** but **2a** maintains heteroaromatic character; the simple phenyl ring of **3a** should occupy the same space as the pyridyl ring of **2a**, though the intermolecular forces between the rings and the binding pocket residues should differ. Thus, these amine substrates should serve to probe both electronic and steric effects of the mutations in the amine binding pocket.

2. Results & Discussion.

2.1. Expression and Purification of WT AspRedAm and GDH.

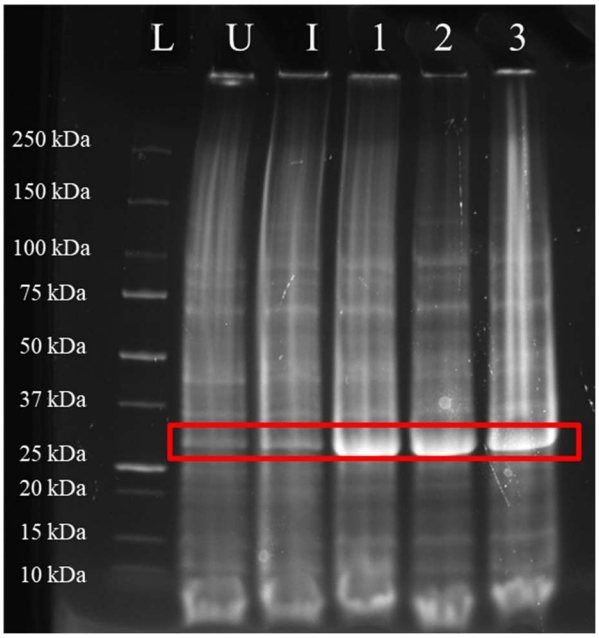

Figure 11. Optimization of WT AspRedAm expression conditions with EtOH supplementation. SDS-PAGE analysis of BL-21 cell lysates harbouring the pET-28a-His-AspRedAm plasmid. Lysates were obtained from cells induced with IPTG and grown in 2xYT media supplemented with **(1)** 1% EtOH, **(2)** 2% EtOH, or **(3)** 3% EtOH (v/v). **(U)** Lysate of cells not induced with IPTG. **(I)** Lysate of cells grown in 2xYT media and induced with IPTG.

A pET-28a(+) expression vector harbouring a codon-optimized recombinant gene sequence for WT *Asp*RedAm (pET-28a-His-*Asp*RedAm) was generously provided by the Turner group from the University of Manchester.[119] For expression, the pET-28a-His-*Asp*RedAm vector was transformed into chemically competent BL-21 cells which were plated and cultured with kanamycin as the antibiotic selection marker; a 2x YT broth was used as the expression media and IPTG was used to induce expression. To increase the yield of expressed enzyme, the expression media was supplemented with 3% EtOH (v/v). It has been shown that cell growth in the presence of dilute organic solvents induces the heat-shock response in *E. coli*, increasing the expression of heat-shock protein chaperones. These chaperones increase the yield of active enzyme by preventing protein misfolding and limiting the formation of inclusion bodies.[136] Indeed, supplementing the expression media with EtOH did result in an

increase of the concentration of WT *Asp*RedAm in the cell lysate compared to the expression performed as previously described, in 2xYT media alone,[119] with 3% EtOH resulting in the largest increase. Interestingly, leaky expression of the recombinant wild-type enzyme was also observed when expression was not induced with IPTG (**Figure 11**).

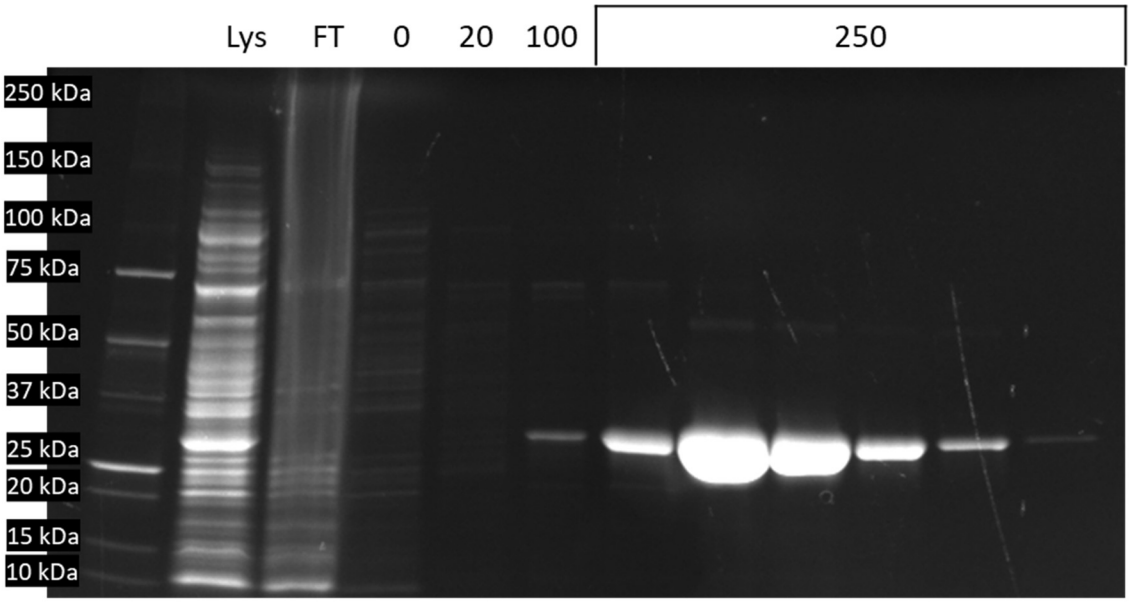

Figure 12. Purification of WT AspRedAm. SDS-PAGE analysis of Ni-IMAC using HisTrap FF column. (**Lys**) cell lysate; (**FT**) flowthrough; (**0-250**) fractions obtained from step gradient of buffered imidazole solutions (100 mM Tris, 300 mM NaCl, 0-250 mM imidazole, pH 8).

The recombinant gene sequence in the pET-28a-His-*Asp*RedAm vector encodes for a recombinant WT *Asp*RedAm with a hexa histidine-tag at the N-terminus of the polypeptide. The histidine-tag enabled efficient purification of the enzyme via affinity chromatography; the recombinant enzyme that was expressed was isolated from the cell lysate using a nickel immobilized-metal affinity chromatography (Ni-IMAC) column and eluted with imidazole. The purification procedure was analyzed by SDS-PAGE (**Figure 12**); fractions containing isolated bands migrating between the 25kDa-37kDa marker corresponded to purified *Asp*RedAm (33.3 kDa) were pooled for use. The yield of WT *Asp*RedAm expressed in 2xYT media containing 3% EtOH (v/v) and purified via Ni-IMAC was ~4 mg/L.

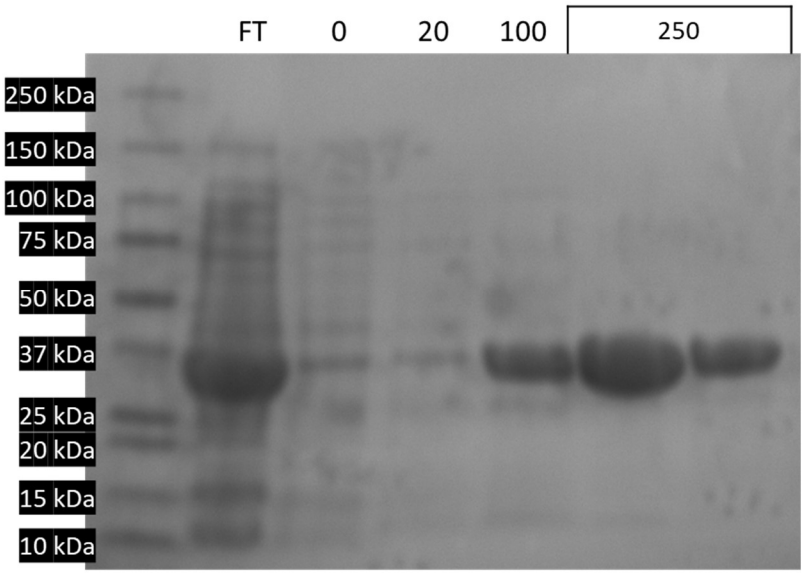

Figure 13. Purification of GDH. SDS-PAGE analysis of Ni-IMAC using HisTrap FF column. (**FT**) Flowthrough; (**0-250**) fractions obtained from step gradient of buffered imidazole solutions (100 mM Tris, 300 mM NaCl, 0-250 mM imidazole, pH 8).

The expression vector containing the gene for a recombinant GDH with a histidine-tag was generously provided by a colleague from the Boddy group. For expression, the vector was transformed into chemically competent BL-21 cells with kanamycin as the selection marker; LB broth was used as the expression media and expression was induced by the addition of IPTG. The recombinant GDH was purified via Ni-IMAC (**Figure 13**) with a yield of ~10 mg/L. While the expression and purification conditions for this enzyme were not optimized, as the yield provided enough GDH for several RedAm assays, the yield of this protocol could be increased should the need arise. The presence of large amounts of GDH in the flowthrough fraction obtained from applying the cell lysates to a Ni-IMAC column suggests that the expression levels of this enzyme are far above the binding capacity of the column that was used. Future efforts at increasing the yield of GDH could be achieved by increasing the size of the column that is used in purification, as it would be able to bind more recombinant protein. An alternative approach would be to re-apply the flowthrough fraction to the Ni-IMAC column after eluting the recombinant protein that was initially bound.

2.2. Assessing the Catalytic Activity of AspRedAm

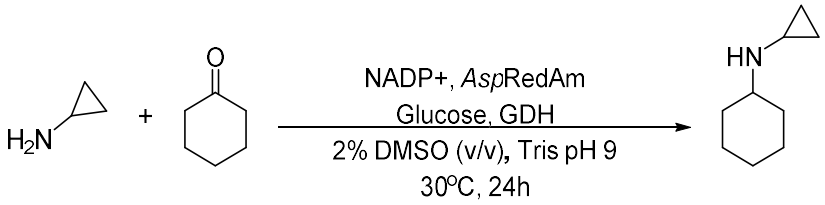

Scheme 19. The reductive amination of cyclohexanone with cyclopropylamine catalyzed by *Asp*RedAm was used as a model biotransformation to assess the catalytic activity of *Asp*RedAm and GDH after expression and storage at -80 °C.

Previously reported conditions for assessing the catalytic activity of *Asp*RedAm involved a buffered aqueous solvent with 2% DMSO (v/v) as a co-solvent. As a consequence of the enzyme's promiscuity, *Asp*RedAm catalyzed reductive aminations have been reported with numerous different amine and carbonyl substrates.[119] These reductive aminations were driven by the oxidation of glucose catalyzed by GDH (**Scheme 18**) which is an established method to used generate NADPH from NADP+ *in situ*.[119,120] To analyze these reductive aminations, the reactions were quenched after 24 h by basifying with NaOH and extracted into methyl *tert*-butyl ether (MTBE); the crude extract was analyzed by gas chromatography coupled to a flame ionization detector (GC-FID). Using this methodology, the reductive amination of cyclopropylamine with cyclohexanone (**Scheme 19**) was previously achieved using a 1:1 molar ratio of amine:ketone with 1 mg/mL of *Asp*RedAm, resulting in 90% conversion observed over a 24 h period. More importantly, more rigorous kinetic studies probing the specific activity of a panel of amine and carbonyl substrates have identified cyclopropylamine and cyclohexanone as ideal substrates for *Asp*RedAm.[119]

Due to these previous findings, the reductive amination of cyclopropylamine with cyclohexanone was chosen as a model reaction to assess the catalytic activity of every batch of *Asp*RedAm and GDH that was expressed and purified. Moreover, this model reaction was also used as a positive control alongside every other set of experimental reductive aminations

to ensure that the enzymes maintained catalytic activity after being stored. However, due to the low yield of *Asp*RedAm after expression and purification, the conditions for this model biotransformation were modified: namely, the amount of RedAm used was lowered from 1 mg/mL to 10 μg/mL, and, to partially counter the reduction in reaction rate as a result of lowering the amount of catalyst, a 2:1 molar ratio of amine:ketone was used. Under these modified conditions, 78% conversion was observed after 24 h which is comparable to the previously reported 90% conversion that was achieved with a 100-fold increase in enzyme loading.

It is worthwhile to note that, due to the nature of assessing conversions observed over an allotted time-period, it is still possible that the reductive amination performed with reduced enzyme loading could achieve 90% conversion if the reaction was quenched after a longer period of time; a slower reaction that is allowed to progress for a longer amount of time can achieve the same yields in the absence of competing side reactions. Therefore, for a more rigorous analysis of this biotransformation, a discontinuous assay could be performed with timed intervals over the course of 24-36 h to assess the progression of the reaction over time. Nonetheless, observing the product of reductive amination under these conditions confirms the catalytic activity of both *Asp*RedAm and GDH (**Figure 14**).

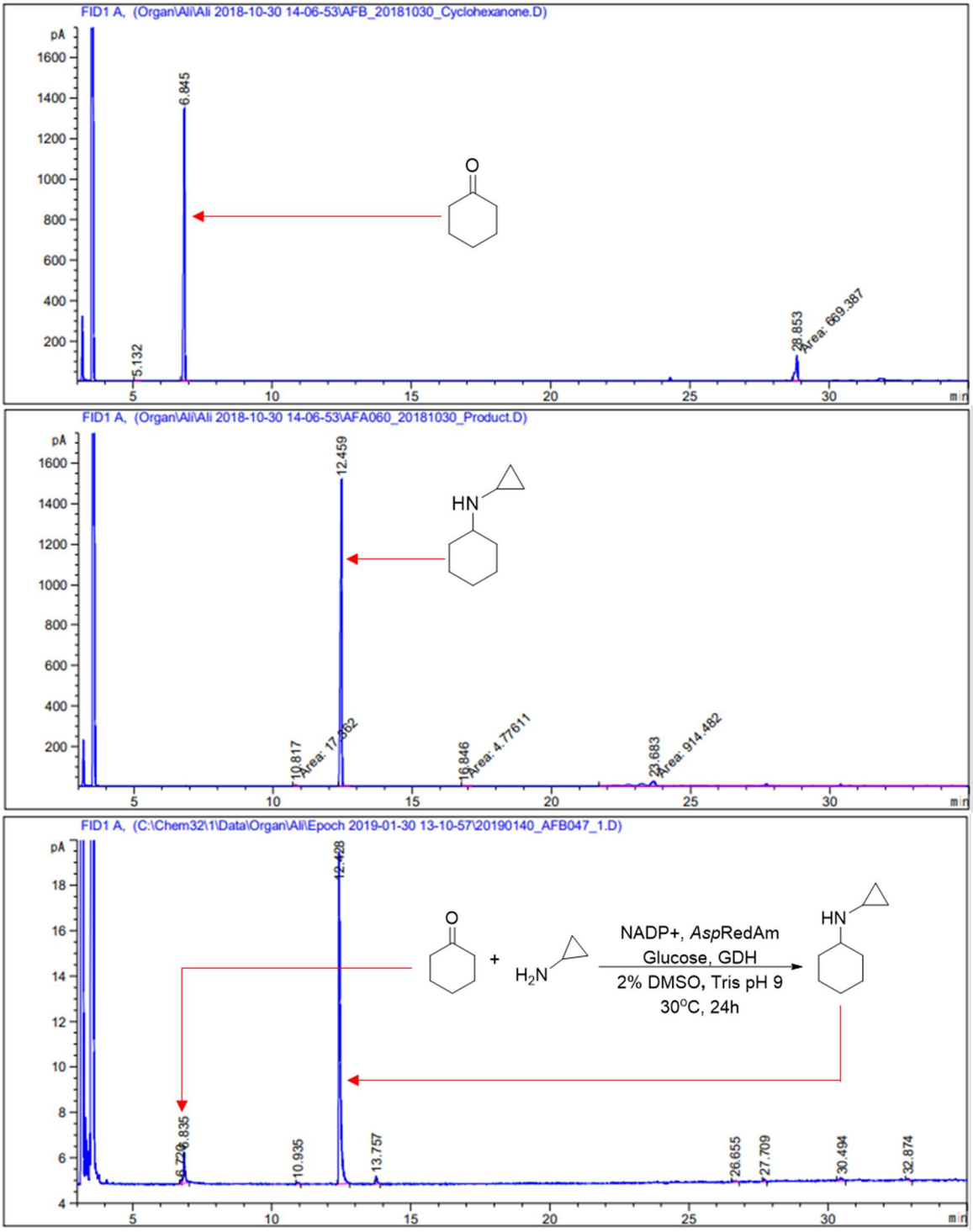

Figure 14. GC-FID analysis of positive control *Asp*RedAm-catalyzed reductive amination of cyclohexanone with cyclopropylamine. (Top) Cyclohexanone standard. (Middle) Reductive amination product standard, *N*-cyclopropylcyclohexylamine. (Bottom) Trace of biotransformation.

2.3. AspRedAm Co-Solvent Screen.

The DG-mediated olefin functionalizations have only been reported to proceed in organic solvents.[53] In particular, our group has optimized protocols for alkene hydrofunctionalizations (directed by **1p**) that occur under ambient temperatures using halogenated alcohols (TFE and HFIP) as solvents.[59] Thus, assessing the activity of *Asp*RedAm in the presence of these halogenated alcohols as co-solvents would provide an understanding of the compatibility between the TM-catalyzed and RedAm-catalyzed transformations. Moreover, compound **1a** (the TDG precursor to **1p**) is not very soluble in aqueous buffers, therefore, a co-solvent screen also serves to determine which/how much co-solvent could be used to increase the solubility of **1a** without hindering the activity of *Asp*RedAm. To this end, the catalytic activity of WT *Asp*RedAm was assayed using a panel of water-miscible organic co-solvents.

Since previously reported *Asp*RedAm catalyzed reductive aminations have been performed with dilute amounts of DMSO, a panel of ACN, THF and DMSO were used to assess the enzyme's compatibility with polar aprotic organic co-solvents. As well, since the conditions for our DG-mediated CH activations have been optimized in fluorinated alcohols, a panel of polar protic co-solvents, including TFE and HFIP along with their corresponding alkyl alcohols EtOH and iPrOH, as well as MeOH, were screened to determine their effect on *Asp*RedAm activity. *Asp*RedAm catalyzed reductive amination in the presence of varying amounts of co-solvent was assessed using previously reported cyclopropylamine and cyclohexanone as substrates[119]. The reactions proceeded for 24 h before a basic workup and extraction; the crude extracts were analyzed by GC-FID to determine conversions.

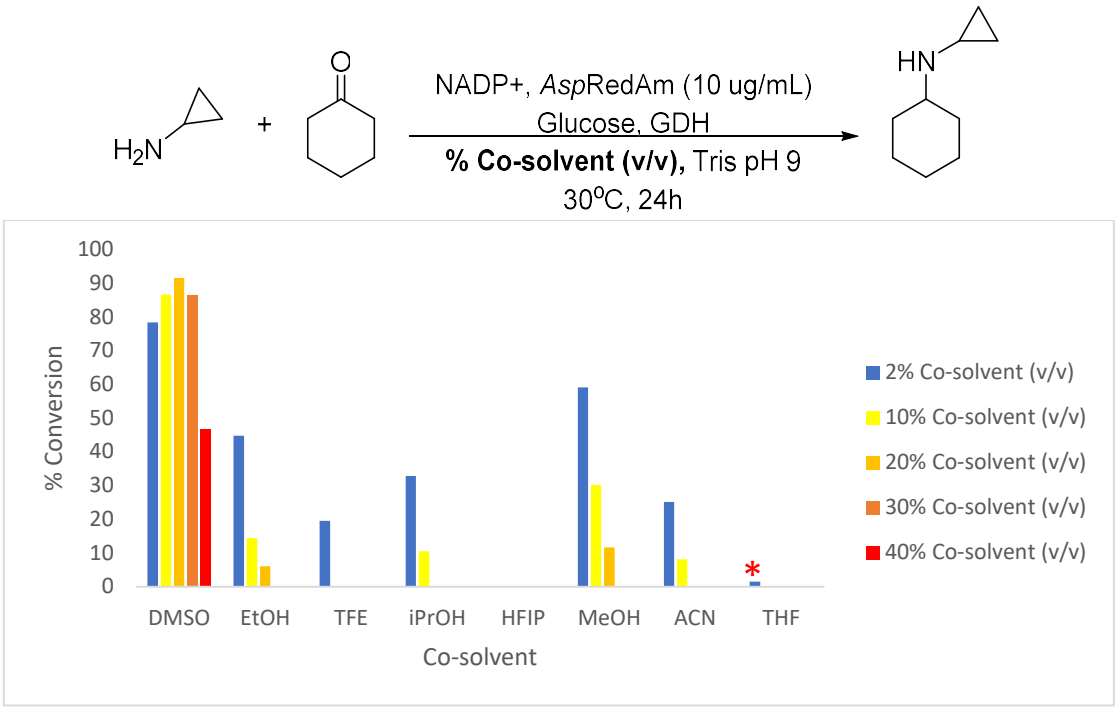

Figure 15. *Asp*RedAm catalyzed reductive amination of cyclohexanone with cyclopropylamine performed with various organic co-solvents. 500 µL reactions with 10 mM cyclohexanone, 20 mM cyclopropylamine, 1 mM NADP+, 30 mM glucose, 0.4 mg/mL GDH, 10 µg/mL *Asp*RedAm, 2-40% co-solvent (v/v) in 200 mM Tris pH 9 were incubated at 30°C for 24 h with shaking (250 rpm). Reactions were quenched with 6 M NaOH, extracted into $CHCl_3$ and % conversion was determined by GC-FID without internal standard. Performed once. (*) Trace conversion. Colours correspond to concentration of co-solvent in Tris buffer (% v/v).

Table 1. Co-solvent screen of *Asp*RedAm-catalyzed reductive amination of cyclohexanone (Ketone) with cyclopropylamine to yield *N*-cyclopropylcyclohexylamine (Product).

Co-Solvent	% v/v	Peak Area (AU)	[Product] (mM)	Peak Area (AU)	[Ketone] (mM)	% Conversion
DMSO	2	107.64	4.3	21.41	1.2	78
	10	84.53	3.4	9.6	0.5	87
	20	124.12	4.9	8.17	0.5	92
	30	121.15	4.8	13.7	0.8	86
	40	62.88	2.6	54.18	3.0	47
ACN	2	18.17	1.0	52.52	2.9	25
	10	0.364	0.3	63.88	3.5	8.1
	20	0	0	65.13	3.6	0
	30	0	0	60.49	3.3	0
	40	0	0	49.03	2.7	0
EtOH	2	57.19	2.4	54.12	3.0	45
	10	11.86	0.7	79.41	4.4	14
	20	0.507	0.3	88.56	4.9	6.1
	30	0	0	64.81	3.6	0
	40	0	0	55.34	3.1	0
TFE	2	11.15	0.7	53.2	2.9	20
	10	0	0	73.92	4.1	0
	20	0	0	86.12	4.8	0
	30	0	0	70.14	3.9	0
	40	0	0	67.59	3.7	0
iPrOH	2	29.64	1.4	51.7	2.9	33
	10	1.51	0.4	54.67	3.0	11
	20	0	0	51.53	2.9	0
	30	0	0	63.49	3.5	0
	40	0	0	60.71	3.4	0
HFIP	2	0	0	64.68	3.6	0
	10	0	0	68.59	3.8	0
	20	0	0	69.15	3.8	0
	30	0	0	73.25	4.1	0
	40	0	0	53.45	3.0	0
MeOH	2	65.4	2.7	34.1	1.9	59
	10	23.78	1.2	49.38	2.7	30
	20	4.22	0.5	62.43	3.5	12
	30	0	0	67.22	3.7	0
	40	0	0	71.53	4.0	0
THF	2	8.72	0.05	55.83	3.1	1.5
	10	0	0	62.08	3.4	0
	20	0	0	58.85	3.3	0
	30	0	0	54.41	3.0	0
	40	0	0	62.01	3.4	0

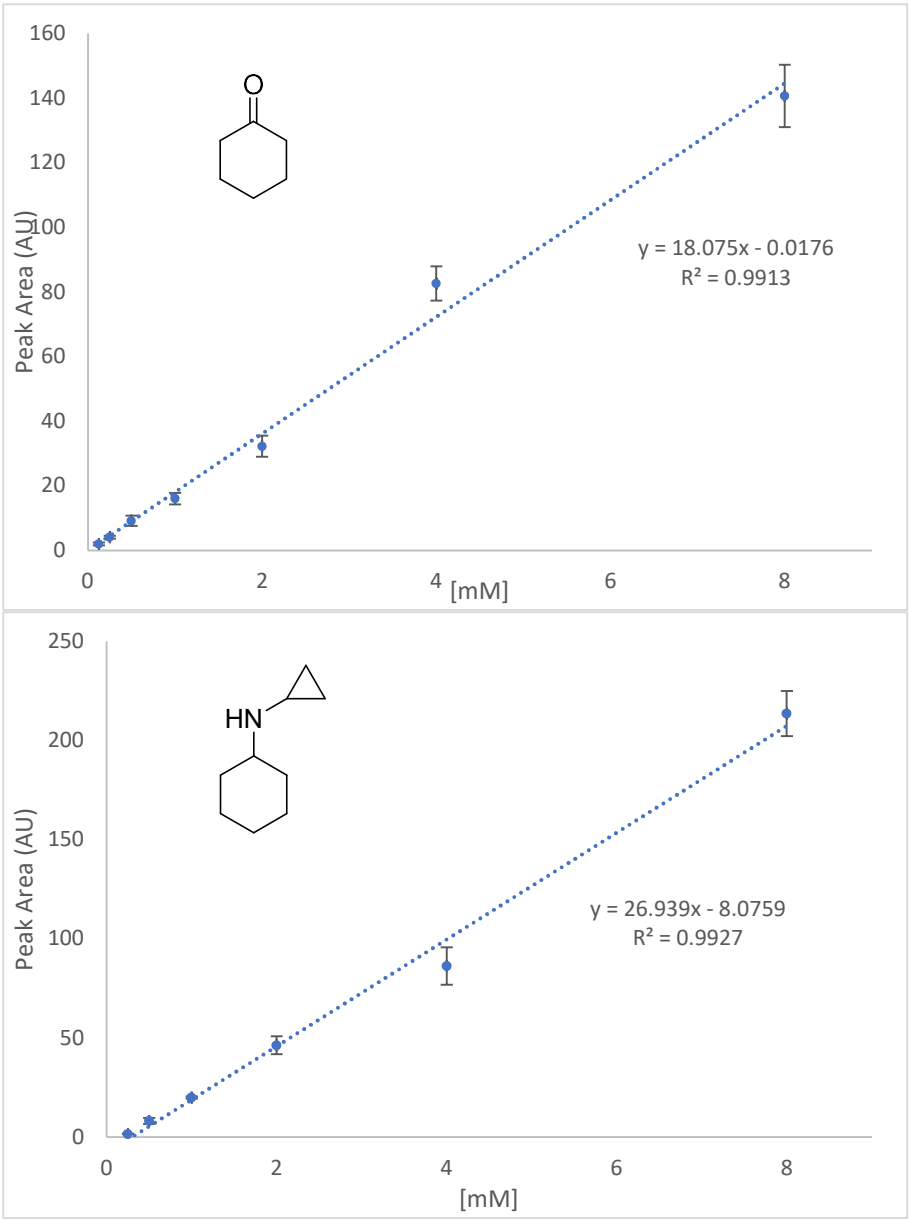

Figure 16. Calibration curves for cyclohexanone (Top) and *N*-cyclopropylcyclohexylamine (Bottom).

Until now, the catalytic activity of *Asp*RedAm has only been reported with a maximum of 2% DMSO used as co-solvent,[119,120,131] therefore, this solvent screen has demonstrated that the activity of *Asp*RedAm is mostly unaffected when up to 30% DMSO is used as co-solvent. While the use of 40% DMSO resulted in reduced conversions, this condition can still be useful when performing *Asp*RedAm-catalyzed reductive aminations of hydrophobic substrates with limited/no solubility in aqueous solutions, though previous work in our group has shown that 60% DMSO prevents activity. A complete lack of conversion is observed at much lower concentrations of the other co-solvents. However, it is important to note that these reductive aminations were carried out in concert a with NADP+/NADPH co-factor recycling achieved by the oxidation of glucose catalyzed by GDH. Therefore, it may be possible that this aspect of the cooperative biotransformation is what is abolished under these conditions and the activity *Asp*RedAm is still viable. Although, the precipitation of *Asp*RedAm was often immediately observed when it was added to solutions with high concentrations of co-solvent (except DMSO), suggesting the incompatibility of these solvents with the catalytic activity of *Asp*RedAm. This was particularly true when HFIP was used as a co-solvent, as the aggregation of *Asp*RedAm was immediately observed when it was added to buffered aqueous solutions with as little as 10% HFIP (v/v).

DMSO, TFE, and HFIP were the main co-solvents of interest in the solvent screen that was performed. It was important to know the upper limit of the concentration of DMSO that could be used for our hydrophobic TDG(**1a**), which was insoluble in the aqueous buffer, even when 40% DMSO was used as a co-solvent. Very limited activity was observed with other polar aprotic co-solvents (THF and ACN), though the contrasting effects of the polar aprotic solvents (DMSO vs. ACN and THF) are not unexpected. DMSO is commonly used as a co-solvent in enzyme assays or as a vehicle for molecular delivery in cell culture/*in vivo*

experiments.[137,138] While DMSO has been shown to inhibit the activity of certain enzymes,[139] it has also been reported that the use of DMSO as a co-solvent can enhance enzyme activity,[140] with the results of the solvent screen suggesting the latter in the case of *Asp*RedAm at moderate concentrations. The increase in conversion that is observed at moderate concentrations of DMSO (10-30% v/v) could be due to a change in the differential binding of the substrates and products; specifically, destabilization of the enzyme-product complex would allow faster release of the product and limit product inhibition as the reaction proceeds to completion.

ACN has been shown to inhibit the activity of other enzymes,[141] and more importantly, the use of ACN to precipitate proteins out of solution has been previously described.[142] Thus, it is understandable that the use of ACN as a co-solvent could decrease enzyme activity, as enzymatic catalysis requires solubilized enzyme in an active conformation *in situ*. The effect of THF on the observed activity is interesting and requires further investigation. While trace amounts of the reductive amination product was observed with dilute amounts of THF (2% v/v), it is unclear whether THF inhibited the activity of *Asp*RedAm or GDH, as it has been reported that THF can completely inhibit dehydrogenase activity.[143] To ascertain whether THF (or other co-solvents used in the screen) are truly affecting the activity of *Asp*RedAm, the solvent screen should be performed with a modified experimental set-up that involves only the solitary activity of *Asp*RedAm, such as reductive aminations with (supra)stoichiometric amounts of NADPH, or oxidative deaminations (the reverse reaction) with NADP+. Furthermore, a fixed-time assay would not report on the stability of the enzyme, thus, assaying the biotransformations at multiple time-points would allow for a more thorough analysis.

In terms of polar protic co-solvents, TFE and HFIP were of interest because the DG-mediated hydrofunctionalization we were interested in performing concurrently had only been achieved in these halogenated solvents.[53,59] The results of the solvent screen suggest that the

biocatalytic and TM-catalyzed transformations are incompatible under these conditions. Indeed, the fluorinated alcohols proved to be poor co-solvents, especially when compared to their aliphatic counterparts (EtOH vs. TFE; iPrOH vs. HFIP). Whereas high concentrations of alcohol co-solvents are known to denature proteins, thereby suppressing enzyme activity,[144] the halogenated alcohols were far more chaotropic than their alkyl counterparts. Such stark differences may be attributed to the fact that TFE and HFIP have lower pKa values compared to EtOH and iPrOH, suggesting that an alkoxide species formed in the basic buffer plays a role in the denaturation of the enzymes. This would be especially true of the acidic HFIP, with a pKa of 9.3,[145,146] that completely eliminated activity at a mere 2% concentration, an extreme result that was not observed in any of the other solvents that were screened.

Despite the observed incompatibility of the biocatalytic reductive amination under conditions that would be conducive to our intended Pd-catalyzed olefin functionalizations, several procedures combining chemo-catalysts and biocatalysts have been reported.[112–115,147–149] Indeed, a recent report of Buchwald-Hartwig cross-coupling performed with biocatalytic aminations lends inspiration to overcoming the encountered incompatibility.[115] Here, a sequential chemoenzymatic cascade was enabled by the use of a designer surfactant that has been shown to allow cross-coupling reactions and metathesis' to proceed in water at room temperature.[150–152] This micellar catalysis strategy could be tailored to the conditions necessary for the DG-mediated Pd-catalyzed olefin functionalizations that we are currently pursuing. Moreover, the use of enzymes in neat organic solvents has been shown to be a productive strategy for repurposing enzymes to perform non-native biocatalysis that would not be compatible with aqueous conditions.[153] Here, the use of lyophilized *Asp*RedAm in neat HFIP or TFE could provide the means to achieve bio-catalyzed reductive aminations in concert with Pd-mediated group-directed CH activations; the lyophilization of the enzyme

could preserve the active fold in a solvation-shell that maintains the catalytic activity of the enzyme in organic solvents. Other strategies to overcome the innate incompatibility of biocatalytic and organometallic-catalytic transformations have involved the separation of the process via semipermeable membranes[112,149] or immiscible phases,[147,148] as well as the incorporation of the organometallic species into supramolecular hosts,[113,114] or immobilization of the enzyme and/or the organometallic catalyst.[112]

2.4. Mutant AspRedAm Variants via Rational Protein Design.

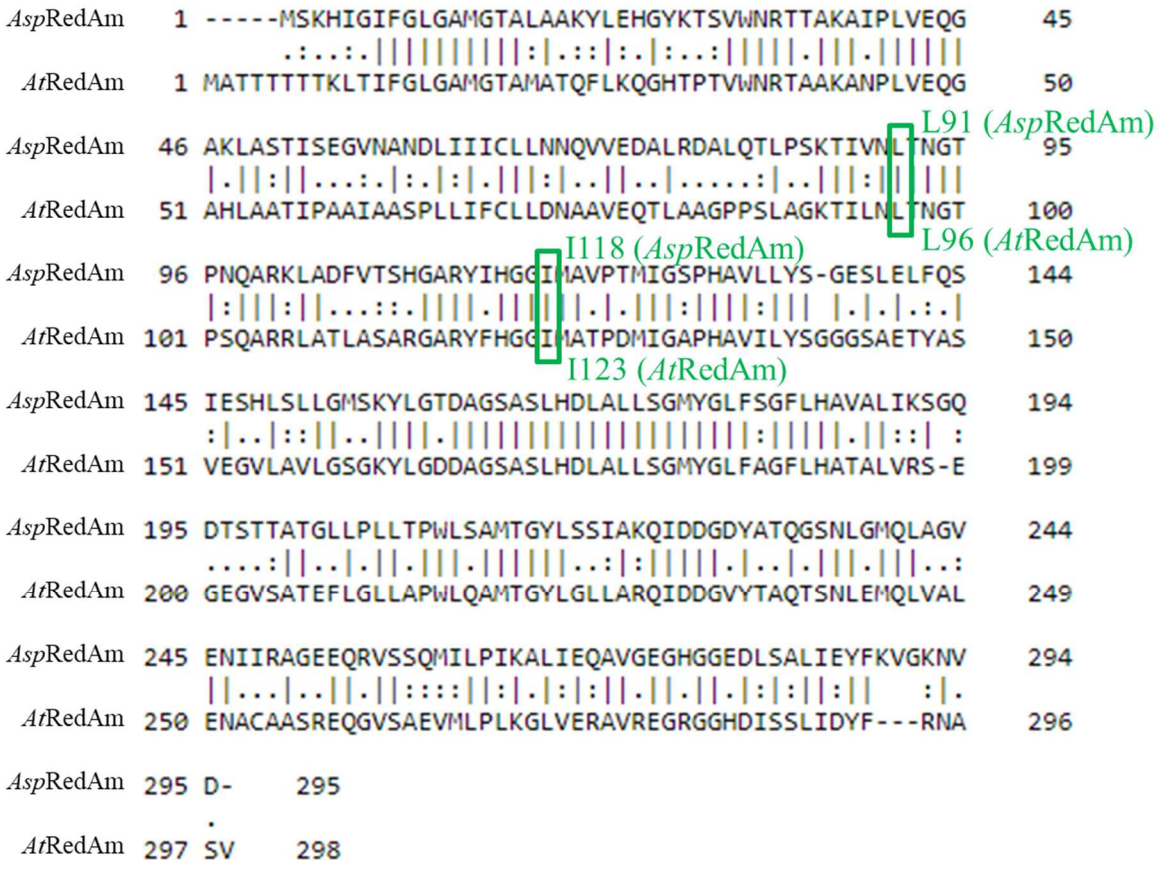

Figure 17. Sequence alignment for RedAms from *Aspergillus oryzae* (*Asp*RedAm) and *Aspergillus terreus* (*At*RedAm). Previously mutated residues on *At*RedAm and analogous residues on *Asp*RedAm targeted for site-directed mutagenesis are highlighted. Pairwise sequence alignment performed using EMBOSS Needle.[154]

The primary and secondary amines that have been reported as substrates for *Asp*RedAm are much smaller structures than compound **1a**, the TDG we have designed for our chemoenzymatic cascade. Thus, to modulate the substrate specificity of *Asp*RedAm, a rational design approach was chosen. The homology between the two fungal RedAms, *Asp*RedAm and *At*RedAm, provided inspiration for our efforts to engineer the amine binding pocket of *Asp*RedAm guided by the previously reported efforts to engineer *At*RedAm. In previous studies, the substrate specificity of *At*RedAm was modulated to achieve reductive aminations with larger amine substrates; the I123A and L96A/I123A mutant variants displayed increased activity with larger amines compared to WT *At*RedAm. Using sequence alignment software, L91 and I118 were identified as analogous residues in *Asp*RedAm and were chosen as key targets for mutagenesis (**Figure 17**). Like previous efforts with *At*RedAm, the L91A and I118A mutant variants of *Asp*RedAm should display different amine substrate specificities compared to the WT enzyme.

For sequencing, the pET-28a-His-*Asp*RedAm vector was transformed into chemically competent DH5α cells and purified using the E.Z.N.A Plasmid DNA Kit (Omega BioTek) before sequencing analysis (Génome Québec). To generate the mutant genes, site-directed mutagenesis was achieved using mutagenic PCR protocols: the I118A mutation was generated using a protocol inspired by the commercially available Q5® Site-Directed Mutagenesis Kit (NEB)[155] and the L91A mutation was generated using the RecA-independent recombination (RAIR) pathway.[156] These methods differ in primer design but both amplify the entire plasmid while introducing the desired mutation, eliminating the need to clone a newly synthesized mutant gene into another expression vector.

The I118A mutation was introduced using back-to-back non-overlapping primers with the mutation on the 5' terminus of the forward primer. Following PCR, a linear product was

obtained that was phosphorylated and ligated by T4 PNK and T4 Ligase, respectively, with the template DNA degraded by DpnI. Serendipitously, this mutation introduced a new NcoI recognition site in the expression vector, enabling the restriction enzyme to cleave the mutated plasmid at two different positions compared to the single NcoI recognition site present on the WT plasmid (**Figure 18**, **A/B**). Once the mutation was confirmed by sequencing analysis, the I118A mutant was expressed on a small scale (50 mL culture) and purified in parallel with the WT enzyme to confirm the fidelity of the mutant polypeptide sequence (**Figure 19**).

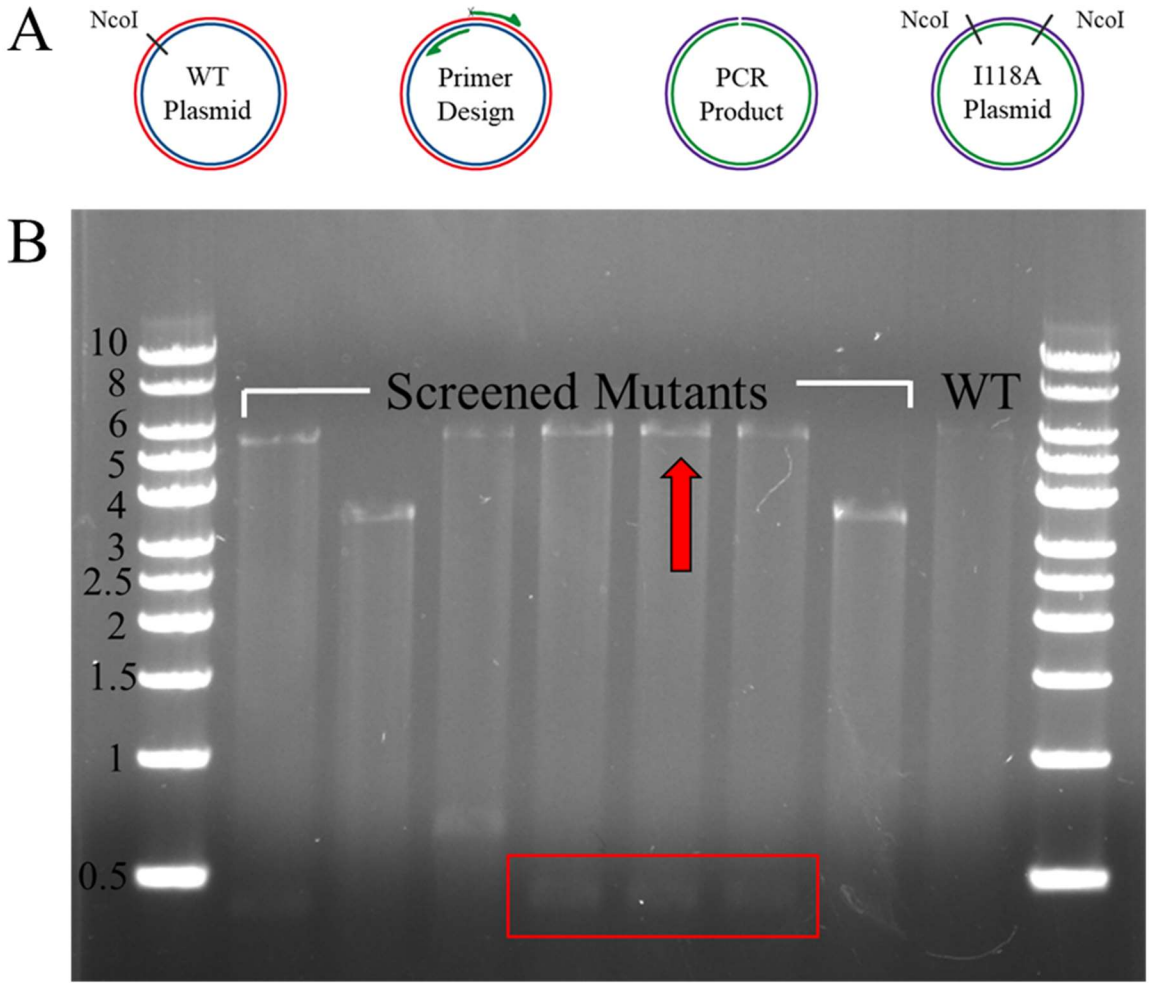

Figure 18. I118A mutation introduced into *Asp*RedAm via mutagenic PCR. (**A**) Primer design utilized to introduce the I118A mutation which generates a linear PCR product that was phosphorylated and ligated prior to the transformation of chemically competent cells. The isolated plasmid harboring the gene for the I118A mutant variant contains two NcoI recognition sites compared to the plasmid harboring the gene for the WT enzyme. (**B**) NcoI restriction digest of isolated plasmids enabled screening for the mutation with the WT plasmid (WT) digested for reference. Isolated plasmids that showed evidence of a double digest (red box) were sent for sequencing to identify a plasmid with the desired mutation (red arrow).

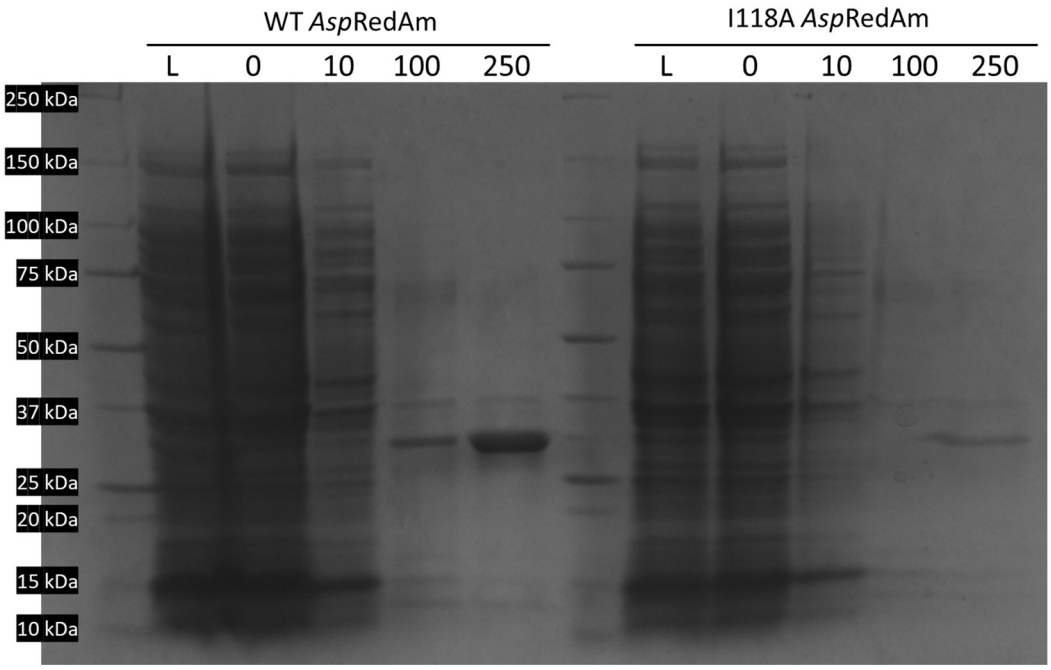

Figure 19. Small scale expression and purification of RedAms. WT *Asp*RedAm (left) and I118A mutant (right) were expressed on a 50 mL scale and purified using Ni-NTA resin in Eppendorf tubes. (**L**) Cell lysates; (**0-250**) Supernatant obtained from washing Ni-NTA resin with buffered imidazole solutions (100 mM Tris, 300 mM NaCl, 0-250 mM imidazole, pH 8).

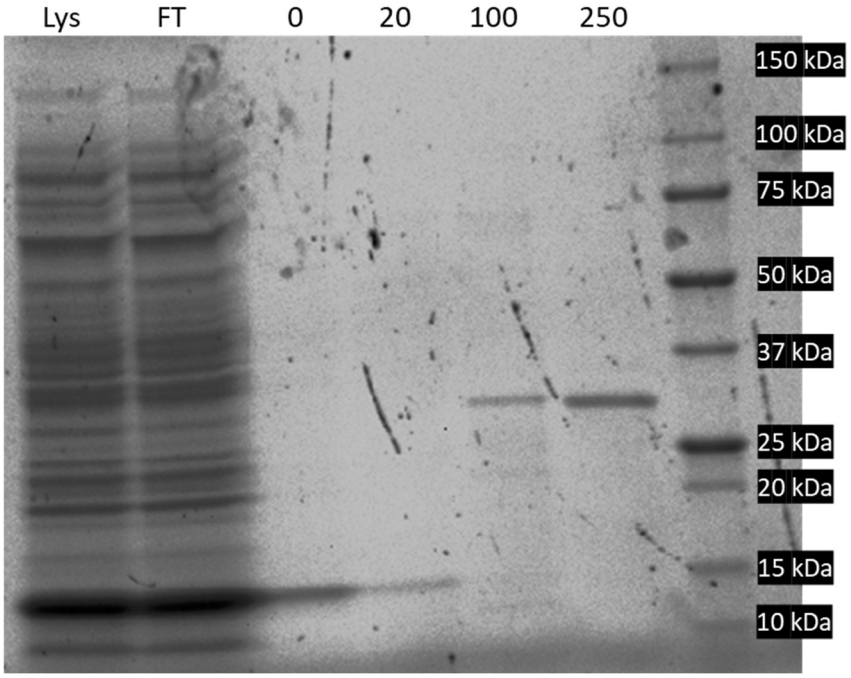

Figure 20. Purification of the I118A mutant variant of *Asp*RedAm. SDS-PAGE analysis of Ni-IMAC using HisTrap FF column. (**Lys**) cell lysate; (**FT**) flowthrough; (**0-250**) fractions obtained from step gradient of buffered imidazole solutions (100 mM Tris, 300 mM NaCl, 0-250 mM imidazole, pH 8).

Once the I118A mutation was confirmed by sequencing analysis and the fidelity of the mutant polypeptide sequence (namely the size and presence of a His-tag) was confirmed by a small-scale expression and purification experiment, the I118A mutant was expressed and purified at normal scale using the same conditions and methods that were used for WT *Asp*RedAm (**Figure 20**). The yield of the I118A mutant expressed in 2xYT media containing 3% EtOH (v/v) and purified via Ni-IMAC was <1 mg/L. This low yield of enzyme prompted the optimization of assay conditions to reduce the amount of RedAm used in each biotransformation from the previously reported loading of 1 mg/mL to 10 μg/mL.

The L91A mutation was introduced via an *in vivo* molecular cloning protocol that utilizes the RAIR pathway to generate circular plasmid DNA from a strand of linear double stranded DNA (dsDNA) with homologous ends. Mutagenic PCR was performed with a pair of overlapping primers with the mutation present in the non-overlapping region of the forward primer. Following PCR and digestion of the template DNA with DpnI, the linear strand of dsDNA that was obtained was used to transform chemically competent DH5α cells; the homologous ends generated from the use of an overlapping primer pair facilitated the *in vivo* recombination of the linear strand into a circularized expression vector (**Figure 21**, **A**). No novel restriction cut sites were introduced into the mutant expression vector for the L91A variant, thus, a restriction digest with NcoI only served to verify the correct size of the plasmid vectors that were sent for sequencing analysis (**Figure 21**, **B**). Once the mutation was confirmed by sequencing analysis, the L91A mutant was expressed and purified using the same conditions and methods that were previously used for the WT and I118A variants of *Asp*RedAm.

Unfortunately, the expression and purification of the L91A was unsuccessful at isolating catalytically active L91A in solution. Further investigation into the expression

conditions revealed that while the L91A variant was indeed expressed by the bacterial cells, the mutant aggregated into inclusion bodies (**Figure 22**).[136,157] Future efforts made towards expressing the L91A variant should aim to address the insolubility that was encountered with this mutant. One possible strategy could involve attempts at recovering and isolating the enzyme from insoluble inclusion body aggregates.[158] This approach would involve the solubilization of the inclusion bodies formed during protein expression, followed by chromatographic isolation and refolding of the expressed protein to yield a bioactive enzyme.

Alternatively, the expression conditions can be modified to address the formation of inclusion bodies directly. Indeed, multiple strategies have been reported to increase the yield of recombinant proteins expressed in prokaryotic systems by reducing the formation of insoluble inclusion body aggregates during expression;[159,160] unfortunately, EtOH supplementation was unsuccessful. Still, there are multiple parameters that could be modified to optimize protein expression with key factors including the concentration of IPTG used to induce expression, the post-induction time, and the temperature at which expression is conducted. Reducing the temperature used to express recombinant protein can help prevent inclusion body formation by reducing the rate of protein expression; the expression of the recombinant protein at a reduced rate would provide more time for the polypeptide to sample different conformations until the catalytically active fold is found. Similarly, inducing expression with lower concentrations of IPTG would help reduce the rate of protein expression through the incomplete inhibition of the *lac* repressor. Finally, reducing the post-induction time could increase the yield of expressed protein by limiting the amount of time that inclusion bodies are given to form.

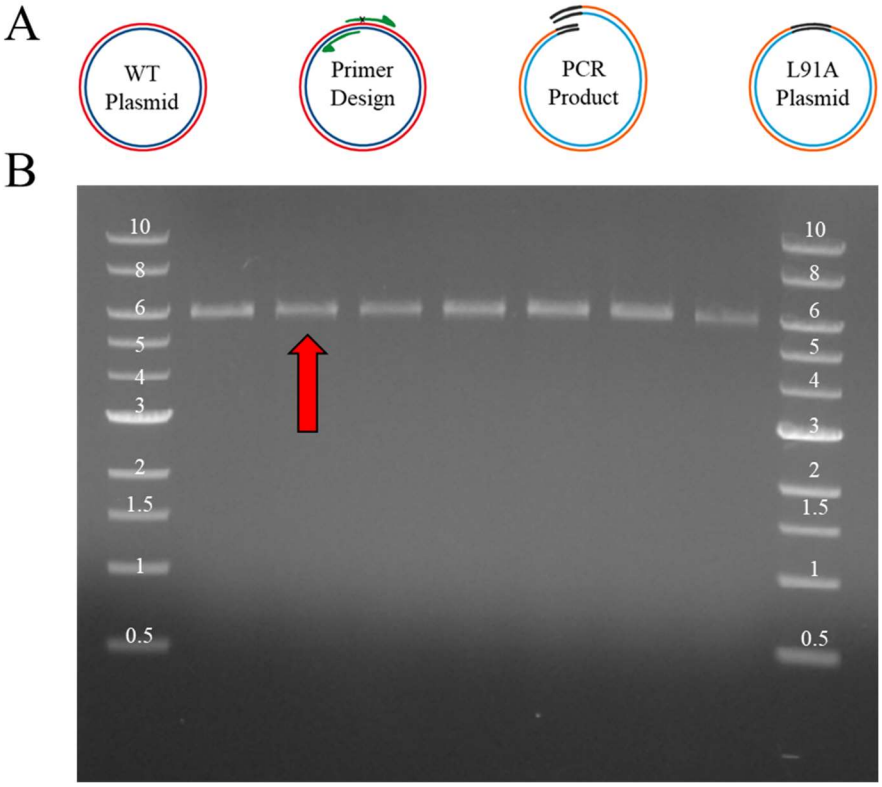

Figure 21. L91A mutation generated via mutagenic PCR and RAIR pathway. (**A**) The primer design used to enable *in vivo* recombination: overlapping primer pairs generate a linear PCR product with homologous ends that is recombined to form a circular plasmid. (**B**) NcoI restriction digest of plasmids isolated from DH5α cells transformed with linear PCR product. Sequencing analysis confirmed the L91A mutation (red arrow).

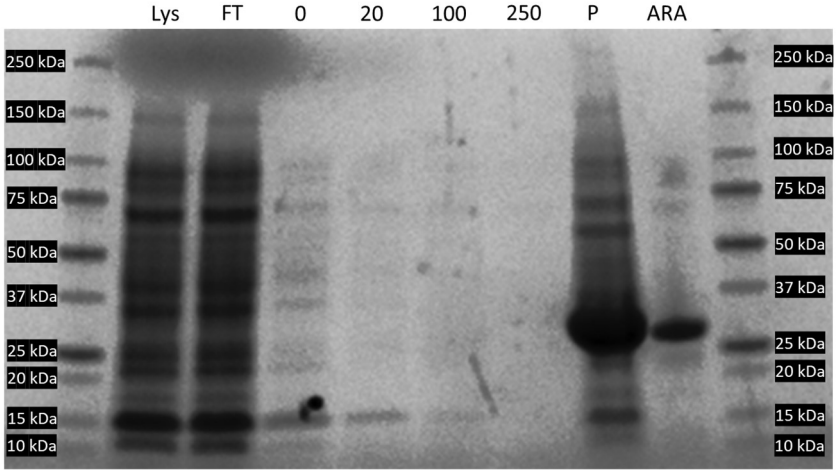

Figure 22. Purification of the L91A mutant variant of *Asp*RedAm. SDS-PAGE analysis of Ni-IMAC using HisTrap FF column. (**Lys**) cell lysate; (**FT**) flowthrough; (**0-250**) fractions obtained from step gradient of buffered imidazole solutions (100 mM Tris, 300 mM NaCl, 0-250 mM imidazole, pH 8); (**P**) cell pellet solubilized in a 8 M urea solution; (**ARA**) purified wild-type *Asp*RedAm ran as reference.

2.5. Reductive Aminations with Mutant AspRedAm Variants.

In some cases, efforts to modulate substrate specificity through mutations in the active site of an enzyme can be deleterious to overall activity, resulting in the expression of an inactive mutant variant. Thus, the reductive amination of cyclohexanone with cyclopropylamine was used as a preliminary assay to ensure the catalytic activity of the novel mutant variants (**Figure 23**). Both WT AspRedAm and the I118A variant showed reductive aminase activity with these previously reported substrates (**Figure 23**). The WT enzyme achieved 90% conversion in 10% DMSO, which decreased to 47-70% with 40% DMSO (**Figure 15** and **23**). The I118A variant achieved lower conversions overall, with 35% conversion observed in 10% DMSO which reduced to 15% conversion observed with 40% DMSO (**Figure 23**). The catalytic activity of the L91A mutant was not tested as its expression did not yield soluble enzyme.

The reductive amination of cyclohexanone with cyclopropylamine catalyzed by the two RedAm variants provides evidence for their catalytic activity. The lower conversions achieved by the I118A mutant may indicate that either this mutation is deleterious to overall activity and/or enzyme stability, or that the mutation has modulated substrate specificity. However, it is important to note that despite any changes in substrate specificity, it should be possible for the I118A mutant to achieve similar conversions as the wild-type enzyme, if the reaction was given more time to proceed; as previously discussed, slower reaction rates can achieve the same conversions as faster rates, if given more time. To determine the overall effect of the mutation on substrate specificity, a panel of previously reported amine substrates should be used in a more rigorous kinetic investigation. Previous studies with the *At*RedAm mutants followed the consumption of NADPH to measure and compare the specific activity observed when the variants were used for the reductive amination of cyclohexanone with a

panel of amine substrates.[120] To conduct a similar analysis for the *Asp*RedAm variants, the reductive amination of cyclohexanone with a panel of previously reported amine substrates could be conducted under specific conditions, with the consumption of NADPH monitored over time.

Alternatively, a more in-depth study would involve using the Michaelis-Menten model of enzyme kinetics[161] to characterize the catalytic activity of the WT and mutant *Asp*RedAm variants. Here, the concentration of the ketone and NADPH should be held at saturation while the concentration of the amine is varied to measure the change in the initial rate of the biotransformation. Monitoring the consumption of NADPH should still be the most facile approach to following the reaction, though aliquots of the reaction could be quenched and analyzed via GC-FID to determine conversion over time. Nevertheless, plotting the rate of the reaction as a function of amine substrate concentration (or a linearization of the hyperbolic curve)[162] could be used to determine the Michaelis constant (K_M – the substrate concentration at which the initial reaction rate is half of what could be maximally achieved under those conditions), the turnover number (k_{cat}), and the specificity constant (k_{cat}/K_M), with the latter being a good measure to assess the differences in substrate specificity displayed by the WT and mutant variants of *Asp*RedAm.

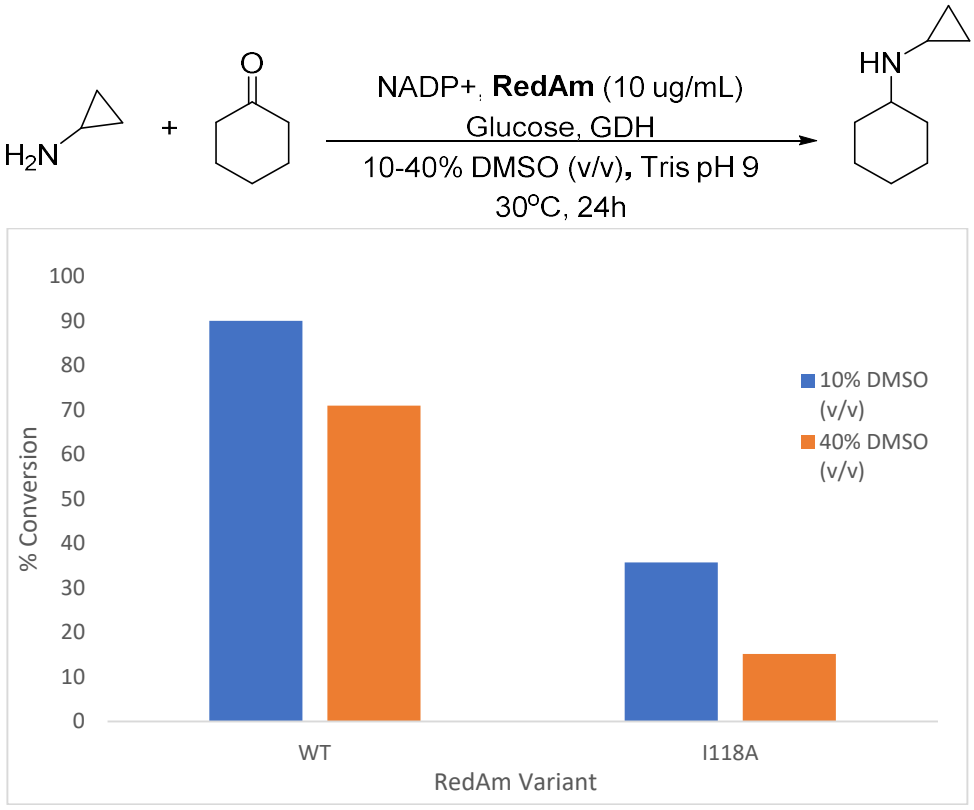

Figure 23. Reductive aminations of cyclohexanone with cyclopropylamine catalyzed by RedAm variants. 500 µL reactions with 10 mM cyclohexanone, 20 mM cyclopropylamine, 1 mM NADP+, 30 mM glucose, 0.4 mg/mL GDH, 10 µg/mL of WT or I118A RedAm variant, 10 or 40% DMSO (v/v) in 200 mM Tris pH 9 were incubated at 30°C for 24 h with shaking (250 rpm). Reactions were quenched with 6 M NaOH, extracted into $CHCl_3$ and % conversion was determined by GC-FID without internal standard. Performed once. Colours correspond to concentration of DMSO in Tris buffer (% v/v).

Table 2. Reductive amination of 4-pentenal with **1a**, **2a**, and **3a**. Reaction conditions and analysis methods: **(1)** 500 µL reactions with 10 mM amine, 50 mM 4-pentenal, 1 mM NADP+, 30 mM glucose, 0.4 mg/mL GDH, 10 µg/mL RedAm variant, and 40% DMSO in 200 mM Tris (pH 9) incubated at 30°C for 24 h with shaking (250 rpm). Reactions were quenched with 6 M NaOH, extracted into $CHCl_3$ and analyzed by GC-FID. **(2)** 1 mg of **1a** in a 500 µL reaction with 50 mM 4-pentenal, 1 mM NADP+, 30 mM glucose, 0.4 mg/mL GDH, 10 µg/mL RedAm variant, and 40% DMSO in 200 mM Tris (pH 9) incubated at 30°C for 24 h with shaking (250 rpm). Reactions were quenched with 6 M NaOH, extracted into $CDCl_3$ and analyzed by NMR.

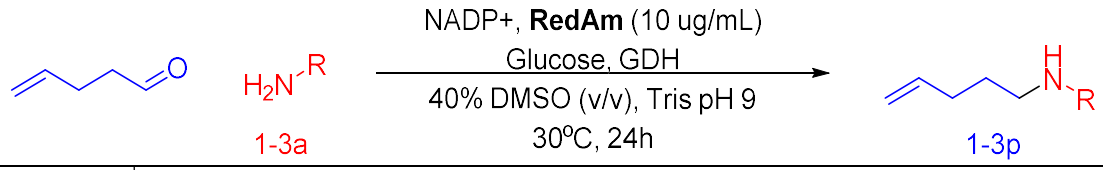

RedAm Variant	Reductive Amination Product		
	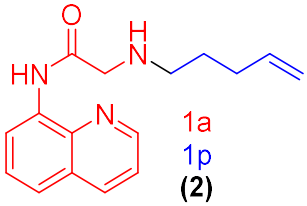 1a 1p **(2)**	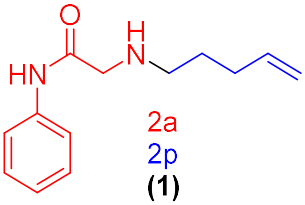 2a 2p **(1)**	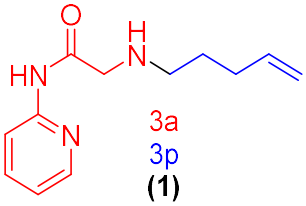 3a 3p **(1)**
*Asp*RedAm	Not Observed	Not Observed	Not Observed
I118A	Not Observed	Not Observed	Not Observed

To determine whether catalytically active mutants of *Asp*RedAm were suitable variants for our proposed concurrent chemoenzymatic cascade, reductive aminations were performed with novel amine substrates (**Figure 10**, **1a-3a**) and 4-pentenal (**Table 1**). Negative controls were either performed without a RedAm, the NADP+ coenzyme, or the aldehyde or amine substrates to determine whether any observed products were the result of enzyme-catalyzed reductive amination (**Figures 24-27**). Reductive aminations performed using **2a** and **3a** as amine substrates, to yield **2p** and **3p** respectively, were assessed using GC-FID analysis. Reductive aminations performed using **1a** as the amine substrate, to yield **1p**, were analyzed by ^{1}H-NMR spectroscopy. The products of reductive amination, **1p-3p**, were never observed with either WT *Asp*RedAm or the I118A mutant. Interestingly, products formed in the presence of the amines and 4-pentenal were observed under these reaction and workup conditions, though their formation was independent of the catalytic activity of the RedAms

(**Figures 24-27**). Reductive aminations were never performed with L91A mutant as this variant was unstable during expression and aggregated in inclusion bodies (**Figure 22**).

The reductive amination that yields **1p** is our main biotransformation of interest, as it enables the loading of **1a** as a TDG for the downstream olefin functionalization. While 4-pentenal has not been reported as a substrate for RedAms,[119,120] previous work in our group has shown that *Asp*RedAm is able to catalyze reductive aminations with this substrate. For example, some glycine-based amines, glycinamide and glycine-methyl ester (but not glycine-*tert*-butyl ester) have also been shown to be compatible substrates for WT *Asp*RedAm catalyzed reductive aminations. The fact that WT *Asp*RedAm tolerates glycinamide and glycine-methyl ester as amine substrates, but not glycine-*tert*-butyl ester, suggests a steric limitation in the amine binding pocket of the enzyme. Therefore, reductive aminations with **2a** could help further probe the size of the amine binding pocket. However, **1a** differs from **2a** not only in size but also due to its heteroarene structure. Thus, the reductive amination with **3a** and 4-pentenal could serve to probe the compatibility of heteroarenes with the amine binding pocket of the enzyme. Unfortunately, when **1a**, **2a**, or **3a** were used as amine substrates, the products of reductive amination (**1p**, **2p**, and **3p** respectively) were not observed with either WT *Asp*RedAm or the I118A mutant (**Figures 24-27**). It is important to note that both variants are catalytically active under these conditions (**Figure 23**). Interestingly, products were observed as a result of a reaction between 4-pentenal and all the amines; these products formed independent of enzyme activity and were even observed when only 4-pentenal and the amines were added to the reaction milieu and worked-up for analysis (**Figures 26** and **27**). GC-MS analysis of the reaction mixtures between 4-pentenal and **2a** or **3a**, carried out with and without RedAm activity, provides evidence for the formation of the imine (not shown). The reductive aminations performed with **1a** were analyzed by ^{1}H-NMR

spectroscopy as the product of the reductive amination (**1p**) was not sufficiently volatile for GC analysis. Here, the same NMR spectra is observed with or without RedAm activity, and the lack of any signals corresponding to the product under the same conditions is again suggestive of imine formation (**Figures 24** and **25**). Unfortunately, no reductive aminations were performed with the L91A mutant, as this variant was only found in the inclusion body aggregates during protein expression.[157]

The analysis of the extracts from the reactions performed with and without RedAm activity suggest that our amine substrates (**1a**, **2a**, and **3a**) are not tolerated in the amine binding pockets of WT *Asp*RedAm and the I118A mutant. Contrasting these amines to those previously reported[119] and our unpublished results, it seems that the steric bulk of (hetero)arene rings prevent the amines from entering the amine binding pocket of *Asp*RedAm. Moreover, the imine reductase activity of *Asp*RedAm has been previously reported, thus, the formation of the imine without any reduced product suggests that no productive interaction occurs between these compounds and the enzyme.

Although there is precedent for modulating the substrate specificity of RedAms through the modification of the amine binding pocket,[120] the notable mutant variant was a I123A variant of *At*RedAm, an *Asp*RedAm homologue derived from *A. terreus*. The I123 residue of *At*RedAm occupies the position equivalent to I118 in *Asp*RedAm. Thus, while the I118A mutation might have modulated substrate specificity, the absence of reductive amination products (**1p-3p**) suggests that the amine binding site is still too encumbered for these amine substrates (**1a-3a**). A double mutant variant of *At*RedAm (L96A/I123A) has also been reported, and while it displayed reduced activity compared to the I123A mutant with the amine substrates that were screened,[120] the potential substrate specificity of this less congested amine binding cavity for larger amine substrates is plausible (**Figure 7**). However, the L96

position of *At*RedAm is equivalent to the L91 residue of *Asp*RedAm, and the L91A variant that was generated expressed exclusively in inclusion bodies (**Figure 22**), presenting a challenge for analyzing its substrate specificity and the potential L91A/I118A *Asp*RedAm double mutant.[157]

Future work in this area could aim to address the challenges of expressing the L91A mutant, as previously discussed; finding a good protocol to isolate the L91A mutant should translate well to the L91A/I118A double mutant if issues regarding inclusion bodies persist. Further work with I118A mutant could involve the testing of new amine substrates to see if the mutation has made any changes to the substrate scope. Since the expression of the L96A/I123A mutant of the homologous *At*RedAm has been reported,[120] assessing its compatibility with **1a** as an amine substrate would be a simpler approach to solving the poor expression of *Asp*RedAm mutants. Moreover, the well-studied, broader class of prokaryotic IREDs presents plentiful opportunity to identify a biocatalyst that is capable of reductively aminating 4-pentenal with **1a**. Indeed, the recently published high throughput screen developed for rapidly interrogating RedAm activity, along with the production of a large IRED library,[130] provides a promising and fastidious strategy to finding a suitable enzyme.

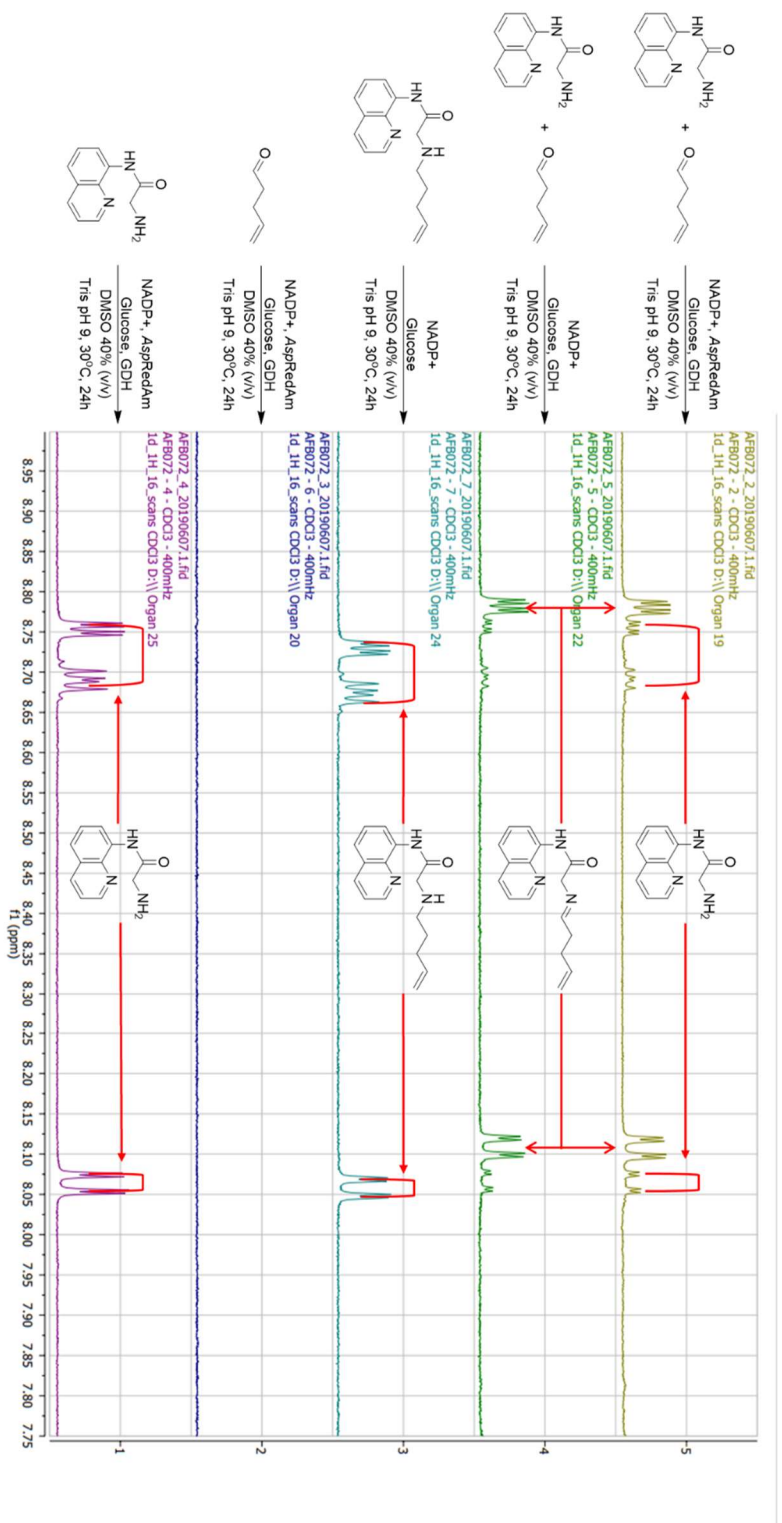

Figure 24. [1]H-NMR spectral analysis of WT AspRedAm catalyzed reductive amination of 4-pentenal with **1a** (7.75 – 9.00 ppm). (Top) Biocatalytic reductive amination. (Top middle) Negative control without WT AspRedAm. (Middle) Reductive amination product, **1p** as reference. (Bottom middle) Starting material, 4-pentenal, as reference. (Bottom) Starting material, **1a**, as reference.

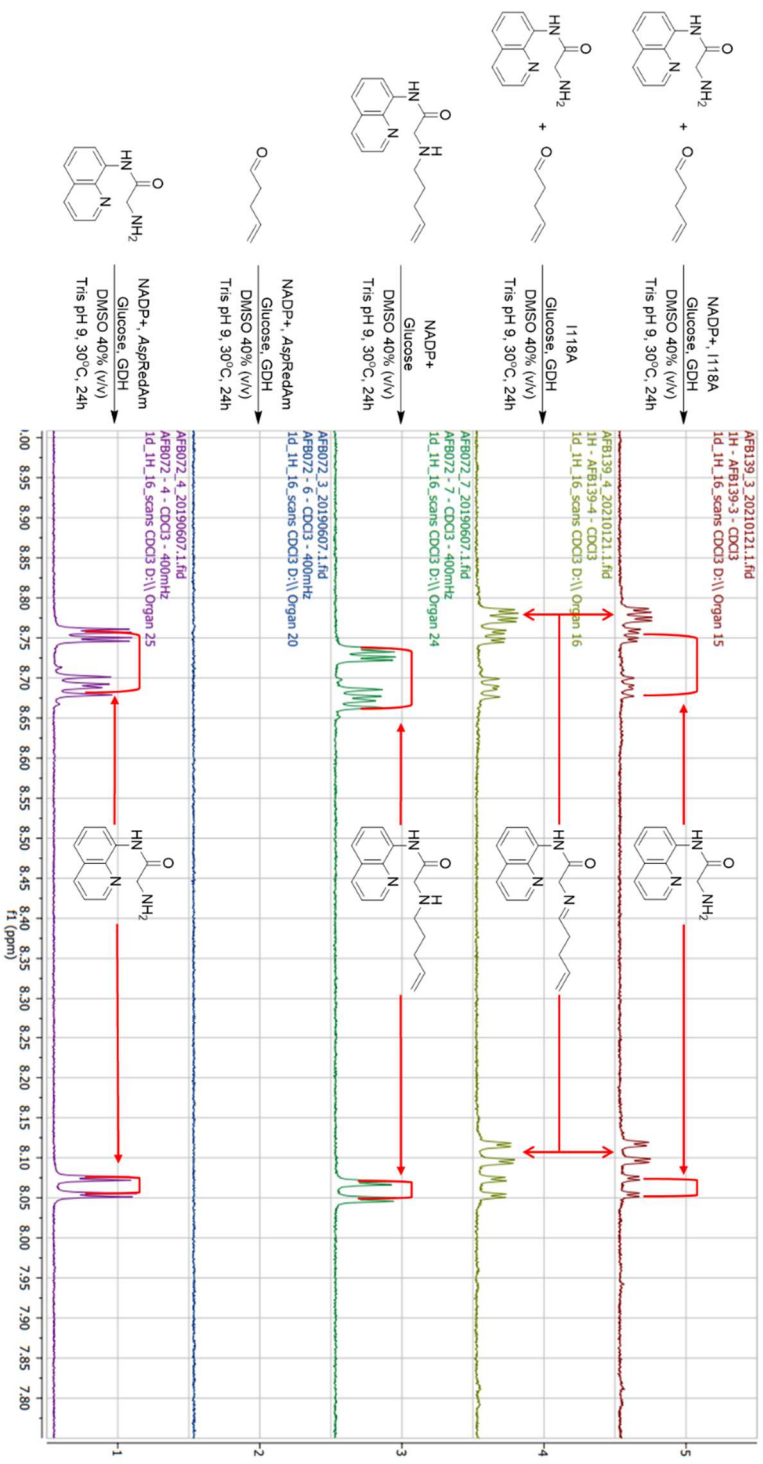

Figure 25. [1]H-NMR spectral analysis of I118A AspRedAm catalyzed reductive amination of 4-pentenal with **1a** (7.75 – 9.00 ppm). (Top) Biocatalytic reductive amination. (Top middle) Negative control without NADP+. (Middle) Reductive amination product, **1p** as reference. (Bottom middle) Starting material, 4-pentenal, as reference. (Bottom) Starting material, **1a**, as reference.

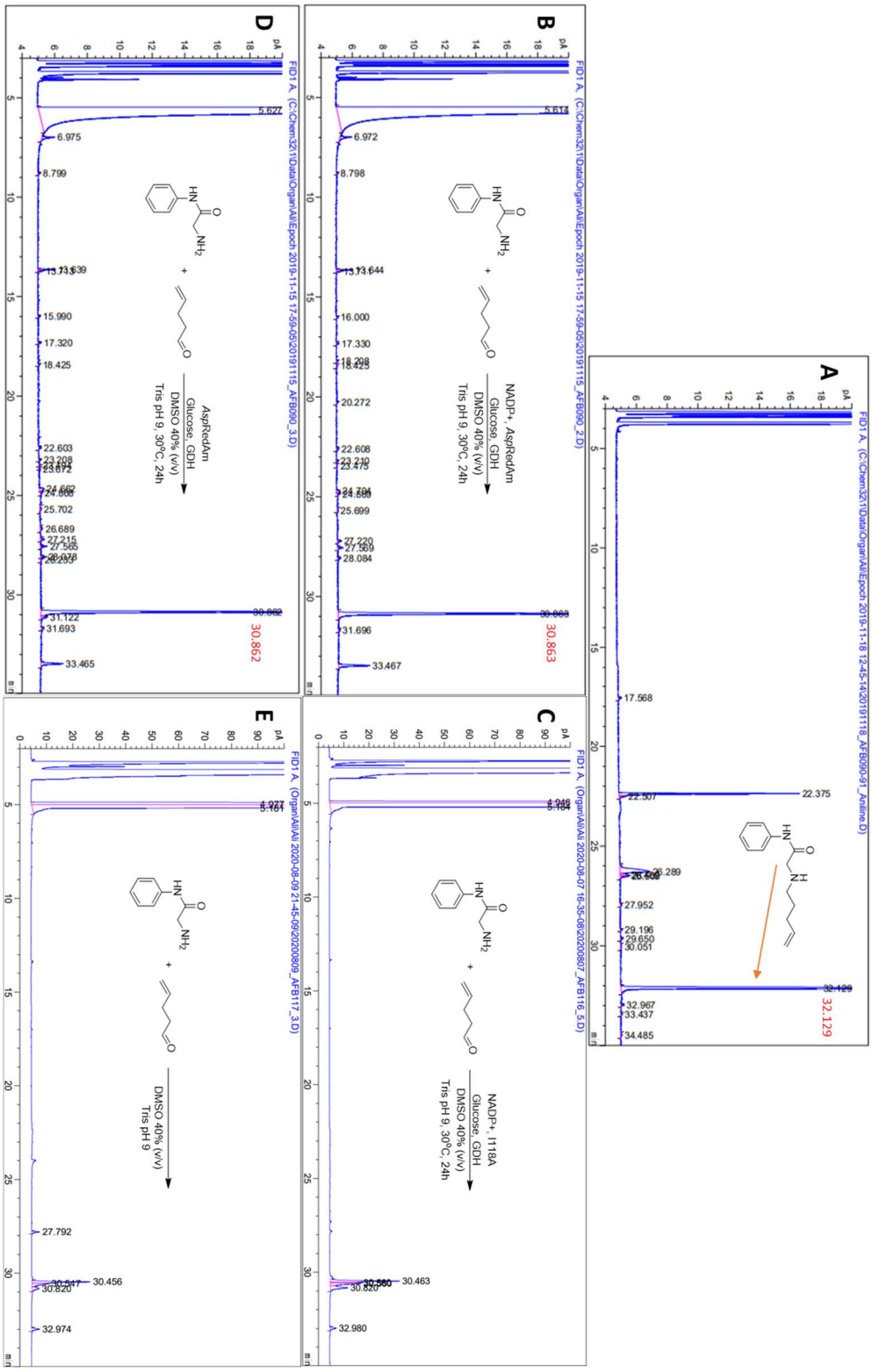

Figure 26. GC-FID analysis of RedAm catalyzed reductive amination of 4-pentenal with **2a. (A)** Trace of **2p** analytical standard (retention time 32.129 min) **(B)** Trace of WT AspRedAm biotransformation. **(C)** Trace of I118A biotransformation. **(D)** Trace of biotransformation negative control without NADP+. **(E)** Trace of **2a** and 4-pentenal under biotransformation conditions.

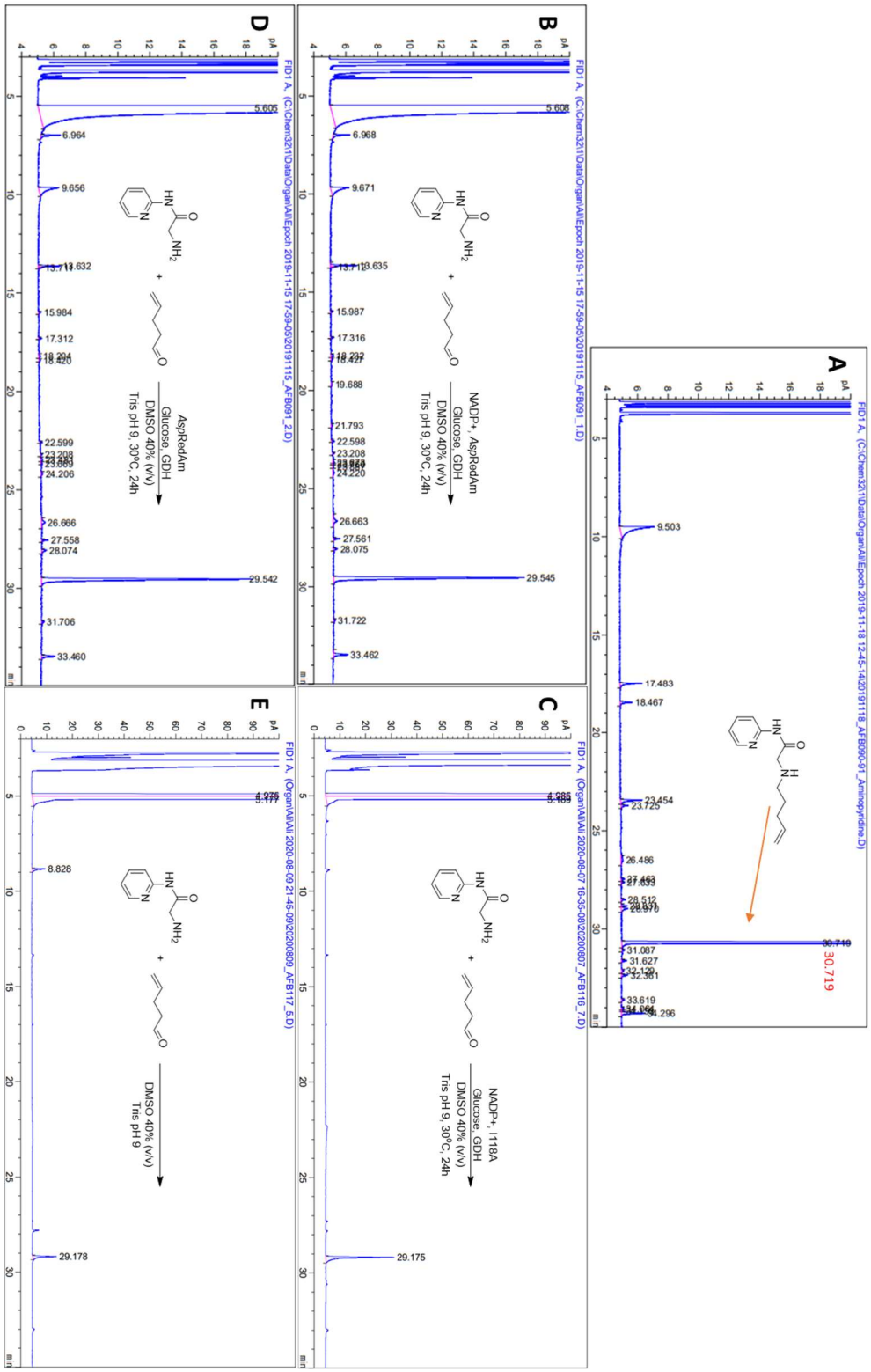

Figure 27. GC-FID analysis of RedAm catalyzed reductive amination of 4-pentenal with **3a. (A)** Trace of **3p** analytical standard (retention time 32.129 min) **(B)** Trace of WT AspRedAm biotransformation. **(C)** Trace of I118A biotransformation. **(D)** Trace biotransformation negative control without NADP+. **(E)** Trace of **3a** and 4-pentenal under biotransformation conditions.

3. Conclusions.

Using EtOH to supplement the culture media, the yield of WT *Asp*RedAm expressed in a prokaryotic system was improved from the previously reported conditions.[119] Moreover, the reaction conditions used to assay RedAm activity was optimized to reduce the amount of enzyme required for each assay by 100-fold. However, future efforts should aim to move away from the use of a fixed time assay in favour of discontinuous or continuous assays that enable more rigorous kinetic analysis. Indeed, while the I118A achieved lower conversion in the fixed time assay, it is unclear whether this reduced activity is due to a change in substrate specificity, decreased catalytic efficiency, or enzyme instability. A kinetic study comparing the RedAm variants with some different amine substrates would provide further insight into the effects of the mutation. Unfortunately, while the L91A mutant was generated, no assays were performed with this variant due to its aggregation into inclusion bodies under the expression conditions. Future efforts with this variant should focus on methods to solubilize and refold the enzymes that aggregate into inclusion bodies or modifying the expression conditions to yield L91A *in situ* by preventing the formation of inclusion bodies; critical parameters to modify include the concentration of IPTG used to induce expression, the temperature of expression, the time of expression post-induction, and the culture media used.

In previous studies, the use of enzymes in the presence of organic co-solvents has yielded mixed results in the effect on catalytic activity.[138–141] The effect of an organic co-solvent on catalytic activity is dependent on the physicochemical properties of the organic co-solvent, the enzyme, and substrate(s), along with their *in situ* interactions, making it difficult to predict *a priori*. The co-solvent screen that was used to assay the activity of *Asp*RedAm has, in part, identified the co-solvent compatibility of this enzyme. While the use of an enzymatic cofactor regenerating process in the assays introduces uncertainty in the

conclusions made from negative results, the increase in conversion achieved with DMSO indicates that it is a good co-solvent to use with *Asp*RedAm catalyzed transformations. Despite the uncertainty associated with a lack of observed conversion, the insolubility of the enzyme in buffers containing TFE and HFIP demonstrates incompatibility between *Asp*RedAm and the fluorinated alcohols used to facilitate the group-directed CH activations we have developed. Although, this insolubility could prove to be beneficial if lyophilized *Asp*RedAm can retain catalytic activity in neat TFE/HFIP. Future interrogations of co-solvent compatibility should aim to obtain more conclusive results with the co-solvents used by assessing *Asp*RedAm catalyzed oxidative deaminations, a RedAm activity that would not need a second enzyme to recycle the cofactor.

While the first biocatalytic reductive amination to load **1a** as a TDG has not yet been accomplished, these preliminary efforts have revealed some of the incompatibilities the biocatalyst (*Asp*RedAm) has operating in a concurrent chemoenzymatic cascade. These incompatibilities include limited tolerance to organic co-solvents (except DMSO), and no observable substrate specificity with our TDG (**1a**) or even smaller substructure-based amine substrates (**2a** and **3a**). Future efforts on this chemoenzymatic cascade must be conducted with these considerations in mind. It has been demonstrated that the heteroarene moiety of our TDG is imperative to its activity as a tridentate DG.[59] Thus, it is necessary to identify an enzyme (RedAm/IRED) that accepts **1a** as an amine substrate to achieve our proposed chemoenzymatic cascade. Engineering *Asp*RedAm via a rational design approach has so far proven to be unsuccessful; the previously reported *At*RedAm mutant variants may be a more optimal starting point for this approach. With the RedAm activity of a large library of IREDs that has recently been catalogued,[130] pursuing these prokaryotic oxidoreductases seems to be a promising alternative. However, the recently reported high throughput screen for RedAm

activity[130] could be coupled with high throughput mutagenesis.[163,164] This would enable the directed evolution of RedAms for our purposes, which is a more remarkable approach to achieving our objectives.

4. Materials and Methods.

4.1. Materials

The pET-28a-His-*Asp*RedAm plasmid[119] was generously provided by the Turner group (University of Manchester). A plasmid containing the gene for recombinant His-tagged GDH (*B. subtilis* S168; EC: 1.1.1.47) was provided by a colleague in the Boddy lab. Compounds **1a-3a** and **1p-3p** were prepared by colleagues in the Organ lab.

Cyclopropylamine and sodium triacetoxyborohydride were purchased from Oakwood Chemicals. Cyclohexanone, HFIP, TFE, Kanamycin, HPLC grade $CHCl_3$, and BSA were purchased from Sigma-Aldrich. NADP+ and 4-pentenal were purchased from Alfa-Aesar. Biotechnology grade NaCl, tryptone, Tris-HCl, and agarose were purchased from BioShop. LB-Miller and yeast extract were purchased from Fisher. Glucose was purchased from MP Biomedicals. Bradford reagent was purchased from Thermo-Fisher. Tris/Glycine/SDS buffer and Mini-PROTEAN TGX stain-free gels were purchased from Bio-Rad. All primers were purchased from IDT.

Incubations were performed in either a MaxQ 6000 incubated/refrigerated stackable shaker (Thermo Scientific), Innova 4330 refrigerated incubator shaker (New Brunswick Scientific), MaxQ 5000 incubator shaker (Barnstead Lab-Line), Innova 42 incubator shaker (New Brunswick Scientific) or an Isotemp Incubator (Fisher Scientific). Large scale centrifugation was achieved with either: a Sorvall Legend RT+ Centrifuge equipped with a swinging bucket rotor (Thermo Scientific) or a FIBERLite F15-8x50c fixed angle rotor, or a Heraeus Megafuge 16 Centrifuge in a refrigerated room. Small scale centrifugation was achieved with a Centrifuge 5415C (Eppendorf). Optical density measurements were performed with an Evolution 300 UV-Vis spectrometer (Thermo Scientific). Plasmid concentrations were quantified using an Eppendorf BioSpectrometer basic (Eppendorf).

Sonication was performed with a Sonic Dismembrator Model 500 (Fisher Scientific). All buffer solutions were pH adjusted using an Accumet Model 15 pH meter (Fisher Scientific). SDS-PAGE was achieved using a PowerPac 300 electrophoresis power supply (Bio-Rad). DNA electrophoresis was achieved with a Fisherbrand FB300 power supply (Fisher Scientific). Agarose and SDS-PAGE gels were imaged with an AlphaImager EC (Alpha Innotech) using AlphaView software.

GC-FID analysis was performed with a 6850 Series II Network GC (Agilent) furnished with a GC-PAC robotic arm (CTC analytics) auto sampling system and equipped with HP-1 Methyl Siloxane column (Agilent, 30m x 320µm, 0.25µm). GC-MS analysis was performed with a 5975B Inert XL EI/CI MSD (Agilent) furnished with a GC-PAC robotic arm auto sampling system and equipped with a HP-5MS 5% Phenyl Methyl Siloxane column (Agilent, 30m x 250µm, 0.25µm). ^{1}H and ^{13}C NMR spectra were obtained using an AVANCE II 400 instrument (Bruker) in $CDCl_3$ using residual protic solvent as an internal standard. Reported chemical shifts (δ) (in parts per million (ppm)) are relative to the residual protic solvent signal ($CHCl_3$ in $CDCl_3$, $^{1}H = 7.26$; $^{13}C = 77.0$).

4.2. Expression and Purification of Recombinant Proteins

4.2.1. General procedure for the transformation of chemically competent E. coli cells.

1-5 µL of the plasmid containing the gene of interest was incubated with 50 µL of chemically competent *E. coli* BL21 (DE3), *E. coli* XL1-Blue, *E. coli* Top10, or *E. coli* DH5α cells on ice for 30 minutes before heat-shock at 42 °C for 30 seconds. The cells were then grown in 1 mL of LB-Miller and incubated at 37 °C for 1 hour at 250 rpm. 50-100 µL of the culture was then plated on LB-agar containing the appropriate antibiotic marker and incubated at 37 °C overnight.

4.2.2. Expression and purification of recombinant AspRedAm and mutants.

The expression and purification of WT *Asp*RedAm and its mutants was adapted from previous reports[119] with modifications inspired from literature.[165] A single colony of *E. coli* BL21 (DE3) (harbouring the desired *Asp*RedAm gene in the pET-28a plasmid) was picked from an LB-agar plate containing 50 µg/mL kanamycin and inoculated into 5 mL LB-Miller with 50 µg/mL kanamycin. This pre-culture was incubated at 37 °C overnight in an orbital shaker at 200-250 rpm. The pre-culture was used as an inoculum for a 0.5-1 L culture in modified 2xYT media (16 g/L tryptone, 10 g/L yeast extract, 5 g/L NaCl, 3% v/v EtOH) containing 50 µg/mL kanamycin as the antibiotic marker. The culture was incubated at 37 °C in an orbital shaker at 200-250 rpm. At an optical density (OD_{600nm}) between 0.3 and 0.6, isopropyl β-D-1-thiogalactopyranoside (IPTG) was added to a final concentration of 1 mM to induce expression. Expression was continued at 18-20 °C and 200-250 rpm for 18 hours.

The cells from the culture were pelleted at 4000 rpm for 20 min at 4 °C and resuspended in 10-20 mL of lysis buffer (0.1 M Tris-HCl at pH 8, 300 mM NaCl, 10% v/v glycerol, 1 µg/mL pepstatin A, 1 µg/mL leupeptin, 1 mg/mL lysozyme) and lysed by sonication (2 min, 2s ON, 2s OFF). The suspension of lysed cells was centrifuged at 10,000

rpm for 1 hour at 4 °C and the supernatant was filtered through a 0.45 µm PVDF syringe filter (Millipore). The filtered supernatant was manually loaded onto a pre-chilled 1 mL His-Trap FF column (GE Healthcare) charged with 1 M $NiCl_2$. Ni-IMAC was performed with a step gradient using pre-chilled buffers (100 mM Tris, 300 mM NaCl, 0-250 mM imidazole, pH 8) and manual flow achieved using a Luer lock syringe. The column was washed with 5 column volumes (CV) of 0 mM imidazole buffer, 5 CV of 20 mM imidazole buffer, 3 CV of 100 mM imidazole buffer, and the protein eluted with 5-8 CV of 250 mM imidazole buffer. Aliquots of fractions were analyzed by SDS-PAGE and those that contained *Asp*RedAm/mutant were pooled. Buffer exchange was achieved using an Amicon Ultra-15 Centrifugal Filter (Merck-Millipore) with a 10 kDa molecular weight cut-off membrane and the protein was concentrated in a buffer containing 100 mM Tris and 300 mM NaCl (pH 7.4). The purified protein was diluted into a solution containing 30% v/v glycerol, flash frozen using liquid N_2, and stored at -80 °C until used.

4.2.3. Expression and purification of GDH.

The expression and purification of GDH was performed like *Asp*RedAm except that 500 mL of LB-Miller with 50 µg/mL kanamycin was used as the expression culture media.

4.3. Biocatalytic Reductive Aminations

4.3.1. General Procedure

Enzyme-catalyzed reductive aminations were performed in 500µL reaction mixtures containing 30 mM D-glucose, 1 mM NADP+ and 0.4 mg/mL GDH in Tris-HCl buffer (200 mM, pH 9.0). Depending on the biotransformation performed, varying amounts of co-solvents, purified *Asp*RedAm or mutants, carbonyl acceptors, and amine nucleophiles were used. The reactions were incubated at 30 ºC for 24 h with shaking at 250 rpm. The reactions

were quenched with 50 µL of 6 M NaOH, extracted into $CHCl_3$/$CDCl_3$ (2 x 0.5mL), dried over Na_2SO_4, and analyzed by NMR, GC-FID, or GC-MS.

4.3.2. Positive Control Biotransformation

Parallel to every *Asp*RedAm-catalyzed reaction, a positive control reductive amination of cyclohexanone with cyclopropylamine was performed as reported in the literature with modifications[119]. Briefly, a 500 µL reaction was prepared as described previously, with 2% DMSO (v/v), 5 mM cyclohexanone, 10 mM cyclopropylamine, and 10 µg/mL of purified RedAm. After workup, the extract was analyzed by GC-FID.

4.3.3. AspRedAm Co-Solvent Screen

500 µL reactions were prepared as has already been described, with 10 mM cyclohexanone, 20 mM cyclopropylamine, and 10 µg/mL of purified *Asp*RedAm. 2-40% DMSO (v/v), MeOH, EtOH, TFE, iPrOH, HFIP, ACN, or THF were used as co-solvents. After workup with 6 M NaOH and extraction into $CHCl_3$, the reactions were analyzed by GC-FID.

Sample Calculations:

Concentration of cyclohexanone in extract:

$$Peak\ Area\ (AU) = 18.075\ (\,{}^{AU}/_{mM}\,) \times [Cyclohexanone](mM) - 0.0176\ (AU)$$

$$[Cyclohexanone](mM) = \frac{Peak\ Area\ (AU) + 0.0176\ (AU)}{18.075\ ({}^{AU}/_{mM})}$$

$$[Cyclohexanone](mM) = \frac{21.4132\ (AU) + 0.0176(AU)}{18.075\ (\,{}^{AU}/_{mM}\,)}$$

$$[Cyclohexanone](mM) = 1.2\ mM$$

Percent Conversion:

$$\%\ Conversion = \frac{[Product](mM)}{[Product](mM) + [Ketone](mM)} \times 100\%$$

$$\%\ Conversion = \frac{4.3\ mM}{(4.3mM + 1.2\ mM)}\ x\ 100\%$$

$$\%\ Conversion = 78\%$$

4.4. Site-directed Mutagenesis

The wild-type *Asp*RedAm plasmid served as a template for the construction of mutants using established site directed mutagenesis protocols. The I118A mutation was generated using a protocol inspired by the commercially available Q5® Site-Directed Mutagenesis Kit (NEB),[155] with modifications. The L91A mutant plasmid was prepared using the previously reported endogenous RAIR pathway.[156] Target mutations were confirmed by sequencing (GenomeQuébec). Primers were designed using Benchling software (https://benchling.com) and are listed below.

Table 3. Primers used for the construction of *Asp*RedAm mutants with the WT *Asp*RedAm plasmid serving as a template for mutagenic PCR.

Primer	Primer Sequence
*Asp*RedAm L91A forward	5' AAAACCATCGTTAACGCGACTAACGGTACTCCGAACCAGGCGC 3'
*Asp*RedAm L91A reverse	5' GTTAACGATGGTTTTAGACGGCAGGGTTTGCAGC 3'
*Asp*RedAm I118A forward	5' GCCATGGCGGTGCCGACC 3'
*Asp*RedAm I118A reverse	5' ACCACCGTGGATGTAACGTGCA 3'

4.4.1. Quickchange Site Directed Mutagenesis

For the I118A mutant, non-complementary but adjacent primers were used with the mutation located at the 5' terminus of the forward primer. PCR reactions were performed with 1 µL of Herculase II Fusion DNA polymerase (Agilent) in a total reaction volume of 50 µL containing 1x Herculase buffer, 400 µM of each dNTP, 500 nM of forward and reverse primers, 35 ng of plasmid DNA template and 6% DMSO. PCR reactions were carried out in a T100 thermocycler (BioRad) using the following program: 95 °C denaturation for 1 min followed by 25 cycles of 95 °C denaturation for 50 s, annealing at 62.4 °C for 50 s, extension at 72 °C for 3 min 40 s, and a final extension at 72 °C for 7 min. Following the PCR reaction, the sample was incubated with 1 µL of DpnI (NEB) at 37 °C for 2 hours followed by heat inactivation at 80 °C for 20 min. The PCR products were purified using E.Z.N.A Gel

Extraction Kit (Omega BioTek) using the manufacturer's spin protocol with modification to exclude steps pertaining to extracting DNA from an agarose gel. Purified PCR products were quantified using an Eppendorf BioSpectrometer basic (Eppendorf). The PCR products were phosphorylated using 1 µL of T4 PNK (NEB) in a 19 µL reaction containing 1x T4 DNA buffer and 1 µg PCR product incubated at 37 °C for 1 hour followed by heat inactivation at 65 °C for 20 min. The phosphorylated PCR products were ligated by incubating the phosphorylation reaction with 1 µL of T4 Ligase (NEB) at 4 °C overnight. 5 µL of the ligation reaction was transformed into chemically competent DH5α cells, plated on LB agar containing 50 µg/mL kanamycin and incubated at 37 °C overnight. Individual colonies were inoculated into 5 mL of LB-Miller media containing 50 µg/mL kanamycin and incubated at 37 °C overnight. The cells were harvested by centrifugation at 14,000 rpm and the mutant plasmid was isolated using the E.Z.N.A Plasmid DNA Kit (Omega BioTek) as per the manufacturer's protocol.

4.4.2. RecA Independent Recombination (RAIR)-Enabled Site Directed Mutagenesis

For the L91A mutant, primers with a 15 bp overlap were used with the mutation adjacent to the overlapping region on the forward primer. PCR reactions were performed with 2 U of Q5 High-Fidelity DNA polymerase (NEB) in a total reaction volume of 50 µL containing 1x Q5 buffer, 400 µM of each dNTP, 500 nM of forward and reverse primers and 12 ng of plasmid DNA template. PCR reactions were carried out in a T100 thermocycler (BioRad) using the following program: 98 °C denaturation for 30 s followed by 25 cycles of 98 °C denaturation for 10 s, annealing at 67.5 °C for 50 s, extension at 72 °C for 3 min 10 s, and a final extension at 72 °C for 2 min. Following the PCR reaction, the sample was incubated with 1 µL of DpnI (NEB) at 37 °C for 2 hours followed by heat inactivation at 80 °C for 20 min. 5 µL of this crude mixture was transformed into chemically competent DH5α cells, plated

on LB agar containing 50 µg/mL kanamycin and incubated at 37 °C overnight. Individual colonies were inoculated into 5 mL of LB-Miller media containing 50 µg/mL kanamycin and incubated at 37 °C overnight. The cells were harvested by centrifugation at 14,000 rpm and the mutant plasmid was isolated using the E.Z.N.A Plasmid DNA Kit (Omega BioTek) as per the manufacturer's protocol.

4.4.3. Restriction Digest of Isolated Plasmids

The size of isolated plasmids was confirmed by a restriction digest and analysis by agarose gel electrophoresis. Briefly, 0.5-1 µg of plasmid DNA was incubated with 1 U of NcoI (NEB) in 1x NEBuffer™ 3.1 (NEB) at 37 °C for 1.5 h with heat inactivation at 80 °C for 15 min. Aliquots of the reaction were loaded on a 0.7% agarose gel (w/v) and analyzed by gel electrophoresis.

4.5. Synthesis of Analytical Standards

_N_-cyclopropylcyclohexylamine

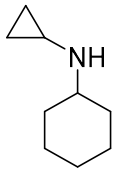

In a round bottom flask, cyclohexanone (0.5 mL, 5.0 mmol) was dissolved in DCM (30 mL) and cyclopropylamine (0.35 mL, 5.0 mmol) was added. A drop of glacial acetic acid was added to the solution and stirred at room temperature for 5 minutes. Sodium triacetoxyborohydride (1.59 g, 7.5 mmol) was added to the flask and the reaction was stirred at room temperature overnight. The reaction was quenched with 12 M HCl and extracted with 45 mL of distilled water (pH 1-2). The aqueous phase was basified with 6 M NaOH (pH 13) and extracted with DCM (3 x 30 mL). The organic phases were pooled, dried over $MgSO_4$ and filtered. The solvent was removed under reduced pressure to yield a yellow oil (583.8 mg, 4.19 mmol, 83.8% yield). **^{1}H-NMR** (400 MHz, $CDCl_3$) 2.56 (tt, J = 10.6, 3.8 Hz, 1H), 2.13 (tt, J = 6.7, 3.7 Hz, 1H), 1.99-1.91 (m, 2H), 1.76-1.68 (m, 2H), 1.65-1.58 (m, 2H), 1.50 (br, 1H), 1.33-1.00 (m, 5H), 0.46-0.29 (m, 4H). **^{13}C-NMR** (400 MHz, $CDCl_3$) 57.4 (CH), 33.9 (CH_2), 28.2 (CH), 26.2 (CH_2), 25.2 (CH_2), 6.5 (CH_2). **MS** *m/z* 139.14 [M^+] found 139.14.

5. References.

(1) Chakrabarty, S.; Romero, E. O.; Pyser, J. B.; Yazarians, J. A.; Narayan, A. R. H. Chemoenzymatic Total Synthesis of Natural Products. *Acc. Chem. Res.* **2021**, *54* (6), 1374–1384. https://doi.org/10.1021/acs.accounts.0c00810.

(2) Pichette Drapeau, M.; Gooßen, L. J. Carboxylic Acids as Directing Groups for C−H Bond Functionalization. *Chem. - A Eur. J.* **2016**, *22* (52), 18654–18677. https://doi.org/10.1002/chem.201603263.

(3) Brown, A. C.; Gibson, J. A Rule for Determining Whether a given Benzene Mono-Derivative Shall Give a Meta-Di-Derivative or a Mixture of Ortho- and Para-Di-Derivatives. *J. Chem. Soc., Trans.* **1892**, *61*, 367–369. https://doi.org/10.1039/CT8926100367.

(4) Wade, L. G. *Organic Chemistry*, 8th ed.; Pearson: Glenview, **2013**.

(5) Clayden, J.; Greeves, N.; Warren, S. *Organic Chemistry*, 2nd ed.; Oxford University Press: New York, **2001**.

(6) Sambiagio, C.; Schönbauer, D.; Blieck, R.; Dao-Huy, T.; Pototschnig, G.; Schaaf, P.; Wiesinger, T.; Zia, M. F.; Wencel-Delord, J.; Besset, T.; Maes, B. U. W.; Schnürch, M. A Comprehensive Overview of Directing Groups Applied in Metal-Catalysed C-H Functionalisation Chemistry. *Chem. Soc. Rev.* **2018**, *47* (17), 6603–6743. https://doi.org/10.1039/c8cs00201k.

(7) Muchowski, J. M.; Solas, D. R. B-Substituted Pyrroles via Electrophilic Substitution of N-Triisopropylsilylpyrrole. *Tetrahedron Lett.* **1983**, *24* (33), 3455–3456.

(8) Morgan, K. J.; Morrey, D. P. The Preparation and Properties of 2- and 3-Nitropyrrole. *Tetrahedron* **1966**, *22*, 57–62.

(9) Snieckus, V. Directed Ortho Metalation. Tertiary Amide and O-Carbamate Directors in Synthetic Strategies for Polysubstituted Aromatics. *Chem. Rev.* **1990**, *90* (6), 879–933. https://doi.org/10.1021/cr00104a001.

(10) Mortier, J.; Moyroud, J.; Bennetau, B.; Cain, P. A. The Carboxylic Acid Group as an Effective Director of Ortho-Lithiation. *J. Org. Chem.* **1994**, *59* (15), 4042–4044. https://doi.org/10.1021/jo00094a007.

(11) Murai, S.; Kakiuchl, F.; Seklne, S.; Tanaka, Y.; Kamatani, A.; Sonoda, M. Efficient Catalytic Addition of Aromatic Carbon-Hydrogen Bonds to Olefins. *Nature* **1993**, *366*, 529–531.

(12) Ryabov, A. D. Mechanisms of Intramolecular Activation of C-H Bonds in Transition-Metal Complexes. *Chem. Rev.* **1990**, *90* (2), 403–424. https://doi.org/10.1021/cr00100a004.

(13) Webster, D. E. Activation of Alkanes by Transition Metal Compounds. In *Advances in Organometallic Chemistry*; **1977**; Vol. 15, pp 147–188. https://doi.org/10.1016/S0065-3055(08)60128-8.

(14) Corbet, J. P.; Mignani, G. Selected Patented Cross-Coupling Reaction Technologies. *Chem. Rev.* **2006**, *106* (7), 2651–2710. https://doi.org/10.1021/cr0505268.

(15) Negishi, E. A Genealogy of Pd-Catalyzed Cross-Coupling. *J. Organomet. Chem.* **2002**, *653* (1–2), 34–40. https://doi.org/10.1016/S0022-328X(02)01273-1.

(16) Johansson Seechurn, C. C. C.; Kitching, M. O.; Colacot, T. J.; Snieckus, V. Palladium-Catalyzed Cross-Coupling: A Historical Contextual Perspective to the 2010 Nobel Prize. *Angew. Chemie - Int. Ed.* **2012**, *51* (21), 5062–5085. https://doi.org/10.1002/anie.201107017.

(17) Chen, Z.; Wang, B.; Zhang, J.; Yu, W.; Liu, Z.; Zhang, Y. Transition Metal-Catalyzed C-H Bond Functionalizations by the Use of Diverse Directing Groups. *Org. Chem. Front.* **2015**, *2* (9), 1107–1295. https://doi.org/10.1039/c5qo00004a.

(18) Simon, M. O.; Genet, J. P.; Darses, S. Ruthenium Chloride as an Efficient Catalytic Precursor for Hydroarylation Reactions via C-H Bond Activation. *Org. Lett.* **2010**, *12* (13), 3038–3041. https://doi.org/10.1021/ol101038c.

(19) Crisenza, G. E. M.; McCreanor, N. G.; Bower, J. F. Branch-Selective, Iridium-Catalyzed Hydroarylation of Monosubstituted Alkenes via a Cooperative Destabilization Strategy. *J. Am. Chem. Soc.* **2014**, *136* (29), 10258–10261. https://doi.org/10.1021/ja505776m.

(20) Pan, S.; Jiang, H.; Zhang, Y.; Chen, D.; Zhang, Y. Synthesis of Unsymmetrically Disubstituted Tetraphenylenes via Carbonyl-Directed C–H Functionalization. *Synlett* **2016**, *27* (13), 1997–2002. https://doi.org/10.1055/s-0035-1561862.

(21) Bakthadoss, M.; Kumar, P. V.; Reddy, T. S. Ruthenium-Catalyzed, Keto-Directed, Site-Selective C–H Activation of Diverse Chromanones with Alkenes. *European J. Org. Chem.* **2017**, *2017* (30), 4439–4444. https://doi.org/10.1002/ejoc.201700513.

(22) Hu, F.; Szostak, M. Ruthenium(0)-Catalyzed Hydroarylation of Alkynes via Ketone-Directed C-H Functionalization Using in Situ -Generated Ruthenium Complexes. *Chem. Commun.* **2016**, *52* (62), 9715–9718. https://doi.org/10.1039/c6cc04537e.

(23) Zhang, B.; Wang, H. W.; Kang, Y. S.; Zhang, P.; Xu, H. J.; Lu, Y.; Sun, W. Y. Rhodium-Catalyzed Direct Ortho C-H Arylation Using Ketone as Directing Group with Boron Reagent. *Org. Lett.* **2017**, *19* (21), 5940–5943. https://doi.org/10.1021/acs.orglett.7b02931.

(24) Li, X.; Wu, G.; Liu, X.; Zhu, Z.; Huo, Y.; Jiang, H. Regioselective C-H Bond Alkynylation of Carbonyl Compounds through Ir(III) Catalysis. *J. Org. Chem.* **2017**, *82* (24), 13003–13011. https://doi.org/10.1021/acs.joc.7b01489.

(25) Lee, P.; Liang, P.; Yu, W. Pd(II)-Catalyzed Direct Ortho-C−H Acylation of Aromatic Ketones by Oxidative Decarboxylation of A-Oxocarboxylic Acids. *Org. Lett.* **2017**, *19*, 2082–2085. https://doi.org/10.1021/acs.orglett.7b00677.

(26) Chiong, H. A.; Pham, Q.-N.; Daugulis, O. Two Methods for Direct Ortho -Arylation of Benzoic Acids. *J. Am. Chem. Soc.* **2007**, *129* (32), 9879–9884. https://doi.org/10.1021/ja071845e.

(27) Kangani, C. O.; Kelley, D. E. One Pot Direct Synthesis of Amides or Oxazolines from Carboxylic Acids Using Deoxo-Fluor Reagent. *Tetrahedron Lett.* **2005**, *46* (51), 8917–8920. https://doi.org/10.1016/j.tetlet.2005.10.068.

(28) Eaddy, J. F. THE NICKEL(I) CATALYZED COUPLING OF A DIARYLZINC WITH AN ARYL CHLORIDE IN THE SYNTHESIS OF XENALIPIN. *Org. Prep. Proced. Int.* **1995**, *27* (3), 367–372. https://doi.org/10.1080/00304949509458470.

(29) Ciske, F. L. An Efficient Synthesis of Dihydroxyfluorenones via in Situ Pd(0)-Catalyzed Cross-Coupling. *Synthesis (Stuttg).* **1998**, *1998* (08), 1195–1198. https://doi.org/10.1055/s-1998-2113.

(30) Kuninobu, Y.; Ohta, K.; Takai, K. Rhenium-Catalyzed Allylation of C–H Bonds of Benzoic and Acrylic Acids. *Chem. Commun.* **2011**, *47* (38), 10791. https://doi.org/10.1039/c1cc12359a.

(31) Giri, R.; Maugel, N.; Li, J.-J.; Wang, D.-H.; Breazzano, S. P.; Saunders, L. B.; Yu, J.-Q. Palladium-Catalyzed Methylation and Arylation of Sp 2 and Sp 3 C−H Bonds in Simple Carboxylic Acids. *J. Am. Chem. Soc.* **2007**, *129* (12), 3510–3511. https://doi.org/10.1021/ja0701614.

(32) Fischer, E.; Speier, A. Darstellung Der Ester. *Berichte der Dtsch. Chem. Gesellschaft* **1895**, *28* (3), 3252–3258. https://doi.org/10.1002/cber.189502803176.

(33) Neises, B.; Steglich, W. Simple Method for the Esterification of Carboxylic Acids. *Angew. Chemie Int. Ed. English* **1978**, *17* (7), 522–524. https://doi.org/10.1002/anie.197805221.

(34) Schneider, C.; Broda, E.; Snieckus, V. Directed Ortho -Metalation–Cross-Coupling Strategies. One-Pot Suzuki Reaction to Biaryl and Heterobiaryl Sulfonamides. *Org. Lett.* **2011**, *13* (14), 3588–3591. https://doi.org/10.1021/ol201175g.

(35) Ros, A.; Fernández, R.; Lassaletta, J. M. Functional Group Directed C-H Borylation. *Chem. Soc. Rev.* **2014**, *43* (10), 3229–3243. https://doi.org/10.1039/c3cs60418g.

(36) Ishiyama, T.; Isou, H.; Kikuchi, T.; Miyaura, N. Ortho-C-H Borylation of Benzoate Esters with Bis(Pinacolato)Diboron Catalyzed by Iridium-Phosphine Complexes. *Chem. Commun.* **2010**, *46* (1), 159–161. https://doi.org/10.1039/b910298a.

(37) Sasaki, I.; Doi, H.; Hashimoto, T.; Kikuchi, T.; Ito, H.; Ishiyama, T. Iridium(i)-Catalyzed Vinylic C–H Borylation of 1-Cycloalkenecarboxylates with Bis(Pinacolato)Diboron. *Chem. Commun.* **2013**, *49* (68), 7546. https://doi.org/10.1039/c3cc44149k.

(38) Wang, G.; Liu, L.; Wang, H.; Ding, Y. S.; Zhou, J.; Mao, S.; Li, P. N,B-Bidentate Boryl Ligand-Supported Iridium Catalyst for Efficient Functional-Group-Directed C-H Borylation. *J. Am. Chem. Soc.* **2017**, *139* (1), 91–94. https://doi.org/10.1021/jacs.6b11867.

(39) Gao, P.; Liu, L.; Shi, Z.; Yuan, Y. Iridium(III)-Catalyzed Regioselective Direct Arylation of Sp2 C-H Bonds with Diaryliodonium Salts. *Org. Biomol. Chem.* **2016**, *14* (29), 7109–7113. https://doi.org/10.1039/c6ob01145d.

(40) Li, J.; Ackermann, L. Carboxylate-Assisted Ruthenium(II)-Catalyzed C-H Activations of Monodentate Amides with Conjugated Alkenes. *Org. Chem. Front.* **2015**, *2* (9), 1035–1039. https://doi.org/10.1039/c5qo00167f.

(41) Dai, H.; Yu, C.; Lu, C.; Yan, H. RhIII-Catalyzed C-H Allylation of Amides and Domino Cycling Synthesis of 3,4-Dihydroisoquinolin-1(2H)-Ones with N-Bromosuccinimide. *European J. Org. Chem.* **2016**, *2016* (7), 1255–1259. https://doi.org/10.1002/ejoc.201501551.

(42) Zhang, L.; Chen, C.; Han, J.; Huang, Z. Bin; Zhao, Y. Ru-Catalyzed Selective C-H Oxidative Olefination with N-Heteroarenes Directed by Pivaloyl Amide. *Org. Chem. Front.* **2016**, *3* (10), 1271–1275. https://doi.org/10.1039/c6qo00327c.

(43) Tischler, O.; Bokányi, Z.; Novák, Z. Activation of C-H Activation: The Beneficial Effect of Catalytic Amount of Triaryl Boranes on Palladium-Catalyzed C-H Activation. *Organometallics* **2016**, *35* (5), 741–746. https://doi.org/10.1021/acs.organomet.5b01017.

(44) Meng, K.; Zhang, J.; Li, F.; Lin, Z.; Zhang, K.; Zhong, G. Amide Directed Cross-Coupling between Alkenes and Alkynes: A Regio- and Stereoselective Approach to Substituted (2Z,4Z)-Dienamides. *Org. Lett.* **2017**, *19* (10), 2498–2501. https://doi.org/10.1021/acs.orglett.7b00695.

(45) Coxon, T. J.; Fernández, M.; Barwick-Silk, J.; McKay, A. I.; Britton, L. E.; Weller, A. S.; Willis, M. C. Exploiting Carbonyl Groups to Control Intermolecular Rhodium-Catalyzed Alkene and Alkyne Hydroacylation. *J. Am. Chem. Soc.* **2017**, *139* (29), 10142–10149. https://doi.org/10.1021/jacs.7b05713.

(46) Yang, L.; Fu, L.; Li, G. Incorporation of Carbon Dioxide into Carbamate Directing Groups: Palladium-Catalyzed Meta -C-H Olefination and Acetoxylation of Aniline Derivatives. *Adv. Synth. Catal.* **2017**, *359* (13), 2235–2240. https://doi.org/10.1002/adsc.201700261.

(47) Bag, S.; Patra, T.; Modak, A.; Deb, A.; Maity, S.; Dutta, U.; Dey, A.; Kancherla, R.; Maji, A.; Hazra, A.; Bera, M.; Maiti, D. Remote Para- C–H Functionalization of Arenes by a D-Shaped Biphenyl Template-Based Assembly. *J. Am. Chem. Soc.* **2015**, *137* (37), 11888–11891. https://doi.org/10.1021/jacs.5b06793.

(48) Patra, T.; Bag, S.; Kancherla, R.; Mondal, A.; Dey, A.; Pimparkar, S.; Agasti, S.; Modak, A.; Maiti, D. Palladium-Catalyzed Directed Para C−H Functionalization of Phenols. *Angew. Chemie - Int. Ed.* **2016**, *55* (27), 7751–7755. https://doi.org/10.1002/anie.201601999.

(49) Li, S.; Cai, L.; Ji, H.; Yang, L.; Li, G. Pd(II)-Catalysed Meta-C–H Functionalizations of Benzoic Acid Derivatives. *Nat. Commun.* **2016**, *7* (1), 10443. https://doi.org/10.1038/ncomms10443.

(50) Modak, A.; Mondal, A.; Watile, R.; Mukherjee, S.; Maiti, D. Remote Meta C–H Bond Functionalization of 2-Phenethylsulphonic Acid and 3-Phenylpropanoic Acid Derivatives. *Chem. Commun.* **2016**, *52* (96), 13916–13919. https://doi.org/10.1039/C6CC08302A.

(51) Yang, K. S.; Gurak, J. A.; Liu, Z.; Engle, K. M. Catalytic, Regioselective Hydrocarbofunctionalization of Unactivated Alkenes with Diverse C-H Nucleophiles. *J. Am. Chem. Soc.* **2016**, *138* (44), 14705–14712. https://doi.org/10.1021/jacs.6b08850.

(52) Liu, Z.; Derosa, J.; Engle, K. M. Palladium(II)-Catalyzed Regioselective Syn-Hydroarylation of Disubstituted Alkynes Using a Removable Directing Group. *J. Am. Chem. Soc.* **2016**, *138* (39), 13076–13081. https://doi.org/10.1021/jacs.6b08818.

(53) O'Duill, M. L.; Matsuura, R.; Wang, Y.; Turnbull, J. L.; Gurak, J. A.; Gao, D. W.; Lu, G.; Liu, P.; Engle, K. M. Tridentate Directing Groups Stabilize 6-Membered Palladacycles in Catalytic Alkene Hydrofunctionalization. *J. Am. Chem. Soc.* **2017**, *139* (44), 15576–15579. https://doi.org/10.1021/jacs.7b08383.

(54) Liu, Z.; Wang, Y.; Wang, Z.; Zeng, T.; Liu, P.; Engle, K. M. Catalytic Intermolecular Carboamination of Unactivated Alkenes via Directed Aminopalladation. *J. Am. Chem. Soc.* **2017**, *139* (32), 11261–11270. https://doi.org/10.1021/jacs.7b06520.

(55) Liu, Z.; Ni, H. Q.; Zeng, T.; Engle, K. M. Catalytic Carbo- and Aminoboration of Alkenyl Carbonyl Compounds via Five- and Six-Membered Palladacycles. *J. Am. Chem. Soc.* **2018**, *140* (9), 3223–3227. https://doi.org/10.1021/jacs.8b00881.

(56) Liu, Z.; Li, X.; Zeng, T.; Engle, K. M. Directed, Palladium(II)-Catalyzed Enantioselective Anti-Carboboration of Alkenyl Carbonyl Compounds. *ACS Catal.* **2019**, *9* (4), 3260–3265. https://doi.org/10.1021/acscatal.9b00181.

(57) Nimmagadda, S. K.; Liu, M.; Karunananda, M. K.; Gao, D.; Apolinar, O.; Chen, J. S.; Liu, P.; Engle, K. M. Catalytic, Enantioselective A-Alkylation of Azlactones with Nonconjugated Alkenes by Directed Nucleopalladation. *Angew. Chemie Int. Ed.* **2019**, *58* (12), 3923–3927. https://doi.org/10.1002/anie.201814272.

(58) Liu, M.; Yang, P.; Karunananda, M. K.; Wang, Y.; Liu, P.; Engle, K. M. C(Alkenyl)–H Activation via Six-Membered Palladacycles: Catalytic 1,3-Diene Synthesis. *J. Am. Chem. Soc.* **2018**, *140* (17), 5805–5813. https://doi.org/10.1021/jacs.8b02124.

(59) Nnamdi, F. U.; Diner, C.; Champagne, P. A.; Organ, M. G. Experimental and Computational Study on the Anti-Markovnikov Hydrofunctionalization of Olefins Using Glycine-Extended AQ-Auxiliaries. *Chem. – A Eur. J.* **2021**, *27* (11), 3855–3860. https://doi.org/10.1002/chem.202004881.

(60) Padmavathi, R. .; Sankar, R. .; Gopalakrishnan, B. .; Parella, R. .; Babu, S. A. . Pd(OAc)2/AgOAc Catalytic System Based Bidentate Ligand Directed Regiocontrolled C–H Arylation and Alkylation of the C-3 Position of Thiophene- and Furan-2-carboxamides. *European J. Org. Chem.* **2015**, *17*, 3727–3742. https://doi.org/https://doi.org/10.1002/ejoc.201500249.

(61) Parella, R. .; Babu, S. A. . Pd(OAc)2-Catalyzed, AgOAc-Promoted Z Selective Directed β-Arylation of Acrylamide Systems and Stereoselective Construction of Z-Cinnamamide Scaffolds. *J. Org. Chem.* **2015**, *80* (24), 12379–12396. https://doi.org/10.1021/acs.joc.5b02264.

(62) Parella, R. .; Babu, S. A. . Regio- and Stereoselective Pd-Catalyzed Direct Arylation of Unactivated Sp3 C(3)–H Bonds of Tetrahydrofuran and 1,4-Benzodioxane Systems. *J. Org. Chem.* **2015**, *80* (4), 2339–2355.

(63) Gopalakrishnan, B. .; Babu, S. A. .; Padmavathi, R. Bidentate Ligand 8-Aminoquinoline-Aided Pd-Catalyzed Diastereoselective β-Arylation of the Prochiral Secondary Sp3 C–H Bonds of 2-Phenylbutanamides and Related Aliphatic Carboxamides.Pdf. *Tetrahedrom* **2015**, *71* (43), 8333–8349.

(64) Affron, D. P.; Bull, J. A. Palladium-Catalyzed Directed C(Sp 3)-H Arylation of Saturated Heterocycles at C-3 Using a Concise Optimization Approach. *European J. Org. Chem.* **2016**, *2016* (1), 139–149. https://doi.org/10.1002/ejoc.201501300.

(65) Parella, R.; Babu, S. A. Pd(II)-Catalyzed Arylation and Intramolecular Amidation of γ-C(Sp 3)–H Bonds: En Route to Arylheteroarylmethane and Pyrrolidone Ring Annulated Furan/Thiophene Scaffolds. *J. Org. Chem.* **2017**, *82* (14), 7123–7150. https://doi.org/10.1021/acs.joc.7b00582.

(66) van der Puyl, V. A.; Derosa, J.; Engle, K. M. Directed, Nickel-Catalyzed Umpolung 1,2-Carboamination of Alkenyl Carbonyl Compounds. *ACS Catal.* **2019**, *9* (1), 224–229. https://doi.org/10.1021/acscatal.8b04516.

(67) Khan, B.; Kant, R.; Koley, D. Nickel(II)-Mediated Regioselective CH Monoiodination of Arenes and Heteroarenes by Using Molecular Iodine. *Adv. Synth. Catal.* **2016**, *358* (14), 2352–2358. https://doi.org/10.1002/adsc.201600177.

(68) Wencel-Delord, J.; Colobert, F. A Remarkable Solvent Effect of Fluorinated Alcohols on Transition Metal Catalysed C-H Functionalizations. *Organic Chemistry Frontiers*. **2016**, pp 394–400. https://doi.org/10.1039/c5qo00398a.

(69) Brown, D. G.; Boström, J. Analysis of Past and Present Synthetic Methodologies on Medicinal Chemistry: Where Have All the New Reactions Gone? *J. Med. Chem.* **2016**, *59* (10), 4443–4458. https://doi.org/10.1021/acs.jmedchem.5b01409.

(70) Boström, J.; Brown, D. G.; Young, R. J.; Keserü, G. M. Expanding the Medicinal Chemistry Synthetic Toolbox. *Nat. Rev. Drug Discov.* **2018**, *17* (10), 709–727. https://doi.org/10.1038/nrd.2018.116.

(71) Roughley, S. D.; Jordan, A. M. The Medicinal Chemist's Toolbox: An Analysis of Reactions Used in the Pursuit of Drug Candidates. *J. Med. Chem.* **2011**, *54* (10), 3451–3479. https://doi.org/10.1021/jm200187y.

(72) Schneider, N.; Lowe, D. M.; Sayle, R. A.; Tarselli, M. A.; Landrum, G. A. Big Data from Pharmaceutical Patents: A Computational Analysis of Medicinal Chemists' Bread and Butter. *J. Med. Chem.* **2016**, *59* (9), 4385–4402. https://doi.org/10.1021/acs.jmedchem.6b00153.

(73) Bhattacharya, T.; Pimparkar, S.; Maiti, D. Combining Transition Metals and Transient Directing Groups for C–H Functionalizations. *RSC Adv.* **2018**, *8* (35), 19456–19464. https://doi.org/10.1039/C8RA03230K.

(74) St John-Campbell, S.; Bull, J. A. Transient Imines as 'next Generation' Directing Groups for the Catalytic Functionalisation of C–H Bonds in a Single Operation. *Org. Biomol. Chem.* **2018**, *16* (25), 4582–4595. https://doi.org/10.1039/C8OB00926K.

(75) Gandeepan, P.; Ackermann, L. Transient Directing Groups for Transformative C–H Activation by Synergistic Metal Catalysis. *Chem* **2018**, *4* (2), 199–222. https://doi.org/10.1016/j.chempr.2017.11.002.

(76) Topczewski, J. J.; Cabrera, P. J.; Saper, N. I.; Sanford, M. S. Palladium-Catalysed Transannular C-H Functionalization of Alicyclic Amines. *Nature* **2016**, *531* (7593), 220–224. https://doi.org/10.1038/nature16957.

(77) Jun, C.-H.; Lee, H.; Hong, J.-B. Chelation-Assisted Intermolecular Hydroacylation: Direct Synthesis of Ketone from Aldehyde and 1-Alkene. *J. Org. Chem.* **1997**, *62* (5), 1200–1201. https://doi.org/10.1021/jo961887d.

(78) Zhang, F.-L.; Hong, K.; Li, T.-J.; Park, H.; Yu, J.-Q. Functionalization of C(Sp3)-H Bonds Using a Transient Directing Group. *Science (80-.).* **2016**, *351* (6270), 252–256. https://doi.org/10.1126/science.aad7893.

(79) Dong, C.; Wu, L.; Yao, J.; Wei, K. Palladium-Catalyzed β-C–H Arylation of Aliphatic Aldehydes and Ketones Using Amino Amide as a Transient Directing Group. *Org. Lett.* **2019**, *21* (7), 2085–2089. https://doi.org/10.1021/acs.orglett.9b00366.

(80) Park, H.; Yoo, K.; Jung, B.; Kim, M. Direct Synthesis of Anthracenes from O-Tolualdehydes and Aryl Iodides through Pd(II)-Catalyzed Sp C H Arylation and Electrophilic Aromatic Cyclization. *Tetrahedron* **2018**, *74* (16), 2048–2055. https://doi.org/10.1016/j.tet.2018.03.006.

(81) Liu, X.-H.; Park, H.; Hu, J.-H.; Hu, Y.; Zhang, Q.-L.; Wang, B.-L.; Sun, B.; Yeung, K.-S.; Zhang, F.-L.; Yu, J.-Q. Diverse Ortho -C(Sp 2)–H Functionalization of Benzaldehydes Using Transient Directing Groups. *J. Am. Chem. Soc.* **2017**, *139* (2), 888–896. https://doi.org/10.1021/jacs.6b11188.

(82) Yang, K.; Li, Q.; Liu, Y.; Li, G.; Ge, H. Catalytic C–H Arylation of Aliphatic Aldehydes Enabled by a Transient Ligand. *J. Am. Chem. Soc.* **2016**, *138* (39), 12775–12778. https://doi.org/10.1021/jacs.6b08478.

(83) Xu, J.; Liu, Y.; Wang, Y.; Li, Y.; Xu, X.; Jin, Z. Pd-Catalyzed Direct Ortho -C–H Arylation of Aromatic Ketones Enabled by a Transient Directing Group. *Org. Lett.* **2017**, *19* (7), 1562–1565. https://doi.org/10.1021/acs.orglett.7b00363.

(84) Jun, C.-H.; Moon, C. W.; Hong, J.-B.; Lim, S.-G.; Chung, K.-Y.; Kim, Y.-H. Chelation-Assisted RhI-Catalyzed Ortho-Alkylation of Aromatic Ketimines or Ketones with Olefins. *Chem. - A Eur. J.* **2002**, *8* (2), 485–492. https://doi.org/10.1002/1521-3765(20020118)8:2<485::AID-CHEM485>3.0.CO;2-1.

(85) Hong, K.; Park, H.; Yu, J.-Q. Methylene C(Sp 3)–H Arylation of Aliphatic Ketones Using a Transient Directing Group. *ACS Catal.* **2017**, *7* (10), 6938–6941. https://doi.org/10.1021/acscatal.7b02905.

(86) Pan, L.; Yang, K.; Li, G.; Ge, H. Palladium-Catalyzed Site-Selective Arylation of Aliphatic Ketones Enabled by a Transient Ligand. *Chem. Commun.* **2018**, *54* (22), 2759–2762. https://doi.org/10.1039/C8CC00980E.

(87) Liu, Y.; Ge, H. Site-Selective C-H Arylation of Primary Aliphatic Amines Enabled by a Catalytic Transient Directing Group. *Nat. Chem.* **2017**, *9* (1), 26–32. https://doi.org/10.1038/nchem.2606.

(88) Xu, Y.; Young, M. C.; Wang, C.; Magness, D. M.; Dong, G. Catalytic C(Sp 3)−H Arylation of Free Primary Amines with an Exo Directing Group Generated In Situ. *Angew. Chemie Int. Ed.* **2016**, *55* (31), 9084–9087. https://doi.org/10.1002/anie.201604268.

(89) Wu, Y.; Chen, Y.-Q.; Liu, T.; Eastgate, M. D.; Yu, J.-Q. Pd-Catalyzed γ-C(Sp 3)–H Arylation of Free Amines Using a Transient Directing Group. *J. Am. Chem. Soc.* **2016**, *138* (44), 14554–14557. https://doi.org/10.1021/jacs.6b09653.

(90) Morin, M. A.; Mallik, D.; Zhang, W.; Pietro, W.; Manthorpe, J. M.; Organ, M. G. Obtaining Kinetics From Continuous Processes: Sampling Multiple Time Points Concurrently With a Single Valve Rotation. *Chemistry–Methods* **2021**, *1* (2), 131–134. https://doi.org/10.1002/cmtd.202100003.

(91) Kwak, J. S.; Bizarri, N.; Sharif, S.; Zhang, W. P.; Mallik, D.; Organ, M. G. The Synthesis of Warfarin Using a Reconfigurable-Reactor Platform Integrated to a Multiple-Variable Optimization Tool. *Chem. – A Eur. J.* **2020**, *26* (67), 15505–15508. https://doi.org/10.1002/chem.202003700.

(92) Li, X.; Cao, X.; Xiong, J.; Ge, J. Enzyme–Metal Hybrid Catalysts for Chemoenzymatic Reactions. *Small* **2020**, *16* (15), 1–14. https://doi.org/10.1002/smll.201902751.

(93) Köhler, V.; Turner, N. J. Artificial Concurrent Catalytic Processes Involving Enzymes. *Chem. Commun.* **2015**, *51* (3), 450–464. https://doi.org/10.1039/c4cc07277d.

(94) Dumeignil, F.; Guehl, M.; Gimbernat, A.; Capron, M.; Ferreira, N. L.; Froidevaux, R.; Girardon, J. S.; Wojcieszak, R.; Dhulster, P.; Delcroix, D. From Sequential Chemoenzymatic Synthesis to Integrated Hybrid Catalysis: Taking the Best of Both Worlds to Open up the Scope of Possibilities for a Sustainable Future. *Catal. Sci. Technol.* **2018**, *8* (22), 5708–5734. https://doi.org/10.1039/c8cy01190g.

(95) Gröger, H.; Hummel, W. Combining the 'Two Worlds' of Chemocatalysis and Biocatalysis towards Multi-Step One-Pot Processes in Aqueous Media. *Curr. Opin. Chem. Biol.* **2014**, *19* (1), 171–179. https://doi.org/10.1016/j.cbpa.2014.03.002.

(96) Wang, Y.; Zhao, H. Tandem Reactions Combining Biocatalysts and Chemical Catalysts for Asymmetric Synthesis. *Catalysts* **2016**, *6* (12). https://doi.org/10.3390/catal6120194.

(97) Makkee, M.; Kieboom, A. P. G.; Van Bekkum, H.; Roels, J. A. Combined Action of Enzyme and Metal Catalyst, Applied to the Preparation of D-Mannitol. *J. Chem. Soc. Chem. Commun.* **1980**, No. 19, 930–931. https://doi.org/10.1039/c39800000930.

(98) Dinh, P. M.; Howarth, J. A.; Hudnott, A. R.; Williams, J. M. J.; Harris, W. Catalytic Racemisation of Alcohols: Applications of Enzymatic Resolution Reactions. *Tetrahedron Lett.* **1996**, *37* (42), 7623–7626. https://doi.org/10.1016/0040-4039(96)01677-2.

(99) Allen, J. V.; Williams, J. M. J. Dynamic Kinetic Resolution with Enzyme and Palladium Combinations. *Tetrahedron Lett.* **1996**, *37* (11), 1859–1862. https://doi.org/10.1016/0040-4039(96)00136-0.

(100) Stürmer, R. Enzymes and Transition Metal Complexes in Tandem—A New Concept for Dynamic Kinetic Resolution. *Angew. Chemie Int. Ed. English* **1997**, *36* (11), 1173–1174. https://doi.org/10.1002/anie.199711731.

(101) Ward, R. S. Dynamic Kinetic Resolution. *Tetrahedron: Asymmetry* **1995**, *6* (7), 1475–1490. https://doi.org/10.1016/0957-4166(95)00179-S.

(102) Turner, N. J. Deracemisation Methods. *Curr. Opin. Chem. Biol.* **2010**, *14* (2), 115–121. https://doi.org/10.1016/j.cbpa.2009.11.027.

(103) Turner, N. J. Enzyme Catalysed Deracemisation and Dynamic Kinetic Resolution Reactions. *Curr. Opin. Chem. Biol.* **2004**, *8* (2), 114–119. https://doi.org/10.1016/j.cbpa.2004.02.001.

(104) Faber, K.; Fessner, W. D.; Turner, N. J. Engineering Biocatalysts for Synthesis Including Cascade Processes. *Adv. Synth. Catal.* **2015**, *357* (8), 1565–1566. https://doi.org/10.1002/adsc.201500450.

(105) Höhne, M. Engineering Imine Reductases for Industrial Applications. *Nat. Catal.* **2019**, *2* (10), 841–842. https://doi.org/10.1038/s41929-019-0366-8.

(106) Payne, J. T.; Andorfer, M. C.; Lewis, J. C. Engineering Flavin-Dependent Halogenases. *Methods Enzymol.* **2016**, *575*, 93–126. https://doi.org/10.1016/bs.mie.2016.03.024.

(107) Vieille, C.; Burdette, D. S.; Zeikus, J. G. Thermozymes. *Biotechnol. Annu. Rev.* **1996**, *2* (C), 1–83. https://doi.org/10.1016/S1387-2656(08)70006-1.

(108) Kumar, S.; Dangi, A. K.; Shukla, P.; Baishya, D.; Khare, S. K. Thermozymes: Adaptive Strategies and Tools for Their Biotechnological Applications. *Bioresour. Technol.* **2019**, *278*, 372–382. https://doi.org/10.1016/j.biortech.2019.01.088.

(109) Burda, E.; Hummel, W.; Gröger, H. Modular Chemoenzymatic One-Pot Syntheses in Aqueous Media: Combination of a Palladium-Catalyzed Cross-Coupling with an Asymmetric Biotransformation. *Angew. Chemie Int. Ed.* **2008**, *47* (49), 9551–9554. https://doi.org/10.1002/anie.200801341.

(110) Tenbrink, K.; Seßler, M.; Schatz, J.; Gröger, H. Combination of Olefin Metathesis and Enzymatic Ester Hydrolysis in Aqueous Media in a One-Pot Synthesis. *Adv. Synth. Catal.* **2011**, *353* (13), 2363–2367. https://doi.org/10.1002/adsc.201100403.

(111) de Souza de Oliveira, C.; de Andrade, K. T.; Omori, A. T. One-Pot Chemoenzymatic Synthesis of Chiral Disubstituted 1,2,3-Triazoles in Aqueous Media. *J. Mol. Catal. B Enzym.* **2013**, *91*, 93–97. https://doi.org/10.1016/j.molcatb.2013.03.004.

(112) Simons, C.; Hanefeld, U.; Arends, I. W. C. E.; Maschmeyer, T.; Sheldon, R. A. A One-Pot Enantioselective Chemo-Enzymatic Synthesis of Amino Acids in Water. *Adv. Synth. Catal.* **2006**, *348* (4–5), 471–475. https://doi.org/10.1002/adsc.200505395.

(113) Wang, Z. J.; Clary, K. N.; Bergman, R. G.; Raymond, K. N.; Toste, F. D. A Supramolecular Approach to Combining Enzymatic and Transition Metal Catalysis. *Nat. Chem.* **2013**, *5* (2), 100–103. https://doi.org/10.1038/nchem.1531.

(114) Köhler, V.; Wilson, Y. M.; Dürrenberger, M.; Ghislieri, D.; Churakova, E.; Quinto, T.; Knörr, L.; Häussinger, D.; Hollmann, F.; Turner, N. J.; Ward, T. R. Synthetic Cascades Are Enabled by Combining Biocatalysts with Artificial Metalloenzymes. *Nat. Chem.* **2013**, *5* (2), 93–99. https://doi.org/10.1038/nchem.1498.

(115) Cosgrove, S. C.; Thompson, M. P.; Ahmed, S. T.; Parmeggiani, F.; Turner, N. J. One-Pot Synthesis of Chiral N-Arylamines by Combining Biocatalytic Aminations with Buchwald–Hartwig N-Arylation. *Angew. Chemie - Int. Ed.* **2020**, *59* (41), 18156–18160. https://doi.org/10.1002/anie.202006246.

(116) Wu, S.; Zhou, Y.; Gerngross, D.; Jeschek, M.; Ward, T. R. Chemo-Enzymatic Cascades to Produce Cycloalkenes from Bio-Based Resources. *Nat. Commun.* **2019**, *10* (1), 5060. https://doi.org/10.1038/s41467-019-13071-y.

(117) Song, J.-W.; Jeon, E.-Y.; Song, D.-H.; Jang, H.-Y.; Bornscheuer, U. T.; Oh, D.-K.; Park, J.-B. Multistep Enzymatic Synthesis of Long-Chain α,ω-Dicarboxylic and ω-Hydroxycarboxylic Acids from Renewable Fatty Acids and Plant Oils. *Angew. Chemie Int. Ed.* **2013**, *52* (9), 2534–2537. https://doi.org/10.1002/anie.201209187.

(118) Lenz, M.; Borlinghaus, N.; Weinmann, L.; Nestl, B. M. Recent Advances in Imine Reductase-Catalyzed Reactions. *World J. Microbiol. Biotechnol.* **2017**, *33* (11), 1–10. https://doi.org/10.1007/s11274-017-2365-8.

(119) Aleku, G. A.; France, S. P.; Man, H.; Mangas-Sanchez, J.; Montgomery, S. L.; Sharma, M.; Leipold, F.; Hussain, S.; Grogan, G.; Turner, N. J. A Reductive Aminase from Aspergillus Oryzae. *Nat. Chem.* **2017**, *9* (10), 961–969. https://doi.org/10.1038/nchem.2782.

(120) Sharma, M.; Mangas-Sanchez, J.; France, S. P.; Aleku, G. A.; Montgomery, S. L.; Ramsden, J. I.; Turner, N. J.; Grogan, G. A Mechanism for Reductive Amination Catalyzed by Fungal Reductive Aminases. *ACS Catal.* **2018**, *8* (12), 11534–11541. https://doi.org/10.1021/acscatal.8b03491.

(121) Natte, K.; Neumann, H.; Jagadeesh, R. V.; Beller, M. Convenient Iron-Catalyzed Reductive Aminations without Hydrogen for Selective Synthesis of N-Methylamines. *Nat. Commun.* **2017**, *8* (1), 1–9. https://doi.org/10.1038/s41467-017-01428-0.

(122) Stemmler, T.; Westerhaus, F. A.; Surkus, A.-E.; Pohl, M.-M.; Junge, K.; Beller, M. General and Selective Reductive Amination of Carbonyl Compounds Using a Core–Shell Structured Co 3 O 4 /NGr@C Catalyst. *Green Chem.* **2014**, *16* (10), 4535–4540. https://doi.org/10.1039/C4GC00536H.

(123) Gao, G.; Du, S.; Yang, Y.; Lei, X.; Huang, H.; Chang, M. Direct Asymmetric Reductive Amination for the Synthesis of (S)-Rivastigmine. *Molecules* **2018**, *23* (9). https://doi.org/10.3390/molecules23092207.

(124) Mangas-Sanchez, J.; France, S. P.; Montgomery, S. L.; Aleku, G. A.; Man, H.; Sharma, M.; Ramsden, J. I.; Grogan, G.; Turner, N. J. Imine Reductases (IREDs). *Curr. Opin. Chem. Biol.* **2017**, *37*, 19–25. https://doi.org/10.1016/j.cbpa.2016.11.022.

(125) Mitsukura, K.; Suzuki, M.; Tada, K.; Yoshida, T.; Nagasawa, T. Asymmetric Synthesis of Chiral Cyclic Amine from Cyclic Imine by Bacterial Whole-Cell Catalyst of Enantioselective Imine Reductase. *Org. Biomol. Chem.* **2010**, *8* (20), 4533. https://doi.org/10.1039/C0OB00353K.

(126) Mitsukura, K.; SUZUKI, M.; SHINODA, S.; KURAMOTO, T.; YOSHIDA, T.; NAGASAWA, T. Purification and Characterization of a Novel (R)-Imine Reductase from Streptomyces Sp. GF3587. *Biosci. Biotechnol. Biochem.* **2011**, *75* (9), 1778–1782. https://doi.org/10.1271/bbb.110303.

(127) Fademrecht, S.; Scheller, P. N.; Nestl, B. M.; Hauer, B.; Pleiss, J. Identification of Imine Reductase-Specific Sequence Motifs. *Proteins Struct. Funct. Bioinforma.* **2016**, *84* (5), 600–610. https://doi.org/10.1002/prot.25008.

(128) Scheller, P. N.; Fademrecht, S.; Hofelzer, S.; Pleiss, J.; Leipold, F.; Turner, N. J.; Nestl, B. M.; Hauer, B. Enzyme Toolbox: Novel Enantiocomplementary Imine Reductases. *ChemBioChem* **2014**, *15* (15), 2201–2204. https://doi.org/10.1002/cbic.201402213.

(129) Cosgrove, S. C.; Brzezniak, A.; France, S. P.; Ramsden, J. I.; Mangas-Sanchez, J.; Montgomery, S. L.; Heath, R. S.; Turner, N. J. Imine Reductases, Reductive Aminases, and Amine Oxidases for the Synthesis of Chiral Amines: Discovery, Characterization, and Synthetic Applications. *Methods Enzymol.* **2018**, *608*, 131–149. https://doi.org/10.1016/bs.mie.2018.04.022.

(130) Marshall, J.; Yao, P.; Montgomery, S.; Finnigan, J.; Thorpe, T.; Palmer, R.; Mangas-Sanchez, J.; Duncan, R.; Heath, R.; Graham, K.; Cook, D.; Charnock, S.; Turner, N. Screening and Characterisation of a Diverse Panel of Metagenomic Imine Reductases for Biocatalytic Reductive Amination. *Nat. Chem.* **2020**. https://doi.org/10.1038/s41557-020-00606-w.

(131) Ramsden, J. I.; Heath, R. S.; Derrington, S. R.; Montgomery, S. L.; Mangas-Sanchez, J.; Mulholland, K. R.; Turner, N. J. Biocatalytic N-Alkylation of Amines Using Either Primary Alcohols or Carboxylic Acids via Reductive Aminase Cascades. *J. Am. Chem. Soc.* **2019**, *141* (3), 1201–1206. https://doi.org/10.1021/jacs.8b11561.

(132) Aleku, G. A.; Mangas-Sanchez, J.; Citoler, J.; France, S. P.; Montgomery, S. L.; Heath, R. S.; Thompson, M. P.; Turner, N. J. Kinetic Resolution and Deracemization of Racemic Amines Using a Reductive Aminase. *ChemCatChem* **2018**, *10* (3), 515–519. https://doi.org/10.1002/cctc.201701484.

(133) The PyMOL Molecular Graphics System. Schrödinger, LLC.

(134) Xu, H. J.; Lu, Y.; Farmer, M. E.; Wang, H. W.; Zhao, D.; Kang, Y. S.; Sun, W. Y.; Yu, J. Q. Rh(III)-Catalyzed Meta-C-H Olefination Directed by a Nitrile Template. *J. Am. Chem. Soc.* **2017**, *139* (6), 2200–2203. https://doi.org/10.1021/jacs.6b13269.

(135) Gair, J. J.; Qiu, Y.; Chan, N. H.; Filatov, A. S.; Lewis, J. C. Rhodium Complexes of 2,6-Bis(Dialkylphosphinomethyl)Pyridines: Improved C–H Activation, Expanded Reaction Scope, and Catalytic Direct Arylation. *Organometallics* **2017**, *36* (24), 4699–4706. https://doi.org/10.1021/acs.organomet.7b00532.

(136) Thomas, J. G.; Baneyx, F. Protein Misfolding and Inclusion Body Formation in Recombinant Escherichia Coli Cells Overexpressing Heat-Shock Proteins. *J. Biol. Chem.* **1996**, *271* (19), 11141–11147. https://doi.org/10.1074/jbc.271.19.11141.

(137) Misuri, L.; Cappiello, M.; Balestri, F.; Moschini, R.; Barracco, V.; Mura, U.; Del-Corso, A. The Use of Dimethylsulfoxide as a Solvent in Enzyme Inhibition Studies: The Case of Aldose Reductase. *J. Enzyme Inhib. Med. Chem.* **2017**, *32* (1), 1152–1158. https://doi.org/10.1080/14756366.2017.1363744.

(138) Watanabe, K.; Ueji, S. Dimethyl Sulfoxide as a Co-Solvent Dramatically Enhances the Enantioselectivity in Lipase-Catalysed Resolutions of 2-Phenoxypropionic Acyl Derivatives. *J. Chem. Soc. Perkin Trans. 1* **2001**, No. 12, 1386–1390. https://doi.org/10.1039/b100182p.

(139) Sharma, S.; Raymond, E.; Soda, H.; Izbicka, E.; Davidson, K.; Lawrence, R.; Von Hoff, D. D. Dimethyl Sulfoxide (DMSO) Causes a Reversible Inhibition of Telomerase Activity in a Burkitt Lymphoma Cell Line. *Leuk. Res.* **1998**, *22* (8), 663–670. https://doi.org/10.1016/S0145-2126(97)00188-4.

(140) Wiggers, H. J.; Cheleski, J.; Zottis, A.; Oliva, G.; Andricopulo, A. D.; Montanari, C. A. Effects of Organic Solvents on the Enzyme Activity of Trypanosoma Cruzi Glyceraldehyde-3-Phosphate Dehydrogenase in Calorimetric Assays. *Anal. Biochem.* **2007**, *370* (1), 107–114. https://doi.org/10.1016/j.ab.2007.06.042.

(141) Busby, W. F.; Ackermann, J. M.; Crespi, C. L. Effect of Methanol, Ethanol, Dimethyl Sulfoxide, and Acetonitrile on in Vitro Activities of CDNA-Expressed Human Cytochromes P-450. *Drug Metab. Dispos.* **1999**, *27* (2), 246–249.

(142) Polson, C.; Sarkar, P.; Incledon, B.; Raguvaran, V.; Grant, R. Optimization of Protein Precipitation Based upon Effectiveness of Protein Removal and Ionization Effect in Liquid Chromatography–Tandem Mass Spectrometry. *J. Chromatogr. B* **2003**, *785* (2), 263–275. https://doi.org/10.1016/S1570-0232(02)00914-5.

(143) Lv, Z.; Yao, Y.; Lv, Z.; Min, H. Effect of Tetrahydrofuran on Enzyme Activities in Activated Sludge. *Ecotoxicol. Environ. Saf.* **2008**, *70* (2), 259–265. https://doi.org/10.1016/j.ecoenv.2007.06.001.

(144) Mozhaev, V. V.; Khmelnitsky, Y. L.; Sergeeva, M. V.; Belova, A. B.; Klyachko, N. L.; Levashov, A. V.; Martinek, K. Catalytic Activity and Denaturation of Enzymes in Water/Organic Cosolvent Mixtures. Alpha-Chymotrypsin and Laccase in Mixed Water/Alcohol, Water/Glycol and Water/Formamide Solvents. *Eur. J. Biochem.* **1989**, *184* (3), 597–602. https://doi.org/10.1111/j.1432-1033.1989.tb15055.x.

(145) Apffel, A.; Chakel, J. A.; Fischer, S.; Lichtenwalter, K.; Hancock, W. S. Analysis of Oligonucleotides by HPLC-Electrospray Ionization Mass Spectrometry. *Anal. Chem.* **1997**, *69* (7), 1320–1325. https://doi.org/10.1021/ac960916h.

(146) Kida, T.; Sato, S.; Yoshida, H.; Teragaki, A.; Akashi, M. 1,1,1,3,3,3-Hexafluoro-2-Propanol (HFIP) as a Novel and Effective Solvent to Facilely Prepare Cyclodextrin-Assembled Materials. *Chem. Commun.* **2014**, *50* (91), 14245–14248. https://doi.org/10.1039/C4CC06690A.

(147) Denard, C. A.; Huang, H.; Bartlett, M. J.; Lu, L.; Tan, Y.; Zhao, H.; Hartwig, J. F. Cooperative Tandem Catalysis by an Organometallic Complex and a Metalloenzyme. *Angew. Chemie - Int. Ed.* **2014**, *53* (2), 465–469. https://doi.org/10.1002/anie.201305778.

(148) Wen, Y. Q.; Hertzberg, R.; Gonzalez, I.; Moberg, C. Minor Enantiomer Recycling: Application to Enantioselective Syntheses of Beta Blockers. *Chem. - A Eur. J.* **2014**, *20* (13), 3806–3812. https://doi.org/10.1002/chem.201303890.

(149) Hildebrand, F.; Lütz, S. Stable Electroenzymatic Processes by Catalyst Separation. *Chem. - A Eur. J.* **2009**, *15* (20), 4998–5001. https://doi.org/10.1002/chem.200900219.

(150) Lipshutz, B. H.; Chung, D. W.; Rich, B. Aminations of Aryl Bromides in Water at Room Temperature. *Adv. Synth. Catal.* **2009**, *351* (11–12), 1717–1721. https://doi.org/10.1002/adsc.200900323.

(151) Lipshutz, B. H.; Ghorai, S.; Abela, A. R.; Moser, R.; Nishikata, T.; Duplais, C.; Krasovskiy, A.; Gaston, R. D.; Gadwood, R. C. TPGS-750-M: A Second-Generation Amphiphile for Metal-Catalyzed Cross-Couplings in Water at Room Temperature. *J. Org. Chem.* **2011**, *76* (11), 4379–4391. https://doi.org/10.1021/jo101974u.

(152) Isley, N. A.; Dobarco, S.; Lipshutz, B. H. Installation of Protected Ammonia Equivalents onto Aromatic & Heteroaromatic Rings in Water Enabled by Micellar Catalysis. *Green Chem.* **2014**, *16* (3), 1480. https://doi.org/10.1039/c3gc42188k.

(153) Klibanov, A. M. Improving Enzymes by Using Them in Organic Solvents. *Nature* **2001**, *409* (6817), 241–246. https://doi.org/10.1038/35051719.

(154) Madeira, F.; Park, Y. mi; Lee, J.; Buso, N.; Gur, T.; Madhusoodanan, N.; Basutkar, P.; Tivey, A. R. N.; Potter, S. C.; Finn, R. D.; Lopez, R. The EMBL-EBI Search and Sequence Analysis Tools APIs in 2019. *Nucleic Acids Res.* **2019**, *47* (W1), W636–W641. https://doi.org/10.1093/nar/gkz268.

(155) New England Biolabs. Q5® Site-Directed Mutagenesis Kit Protocol (E0554).

(156) Watson, J. F.; García-Nafría, J. In Vivo DNA Assembly Using Common Laboratory Bacteria: A Re-Emerging Tool to Simplify Molecular Cloning. *J. Biol. Chem.* **2019**, *294* (42), 15271–15281. https://doi.org/10.1074/jbc.REV119.009109.

(157) García-Fruitós, E. Inclusion Bodies: A New Concept. *Microb. Cell Fact.* **2010**, *9* (1), 80. https://doi.org/10.1186/1475-2859-9-80.

(158) Singh, A.; Upadhyay, V.; Upadhyay, A. K.; Singh, S. M.; Panda, A. K. Protein Recovery from Inclusion Bodies of Escherichia Coli Using Mild Solubilization Process. *Microb. Cell Fact.* **2015**, *14* (1), 1–10. https://doi.org/10.1186/s12934-015-0222-8.

(159) Qing, G.; Ma, L.-C.; Khorchid, A.; Swapna, G. V. T.; Mal, T. K.; Takayama, M. M.; Xia, B.; Phadtare, S.; Ke, H.; Acton, T.; Montelione, G. T.; Ikura, M.; Inouye, M. Cold-Shock Induced High-Yield Protein Production in Escherichia Coli. *Nat. Biotechnol.* **2004**, *22* (7), 877–882. https://doi.org/10.1038/nbt984.

(160) Gutiérrez-González, M.; Farías, C.; Tello, S.; Pérez-Etcheverry, D.; Romero, A.; Zúñiga, R.; Ribeiro, C. H.; Lorenzo-Ferreiro, C.; Molina, M. C. Optimization of Culture Conditions for the Expression of Three Different Insoluble Proteins in Escherichia Coli. *Sci. Rep.* **2019**, *9* (1), 16850. https://doi.org/10.1038/s41598-019-53200-7.

(161) Johnson, K. A.; Goody, R. S. The Original Michaelis Constant: Translation of the 1913 Michaelis–Menten Paper. *Biochemistry* **2011**, *50* (39), 8264–8269. https://doi.org/10.1021/bi201284u.

(162) Lineweaver, H.; Burk, D. The Determination of Enzyme Dissociation Constants. *J. Am. Chem. Soc.* **1934**, *56* (3), 658–666. https://doi.org/10.1021/ja01318a036.

(163) Heydenreich, F. M.; Miljuš, T.; Jaussi, R.; Benoit, R.; Milić, D.; Veprintsev, D. B. High-Throughput Mutagenesis Using a Two-Fragment PCR Approach. *Sci. Rep.* **2017**, *7* (1), 6787. https://doi.org/10.1038/s41598-017-07010-4.

(164) Strain-Damerell, C.; Burgess-Brown, N. A. High-Throughput Site-Directed Mutagenesis. In *High-Throughput Protein Production and Purification.*; Vincentelli, R., Ed.; Humana: New York, NY, **2019**; pp 281–296. https://doi.org/10.1007/978-1-4939-9624-7_13.

(165) Chhetri, G.; Kalita, P.; Tripathi, T. An Efficient Protocol to Enhance Recombinant Protein Expression Using Ethanol in Escherichia Coli. *MethodsX* **2015**, *2*, 385–391. https://doi.org/10.1016/j.mex.2015.09.005.